EPR spectroscopy of oxygen-tolerant [NiFe]-hydrogenases

vorgelegt von

Diplom-Chemiker

Miguel Florian Saggu

aus Schwerte

Von der Fakultät II - Mathematik und Naturwissenschaften

der Technischen Universität Berlin

zur Erlangung des akademischen Grades

Doktor der Naturwissenschaften

- Dr. rer. nat. -

genehmigte Dissertation

Promotionsausschuss:

Vorsitzender:	Prof. Dr. Thomas Friedrich
Berichter:	Prof. Dr. Peter Hildebrandt
Berichter:	Prof. Dr. Robert Bittl
Tag der wissenschaftlichen Aussprache:	09. Dezember 2009

Berlin 2010
D 83

Abstract

Hydrogenases are metalloenzymes and play a pivotal role in the energy metabolism of a variety of microorganisms. They catalyze the reversible cleavage of molecular hydrogen into two protons and two electrons. However, one drawback is their catalytic inactivation upon exposure to oxygen. [FeFe]-hydrogenases are irreversibly inactivated by oxygen, whereas [NiFe]-hydrogenases usually are reversibly inactivated to the so-called 'ready' and 'unready' states. Only a few [NiFe]-hydrogenases show a remarkable oxygen-tolerance, e.g. the [NiFe]-hydrogenases from the 'Knallgasbacterium' *Ralstonia eutropha* H16 investigated in this work. *Re* H16 harbors three different [NiFe]-hydrogenases, all of them being able to oxidize molecular hydrogen under ambient oxygen concentrations. The goal of this work was to understand the origin of this oxygen-tolerance on a molecular level and to study structure/function-relationships of the involved cofactors using a combination of EPR and FTIR spectroscopy. EPR spectroscopy can be applied to detect all paramagnetic species and to obtain information about their electronic and in its more advanced variant the geometric structure, respectively. FTIR spectroscopy applied to hydrogenases specifically monitors the stretching modes of the inorganic ligands at the Fe to follow redox changes of the [NiFe] center. An important aspect of this thesis was to study biological systems in their native environment, e.g. in whole cells or membrane fragments.

The membrane-bound [NiFe]-hydrogenase (MBH) from *Re* H16 was studied mainly in its native environment, i.e. in membrane fragments that harbor over-produced MBH. All catalytically active redox states of the [NiFe] center were identified. However, the 'unready' Ni_u-A, observed in standard [NiFe]-hydrogenases could not be detected, which seems to be a common feature of all oxygen-tolerant [NiFe]-hydrogenases. It was shown, that the MBH contains an additional high-potential paramagnetic center. Concomitant electrochemical experiments revealed that the MBH can be reactivated very fast at high potentials, which might indicate an important role of the additional high-potential center. This center could influence the catalytic cycle by providing electrons to avoid Ni_u-A formation.

The hyperfine structure of the Ni_r-B state (oxidized enzyme) was investigated in more detail by pulsed EPR methods, namely ENDOR and ESEEM spectroscopy. The results were compared with the standard [NiFe]-hydrogenase from *D. vulgaris* Miyazaki F. Both hydrogenases showed a similar spin density distribution in their [NiFe] center indicating that the spatial structures of the active sites are identical. Two large hf-couplings arising from the β-protons of one bridging cysteine sulfur were resolved and simulated in orientation-selective ENDOR spectra. With ESEEM spectroscopy a nitrogen located in a histidine residue in the second coordination sphere of the Ni was detected, which is a known property of many [NiFe]-hydrogenases. This histidine is hydrogen-bonded to the same bridging sulfur.

Another interesting feature of oxygen-tolerant membrane-bound [NiFe]-hydrogenases is the presence of two additional cysteine residues in the vicinity of the proximal [4Fe4S]-cluster. Muta-

tions of these cysteines revealed that these residues are responsible for an alteration of the proximal [4Fe4S] center, resulting in the additional paramagnetic center(s) detectable at high redox potentials.

The oxygen-tolerant soluble hydrogenase (SH) from *Re* H16 and the closely related bidirectional hydrogenase from *Synechocystis* PCC 6803 were investigated as well. The SH has been studied *in situ* in its natural environment in whole cells. It was found, that under these conditions the [NiFe] active site exhibited a standard-type coordination with one CO and two CN^--ligands at the Fe, which is in contrast to previous studies on purified SH. For comparison, the soluble hydrogenase from the oxygenic phototrophic cyanobacterium *Synechocystis* PCC 6803 was characterized with EPR and FTIR spectroscopy. The active site Fe was also found to be coordinated with a standard set of inorganic ligands, one CO and two CN^-. Practically all ready and catalytically active states known from standard [NiFe]-hydrogenases were identified for this enzyme including two different FeS clusters and a flavin-type radical. Both soluble hydrogenases reveal strong similarities with respect to the redox states and FeS clusters. However, no paramagnetic Ni_r-B/Ni_u-A EPR-signals could be observed in both hydrogenases, which might be related to a coupling with another paramagnetic species in close vicinity. The *Synechocystis* hydrogenase can be rapidly activated with hydrogen under anaerobic conditions. Because of its spectral and catalytic properties, the SH from *Synechocystis* represents a link between standard and oxygen-tolerant [NiFe]-hydrogenases.

The unusual oxygen-tolerance of the *Ralstonia* hydrogenases, at least for the MBH, is probably connected with a modified proximal FeS center of yet unknown structure. Possibly a similar paramagnetic species exists close to the [NiFe] center also in SH and could be the reason for its O_2-tolerance.

Zusammenfassung

Hydrogenasen sind Metalloenzyme und spielen eine entscheidende Rolle im Metabolismus einer Vielzahl von Mikroorganismen. Diese Enzyme katalysieren die reversible Spaltung von molekularem Wasserstoff in zwei Protonen und zwei Elektronen. Allerdings werden sie durch Sauerstoff katalytisch inaktiviert. [FeFe]-Hydrogenasen werden irreversibel inaktiviert, während [NiFe]-Hydrogenasen normalerweise reversibel inaktiviert werden zu den so genannten 'ready' und 'unready' Zuständen. Einige [NiFe]-Hydrogenasen zeigen allerdings eine bemerkenswerte Sauerstofftoleranz, z.B. die in dieser Arbeit untersuchten [NiFe]-Hydrogenasen des 'Knallgasbakteriums' *Ralstonia eutropha* H16. *Re* H16 enthält drei unterschiedliche [NiFe]-Hydrogenasen, von denen alle in der Lage sind, molekularen Wasserstoff unter natürlichen Sauerstoffkonzentrationen zu oxidieren. Ziel dieser Arbeit war es, die Ursache der Sauerstofftoleranz auf molekularer Ebene zu verstehen und Struktur/Funktions-Beziehungen der beteiligten Kofaktoren zu studieren unter Verwendung einer Kombination aus EPR und FTIR Spektroskopie. EPR Spektroskopie kann angewendet werden, um alle paramagnetischen Zustände zu detektieren und Informationen über die elektronische und damit räumliche Struktur zu erhalten. Mit FTIR Spektroskopie können die Streckschwingungen der diatomigen Liganden am Fe beobachtet werden, um Redoxänderungen des [NiFe] Zentrums zu verfolgen. Ein wichtiger Aspekt dieser Arbeit war die Untersuchung biologischer Systeme in möglichst nativer Umgebung, z.B. in ganzen Zellen oder Membranfragmenten.

Die Membran-gebundene [NiFe]-Hydrogenase (MBH) von *Re* H16 wurde hauptsächlich in ihrer natürlichen Umgebung untersucht, d.h. in Membranfragmenten, die überproduzierte MBH enthielten. Alle katalytisch aktiven Redoxzustände des [NiFe] Zentrums wurden identifiziert. Allerdings konnte der 'unready' Zustand Ni_u-A, bekannt aus Standard-[NiFe]-Hydrogenasen, nicht detektiert werden, was eine gemeinsame Eigenschaft sauerstofftoleranter [NiFe]-Hydrogenasen zu sein scheint. Es konnte gezeigt werden, dass die MBH ein zusätzliches 'high-potential' paramagnetisches Zentrum enthält. Elektrochemische Untersuchungen haben gezeigt, dass die MBH bei hohen Potentialen sehr schnell reaktiviert werden kann, was auf eine wichtige Rolle des zusätzlichen Zentrums hinweisen könnte. Dieses Zentrum könnte den katalytischen Zyklus beeinflussen, indem es Elektronen zur Verfügung stellt, die eine Bildung des Ni_u-A verhindern.

Die Hyperfeinstruktur des Ni_r-B Redoxzustandes (oxidiertes Enzym) wurde detailliert mit Puls-EPR Methoden untersucht, hauptsächlich mit ENDOR und ESEEM Spektroskopie. Die erhaltenen Resultate wurden verglichen mit der Standard-[NiFe]-Hydrogenase von *D. vulgaris* Miyazaki F. Beide Hydrogenasen zeigten eine ähnliche Spindichte-Verteilung in ihrem [NiFe] Zentrum, was auf eine vergleichbare Geometrie schliessen lässt. Hyperfeinkopplungen von zwei β-Protonen eines verbrückenden Cystein-Schwefels konnten aufgelöst und simuliert werden. Mittels ESEEM Spektroskopie konnte die Anwesenheit eines Histidin Stickstoffs in der zweiten Koordinationssphäre des Ni nachgewiesen werden, was eine Eigenschaft vieler [NiFe]-Hydrogenasen ist. Dieses Histidin ist über eine Wasserstoffbrücke an dasselbe verbrückende Schwefelatom koordiniert.

Eine interessante Eigenschaft sauerstofftoleranter Membran-gebundener [NiFe]-Hydrogenasen ist die Anwesenheit von zwei zusätzlichen Cysteinen in der Nähe des proximalen [4Fe4S] Zentrums. Durch Mutationen dieser beiden Cysteine konnte gezeigt werden, dass eine Modifikation des proximalen [4Fe4S] Zentrums auf sie zurückzuführen ist. Beide scheinen essentiell für die Anwesenheit des zusätzlichen paramagnetischen Zentrums bei hohen Redoxpotentialen zu sein.

Die sauerstofftolerante lösliche Hydrogenase (SH) von *Re* H16 and die eng verwandte Hydrogenase von *Synechocystis* PCC 6803 wurden ebenfalls charakterisiert. Die SH wurde *in situ* in ihrer natürlicher Umgebung in ganzen Zellen studiert. Unter diesen Bedingungen verhielt sich das aktive Zentrum wie ein Standard [NiFe] Zentrum mit einem CO und zwei CN^--Liganden am Fe, im Gegensatz zu früheren Studien an gereinigter SH. Als Vergleich dazu wurde die lösliche Hydrogenase von *Synechocystis* PCC 6803 charakterisiert. Das Fe im aktiven Zentrum ist mit dem Standardsatz anorganischer Liganden, einem CO und zwei CN^-, koordiniert. Praktisch alle 'ready' und katalytisch aktiven Zustände bekannt aus Standard-[NiFe]-Hydrogenasen konnten für dieses Enzym identifiziert werden inklusive zwei verschiedene FeS Zentren und ein typisches Flavin Radikal. Beide löslichen Hydrogenasen zeigten starke Ähnlichkeiten hinsichtich ihrer Redoxzustände und FeS Zentren. Allerdings konnten keine paramagnetischen Ni_r-B/Ni_u-A EPR Signale beobachtet werden, was auf eine Kopplung mit einem anderen benachbarten paramagnetischen Zentrum schliessen lässt. Die *Synechocystis* Hydrogenase konnte unter anaeroben Bedingungen schnell mit Wasserstoff aktiviert werden. Aufgrund ihres spektroskopischen und katalytischen Verhaltens ist die SH von *Synechocystis* zwischen Standard- und sauerstofftoleranten [NiFe]-Hydrogenasen anzuordnen.

Es ist bekannt, dass das proximale FeS Zentrum essentiell für Hydrogenasen ist. Die ungewöhnliche Sauerstofftoleranz der *Ralstonia* Hydrogenasen ist zumindest in der MBH wahrscheinlich verbunden mit einem modifizierten FeS Zentrum von dem die Struktur bis jetzt nicht bekannt ist. Möglicherweise existiert eine ähnliche paramagnetische Spezies in der Nähe des [NiFe] Zentrums in der SH, was auch dort die Ursache der O_2-Toleranz sein könnte.

List of publications

Publications in peer-reviewed scientific journals

1. M. Saggu, I. Zebger, M. Ludwig, O. Lenz, B. Friedrich, P. Hildebrandt and F. Lendzian, *Spectroscopic insights into the oxygen-tolerant membrane-associated [NiFe]-hydrogenase of Ralstonia eutropha H16*, J. Biol. Chem., **2009**, *284*, 16264-16276.

2. F. Germer, I. Zebger, M. Saggu, F. Lendzian, R. Schulz and J. Appel, *Overexpression, isolation and spectroscopic characterization of the bidirectional [NiFe]-hydrogenase from Synechocystis sp. PCC 6803*, J. Biol. Chem., **2009**, *284*, 36462-36472.

3. M. Saggu, C. Teutloff, M. Ludwig, M. Brecht, M. Pandelia, O. Lenz, B. Friedrich, W. Lubitz, P. Hildebrandt, F. Lendzian and R. Bittl, *Comparative investigation of the ready oxidized state of the membrane bound [NiFe]-hydrogenases from Ralstonia eutropha H16 and D. vulgaris Miyazaki F by pulsed EPR spectroscopy*, Phys. Chem. Chem. Phys., **2009**, in press.

4. M. Horch, M. Saggu, L. Lauterbach, O. Lenz, P. Hildebrandt, F. Lendzian, R. Bittl and I. Zebger, *In situ investigation of the soluble hydrogenase from R. eutropha H16 in whole cells: a combined EPR and FTIR spectroscopic study*, **2009**, to be submitted.

5. M. Saggu, M. Ludwig, O. Lenz, B. Friedrich, P. Hildebrandt, R. Bittl, F. Lendzian and I. Zebger, *Impact of amino acid substitutions near the catalytic site on the spectral properties of an O_2-tolerant membrane-bound [NiFe]-hydrogenase*, Chem. Phys. Chem., **2010**, accepted.

6. T. Goris, M. Saggu, A. Wait, I. Zebger, P. Hildebrandt, R. Bittl, F. Armstrong, F. Lendzian, B. Friedrich and O. Lenz, *An unusual proximal iron-sulfur cluster plays a crucial role in the oxygen-tolerance of the membrane-bound hydrogenase of Ralstonia eutropha*, **2009**, in preparation.

Proceedings

1. M. Saggu, I. Zebger, M. Ludwig, O. Lenz, B. Friedrich, P. Hildebrandt and F. Lendzian, *EPR and vibrational spectroscopic investigations of the oxygen-tolerant membrane-bound hydrogenase from Ralstonia eutropha H16*, Proceedings of the European Conference on Metallobiolomics, HMI Berlin, Germany, 2008, 21-25, Herbert Utz Verlag, ISBN: 978-3-8316-0827-0.

Talks at scientific conferences

1. M. Saggu, I. Zebger, M. Ludwig, O. Lenz, B. Friedrich, P. Hildebrandt and F. Lendzian
   EPR and FTIR characterization of the membrane-bound [NiFe]-hydrogenase from *R. eutropha* H16
   Iron-Sulfur proteins. A satellite meeting of the European Iron Club, 13. September 2007, London, UK

2. M. Saggu, I. Zebger, M. Ludwig, O. Lenz, B. Friedrich, P. Hildebrandt and F. Lendzian
   Actual EPR and FTIR spectroscopic data on MBH proteins
   SFB498-Unicat Workshop, 4. Dezember 2007, Berlin

3. M. Saggu, I. Zebger, M. Ludwig, O. Lenz, B. Friedrich, P. Hildebrandt and F. Lendzian
   EPR characterization of the membrane-bound [NiFe]-hydrogenase from *R. eutropha* H16
   SFB Miniworkshop, 25. April 2008, Berlin

4. M. Saggu, M. Ludwig, B. Friedrich, P. Hildebrandt and F. Lendzian
   EPR spectroscopy of hydrogenases
   ITQB Workshop: Structure, dynamics and function of proteins, 17.-19. September 2008, Lissabon, Portugal

5. M. Saggu
   EPR investigation of the MBH and variants
   Unicat Miniworkshop Project B2: Structure-function analysis of oxygen-tolerant hydrogenases, 07.-08. Mai 2009, Berlin

6. M. Saggu
   The membrane-bound [NiFe] hydrogenase from *R. eutropha* H16 investigated with EPR spectroscopy
   Minisymposium Hydrogenase, 11. Mai 2009, MPI Mühlheim

Poster contributions

1. M. Saggu, I. Zebger, M. Ludwig, O. Lenz, B. Friedrich, P. Hildebrandt and F. Lendzian
   Vibrational and EPR spectroscopic investigations of the membrane-bound [NiFe]-hydrogenase from *R. eutropha* H16
   Leopoldina Workshop: Molecular Function of Catalysts Involved in BioH_2 Production, 21.-23. Februar 2007, Berlin

2. M. Saggu, I. Zebger, M. Ludwig, O. Lenz, B. Friedrich, P. Hildebrandt and F. Lendzian
   Vibrational and EPR spectroscopic investigations of the membrane-bound [NiFe]-hydrogenase from *R. eutropha* H16
   Hydrogenase and Hydrogen Production 2007: The 8^{th} International Hydrogenase Conference, 05.-10. August 2007, Breckenridge CO, USA

3. M. Saggu, I. Zebger, M. Ludwig, O. Lenz, B. Friedrich, P. Hildebrandt and F. Lendzian
   EPR and FTIR characterization of the membrane-bound [NiFe]-hydrogenase from *R. eutropha* H16
   Iron-Sulfur proteins. A satellite meeting of the European Iron Club, 13. September 2007, London, UK

4. M. Saggu, I. Zebger, M. Ludwig, O. Lenz, B. Friedrich, P. Hildebrandt and F. Lendzian
   Vibrational and EPR spectroscopic investigations of the membrane-bound [NiFe]-hydrogenase from *R. eutropha* H16
   International Symposium of the Collaborative Research Center SFB498 Protein-Cofactor Interactions in Biological Processes, 16.-19. September 2007, Berlin

5. M. Saggu, I. Zebger, M. Ludwig, O. Lenz, B. Friedrich, P. Hildebrandt and F. Lendzian
   Vibrational and EPR spectroscopic investigations of the membrane-bound [NiFe]-hydrogenase from *R. eutropha* H16
   European Conference on Metallobiolomics, 29.-30. November 2007, Berlin

6. M. Saggu, I. Zebger, M. Ludwig, O. Lenz, B. Friedrich, P. Hildebrandt and F. Lendzian
   Spectroscopic insights into the oxygen-tolerant membrane-associated [NiFe] hydrogenase from *Ralstonia eutropha* H16
   Gordon Research Conference on Iron-Sulfur proteins, 08.-13. Juni 2008, New Londen NH, USA

7. M. Saggu, I. Zebger, M. Ludwig, O. Lenz, B. Friedrich, P. Hildebrandt and F. Lendzian
   Spectroscopic insights into the oxygen-tolerant membrane-associated [NiFe] hydrogenase from *Ralstonia eutropha* H16
   SUSSP-64 and COST P15 Training School and 4^{th} European EPR Federation Summer School in Advanced Techniques in EPR, 22. August - 01. September 2008, St. Andrews, UK

8. M. Saggu, I. Zebger, M. Ludwig, O. Lenz, B. Friedrich, P. Hildebrandt and F. Lendzian
   Spectroscopic insights into the oxygen-tolerant membrane-associated [NiFe] hydrogenase from *Ralstonia eutropha* H16
   German Biophysical Society Meeting 2008 - GBSM 2008, 28. September-01. Oktober, Berlin

9. M. Saggu, M. Ludwig, O. Lenz, C. Teutloff, M. Brecht, B. Friedrich, P. Hildebrandt, W. Lubitz, R. Bittl and F. Lendzian
   Comparative Investigation of the Ni_r-B state of the membrane-bound [NiFe]-hydrogenases from *Ralstonia eutropha* H16 and *D. vulgaris* Miyazaki F using pulsed EPR methods
   Inorganic Reactions at the Molecular Level - 38^{th} Meeting of the RSC Inorganic Reaction Mechanisms Group in conjunction with RSC Inorganic Biochemistry Group, 04.-06. Januar 2009, Oxford, UK

10. M. Saggu, S. Frasca, F. Lendzian, P. Hildebrandt, U. Wollenberger and S. Leimkühler
The role of the two [2Fe2S] clusters in *Rhodobacter capsulatus* xanthine dehydrogenase
Gordon Research Conference on Molybdenum and Tungsten Enzymes, 05.-10. Juli 2009, Lucca, Italy

Further publications in peer-reviewed scientific journals

1. S. Schumann, M. Saggu, N. Moeller, S. Anker, F. Lendzian, P. Hildebrandt and S. Leimkühler, *The mechanism of assembly and cofactor insertion into Rhodobacter capsulatus xanthine dehydrogenase*, J. Biol. Chem., **2008**, *283*, 16602-16611.

2. M. F. Tioni, L. I. Llarrull, A. A. Poeylaut-Palena, M. A. Marti, M. Saggu, G. R. Periyannan, E. G. Mata, B. Bennett, D. H. Murgida and A. J. Vila, *Trapping and characterization of a reaction intermediate in carbapenem hydrolysis by B. cereus metallo-beta-lactamase*, J. Am. Chem. Soc., **2008**, *130*, 15852-15863.

3. M. J. Bröcker, D. Wätzlich, F. Uliczka, S. Virus, M. Saggu, F. Lendzian, H. Scheer, W. Ruediger, J. Moser and D. Jahn, *Substrate recognition of nitrogenase-like dark operative protochlorophyllide oxidoreductase from Prochlorococcus marinus*, J. Biol. Chem., **2008**, *283*, 29873-29881.

4. M. Ludwig, T. Schubert, I. Zebger, N. Wisitruangsakul, M. Saggu, A. Strack, O. Lenz, P. Hildebrandt and B. Friedrich, *Concerted Action of Two Novel Auxiliary Proteins in Assembly of the Active Site in a Membrane-bound [NiFe] Hydrogenase*, J. Biol. Chem., **2009**, *284*, 2159-2168.

5. S. Schumann, M. Terao, E. Garattini, M. Saggu, F. Lendzian, P. Hildebrandt and S. Leimkühler, *Site directed mutagenesis of amino acid residues at the active site of mouse aldehyde oxidase AOX1*, PLoS ONE, **2009**, *4*, e5348.

6. M. Neumann, G. Mittelstädt, C. Iobbi-Nivol, M. Saggu, F. Lendzian, P. Hildebrandt and S. Leimkühler, *A periplasmic aldehyde oxidoreductase represents the first molybdopterin cytosine dinucleotide cofactor containing molybdo-flavoenzyme from Escherichia coli*, FEBS J., **2009**, *276*, 2762-2774.

7. M. J. Bröcker, D. Wätzlich, S. Bruchmann, M. Saggu, F. Lendzian, D. Jahn and J. Moser, *Biosynthesis of (Bacterio)chlorophylls: ATP-dependent transient subunit interaction and electron transfer of dark operative protochlorophyllide oxidoreductase*, J. Biol. Chem., **2010**, accepted.

8. M. Saggu, S. Frasca, P. Hildebrandt, F. Lendzian, U. Wollenberger and S. Leimkühler, *The role of the two [2Fe2S]-clusters in Rhodobacter capsulatus xanthine dehydrogenase*, **2009**, in preparation.

Abbreviations

A. aeolicus	*Aquifex aeolicus*
A. ferrooxidans	*Acidithiobacillus ferrooxidans*
CFQ	clear fused quartz
cw	continuous wave
Cys	cysteine
D. baculatum	*Desulfomicrobium baculatum*
D. gigas	*Desulfovibrio gigas*
D. vulgaris	*Desulfovibrio vulgaris*
DFT	density functional theory
ENDOR	electron nuclear double resonance
EPR	electron paramagnetic resonance
ESEEM	electron spin echo envelope modulation
EXAFS	extended x-ray absorption fine structure
FAD	flavin adenine dinucleotide
FMN	flavin mononucleotide
FTIR	fourier-transform infrared spectroscopy
HiPIP	high potential iron-sulfur protein
HYSCORE	hyperfine sublevel correlation spectroscopy
MBH	membrane-bound hydrogenase
MO	molecular orbital
mw	microwave
NAD^+	nicotinamide adenine dinucleotide
$NADP^+$	nicotinamide adenine dinucleotide phosphate
NTA	nitrilotriacetic acid
O.D.	outer diameter
P. pseudoflava	*Pseudomonas pseudoflava*
Re	*Ralstonia eutropha*
RH	regulatory hydrogenase
Rm	*Ralstonia metallidurans*
SEIRA	surface enhanced infrared absorption spectroscopy
SHE	standard hydrogen electrode
SH	soluble hydrogenase
SOC	spin-orbit coupling
XAS	x-ray absorption spectroscopy

List of Symbols

$\mathbb{1}$	unity matrix
Å	Angstrom (1 Å=10^{-10} m)
$\mathbf{A}$	hyperfine-tensor
a_{iso}	isotropic hyperfine interaction
B	magnetic field
$\mathbf{D}$	zero-field-tensor
e	elementary charge ($1.602 \cdot 10^{-19}$ As)
$\mathbf{g}$	g-tensor
g_e	g-factor of free eletron
g_N	nuclear g-factor
h	Planck constant ($6.62606896 \cdot 10^{-34}$ Js)
$\hat{\mathscr{H}}$	spin Hamiltonian
I	nuclear spin
$\hat{\mathbf{I}}$	nuclear spin operator
k_b	Boltzmann constant ($1.3806504 \cdot 10^{-23}$ J/K)
μ_B	Bohr magneton
$\hat{\mathbf{L}}$	orbital angular momentum operator
m_s	magnetic spin quantum number
μ	magnetic moment
μ_e	magnetic moment of electron
μ_N	magnetic moment of nucleus
ν	frequency
$\mathbf{P}$	nuclear quadrupole-tensor
ρ	spin density
λ	spin-orbit coupling constant
S	electron spin
$\hat{\mathbf{S}}$	spin operator
ψ	wavefunction

Contents

1 Introduction and motivation

Molecular hydrogen is the most simple molecule that we know, but one of the most efficient energy storing compounds. The combustion of hydrogen and oxygen in a 'Knallgasreaction' releases a large amount of energy.[1]

$$2H_2(g) + O_2(g) \longrightarrow 2H_2O(l) \;\; \Delta H^0 = -286 \text{ kJ/mol}$$

Nevertheless, hydrogen has a few disadvantages because bond cleavage requires an activation energy of about 400 kJ/mol and cannot be carried out without an appropiate catalyst at ambient conditions.[2] Noble metals like platinum are used as catalysts in fuels cells but they are expensive and can be contaminated easily by CO or H_2S. In nature many microbes circumvent this difficulty using metalloenzymes as catalysts, e.g. hydrogenases,[3] which show similar hydrogen oxidation rates as compared to platinum catalysts.[4] Hydrogenases are important enzymes because the interest in hydrogen as a renewable energy carrier grows year by year. In contrast, the combustion of fossil fuels leads to pollution with CO_2 and these energy sources are not renewable. The membrane-bound hydrogenase from *Rm* CH34 has been already successfully used in a fuel cell to produce electricity.[1,5] Another interesting aspect are photosynthetic organisms like cyanobacteria, which can use photons to oxidize water and release electrons. Under certain conditions the electrons can be delivered to hydrogenases for hydrogen production ('bio-hydrogen'). Unfortunately, the hydrogenases of these organisms are highly sensitive to oxygen that is generated during the water splitting process. To overcome this problem O_2-tolerant hydrogenases are required, which has been successfully demonstrated in a hybrid protein with a PSI subunit from a cyanobacterium fused to the membrane-bound [NiFe]-hydrogenase from *Re* H16 ('light-driven' hydrogen production).[6] Detailed knowledge about the catalytic mechanism could provide the basis for the synthesis of biomimetic catalysts suitable for large-scale hydrogen production.

Hydrogenases play an important role in the energy metabolism of many microorganisms like bacteria, archaea and eukaryotes.[3,7] They catalyze the reversible cleavage of molecular hydrogen into two protons and two electrons. Deuterium exchange isotope experiments have shown that this reaction is heterolytic.[8]

$$H_2 \underset{\text{Evolution}}{\overset{\text{Uptake}}{\rightleftharpoons}} H^+ + H^- \rightleftharpoons 2H^+ + 2e^-$$

In anaerobic organisms the electrons are used as reduction equivalents in the cell metabolism, e.g. for sulfate, nitrate, iron or carbon dioxide reduction.[7] The 'Knallgas' bacterium *Ralstonia eutropha* studied in this work uses the electrons to produce water from oxygen. Many organisms contain more than one type of hydrogenase and their physiological function (uptake or evolution) is then dependent on their specific electron acceptor/donor.

All hydrogenases are classified depending on the metal composition of their active sites into three phylogenetically different groups of [NiFe]-, [FeFe]- and [Fe]-hydrogenases,[9–11] whereas most of them belong to the group of [NiFe]-hydrogenases. A subgroup of [NiFe]-hydrogenases are the [NiFeSe]-hydrogenases in which one of the terminal cysteines is replaced by a selenocysteine.[12] A more detailed description of [NiFe]-hydrogenases will be given in the next sections.

Since the active site is usually deeply buried inside the protein, the electrons produced in hydrogen-cleavage need to be transferred via an electron transfer-chain consisting of iron-sulfur clusters to the electron acceptor or vice versa in case of H_2 evolution.[11]

The [FeFe]-hydrogenases are found in strictly anaerobic organisms, e.g. the nitrogen-fixating bacterium *C. pasteurianum*,[9] and can be build up of only one subunit.[13] The active center is a di-iron center, where both iron atoms are linked by a dithiol ligand in bridging position. This di-iron center is coordinated to the protein via one cysteine residue, that attaches the center in addition to a cubic [4Fe4S]-cluster. The complete active center contains six Fe atoms and is called 'H-cluster'.[13] Most [FeFe]-hydrogenases harbour additional FeS-clusters. Hydrogenases usually have a directional preference in catalysis, but [FeFe]-hydrogenases can be very efficient in catalyzing both uptake and evolution of hydrogen and are therefore called 'bidirectional'.[14]

The third class was originally designated as 'metal-free' hydrogenase because it was believed for a long time that this type of hydrogenase does not contain metal ions at all. The [Fe]-hydrogenase is composed of only one subunit (38 kDa) without iron-sulfur clusters and the presence of an iron atom was just recently discovered.[10,15] In these hydrogenases, which are found in some methanogenic archaea, hydrogen uptake is coupled to methenyl-tetrahydromethanopterin reduction (H_2-forming methylene-tetrahydromethanopterin dehydrogenases (Hmd)).[16] The iron in the active site appeares to be light sensitive.[17] The oxidation state of the iron does not change and the catalytic site is EPR-silent throughout the catalytic cycle. Therefore, the center was mainly investigated with x-ray crystallography, FTIR and EXAFS.[10]

A special feature all hydrogenases share is the coordination of the iron atoms in the active site by inorganic ligands. In the [NiFe] and [FeFe] hydrogenases the iron(s) of the active center carry CO and CN^--ligands[9,11] whereas in the [Fe]-hydrogenase it is only CO.[10,18] This has been detected by FTIR spectroscopy for the first time in the *A. vinosum* [NiFe]-hydrogenase.[19,20] These ligands keep the iron always in a low-spin Fe^{2+} state with a spin S = 0. This special iron ($Fe(CO)_x$) seems to be essential for biological H_2 cycling.[21]

In addition to H_2, most hydrogenases react with O_2, which acts as an inhibitor. In case of [FeFe]-hydrogenases this leads to an irreversible inactivation of the active site, the H-cluster.[14,22] [NiFe]-hydrogenases are usually reversibly inactivated to the 'unready' Ni_u-A and 'ready' Ni_r-B states.[23,24]

This work is mainly focused on the spectroscopic characterization of the membrane-bound [NiFe]-hydrogenase from *Re* H16. Therefore, a combination of EPR and FTIR spectroscopy was employed. The aim was to elucidate the structural and functional basis of the oxygen-tolerance for the MBH, which makes this enzyme suitable for technological applications. Since no crystal structures are available for *Re* H16, the results were compared to the oxygen-sensitive standard [NiFe]-hydrogenase from *D. vulgaris* Miyazaki F. For the regulatory hydrogenase from *Re* H16 it has been shown that a narrow gas channel prevents O_2 from accessing the active site.[25] Similar

gas-channel mutants of the MBH have shown no effect on the oxygen-tolerance.[26] Thus, the O_2-tolerance must have a different origin, which may be a modification of the [NiFe] center (**chapter 5** and **chapter 6**). A second explanation may be an alteration of the iron-sulfer clusters, especially of the proximal cluster (**chapter 7**).

Another part of this work deals with the soluble hydrogenase from *Re* H16. The [NiFe] center was proposed to contain two additional cyanide ligands, which were supposed to shield the [NiFe] site from oxygen. However, a drawback of the purified protein was the non-reproducibility of spectral data and the fact that also signals of a standard [NiFe] center have been found. Here the SH has been investigated in whole cells in its truly native environment, in contrast to earlier work performed on purified SH (**chapter 8**).

For the first time a bidirectional [NiFe]-hydrogenase from a cyanobacterium (*Synechocystis* sp. PCC 6803) has been characterized in a combined EPR and FTIR study (**chapter 9**). This hydrogenase is structurally similar to the SH from *Re* H16 and is according to its activation behaviour located between standard [NiFe]-hydrogenases and the SH.

A summary of the results is presented in **chapter 10**.

2 Materials and methods

2.1 EPR spectroscopy

In this chapter a few aspects of magnetic resonance will be given. The magnetic properties of an electron are described, followed by the quantum mechanical formalism for spins. After this, the experimental techniques are summarized. A more detailed treatment can be found in the literature. [27–30]

2.1.1 Magnetic moment of electron

The electron has a spin, i.e. an angular momentum with S=1/2. The spin is connected with a magnetic dipole moment

$$\hat{\mu}_e = -g_e \mu_B \hat{\mathbf{S}} \tag{2.1}$$

where g_e is the dimensionless electronic g-factor, μ_B the Bohr magneton and $\hat{\mathbf{S}}$ the spin operator. The negative sign indicates that in the case of the electron, spin and magnetic moment have opposite directions. The g-factor describes the ratio between spin and magnetic moment and has a value of g_e = 2.0023193 for a free electron. The interaction energy of a magnetic moment μ from a S=1/2 species and an external magnetic field **B** is

$$E_{1/2} = -\hat{\mu}\mathbf{B} \tag{2.2}$$

From quantum mechanics it is known that the spin can have two possible orientations with respect to **B**, which are described by the magnetic quantum number m_s, that can take only values of +1/2 (directed along **B**) and -1/2 (directed opposite to **B**) for an electron with S=1/2. [31] The magnetic quantum number is the projection of the spin onto the z-axis, which is defined by the magnetic field **B**. The energies of both states are no longer equivalent because the spins exhibit depending on their orientation, a different potential energy. By combining expressions 2.1 and 2.2, the magnetic interaction energy can be rewritten as

$$E_{1/2} = g_e \mu_B B m_s \tag{2.3}$$

Transitions between both states can be induced when the resonance condition and the selection rule $\Delta m_s = \pm 1$ are fulfilled (Figure 2.1). The energy needed in EPR experiments is in the range of microwaves and higher as compared to NMR experiments because the nuclear magneton μ_N is three orders of magnitude smaller as compared to μ_B.

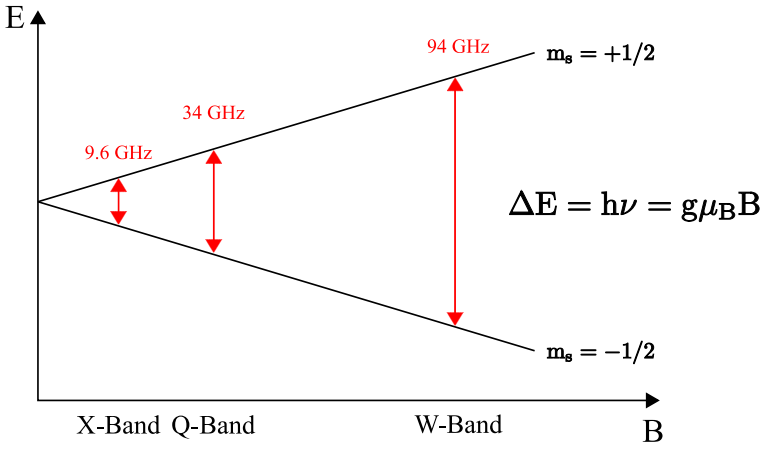

Figure 2.1: Schematic view of electron-Zeeman interaction for a S=1/2 system.

$$\Delta E_{1/2} = g_e \mu_B B \Delta m_s = h\nu \tag{2.4}$$

Due to technical reasons the microwave frequency in EPR experiments is kept constant whereas the magnetic field is swept. Typical microwave working frequencies are 9.6 GHz (X-Band), 34 GHz (Q-Band) and 94 GHz (W-Band). These frequencies are chosen because they are in ranges where no disturbing atmospheric absorptions occur.

In thermodynamical equilibrium the population difference between both spin states is described by a Boltzmann distribution.

$$\frac{N_\uparrow}{N_\downarrow} = e^{-\frac{\Delta E}{k_b T}} \tag{2.5}$$

To obtain a higher population difference either the temperature can be decreased or the energy difference increased (working at higher frequencies).

2.1.2 Spin Hamiltonian

The spin Hamiltonian describes the physical properties of a quantum mechanical system and contains the relevant interactions of the spins with the magnetic field as well as the interactions between them. The complete spin Hamiltonian for a S=1/2 system with k nuclear spins I_k was first introduced by Abragam and Pryce. [32]

$$\hat{\mathscr{H}}_{AP} = \mu_B \mathbf{B} \mathbf{g} \hat{\mathbf{S}} + \mu_N \sum_k \mathbf{B} \mathbf{g}_\mathbf{N} \hat{\mathbf{I}}_\mathbf{k} + \sum_k \hat{\mathbf{S}} \mathbf{A}_\mathbf{k} \hat{\mathbf{I}} + \sum_{I_k \geq 1} \hat{\mathbf{I}}_\mathbf{k} \mathbf{P}_\mathbf{k} \hat{\mathbf{I}}_\mathbf{k} \tag{2.6}$$

The first term describes the electron-Zeeman interaction, the second the nuclear-Zeeman interaction, the third the hyperfine interaction and the last one the nuclear quadrupole interaction. Each interaction is described in more detail in the next sections.

2.1.2.1 Electron-Zeeman interaction

By applying an external magnetic field **B** the interaction between the magnetic moment of the electron and the magnetic field can be described by the electron-Zeeman term

$$\hat{\mathscr{H}}_{eZ} = g_e \mu_B \mathbf{B}\hat{\mathbf{S}} \tag{2.7}$$

where $\hat{\mathbf{S}}$ is the operator of the electron spin. This interaction is the dominant part of the Hamiltonian (high-field approximation). The g-value is sensitive to the chemical environment of the spin and hence a fingerprint. In transition metal complexes, the g-factor usually deviates from g_e of the free electron due to spin-orbit coupling (SOC), i.e. an admixture of orbital angular momentum with L$\neq$0 to the spin. Due to SOC the g-factor becomes orientation-dependent and is treated as an interaction matrix, the so called g-matrix **g**. However, one can always find a principal axis system, in which **g** is diagonal, i.e. a relation between the orientation of the g-matrix and the molecular axis system. The SOC between $\hat{\mathbf{L}}$ and $\hat{\mathbf{S}}$ is described via the following Hamiltonian.

$$\hat{\mathscr{H}}_{SOC} = \lambda \hat{\mathbf{L}}\hat{\mathbf{S}} \tag{2.8}$$

λ is the spin-orbit coupling constant which increases with the atomic mass. The effect of spin-orbit coupling is notably larger when two orbitals have a similar energy difference comparable to the electron-Zeeman energy. For light elements from the first periods the SOC effect is small but for transition metals it can be large and lead to strong deviations from g_e and large anisotropy. With Equation 2.8 the orientation dependence of the Zeeman interaction can be rewritten in the Hamiltonian as

$$\hat{\mathscr{H}}_{eZ} = \mu_B \mathbf{B}(\hat{\mathbf{L}} + g_e\hat{\mathbf{S}}) + \lambda \hat{\mathbf{L}}\hat{\mathbf{S}} \tag{2.9}$$

With second order perturbation theory an expression for the elements of the g-matrix **g** can be obtained as follows

$$\mathbf{g} = g_e \mathbb{1} + 2\lambda \mathbf{\Lambda} \tag{2.10}$$

where $\mathbb{1}$ is the unity matrix and $\mathbf{\Lambda}$ is a symmetric tensor, which can take values of

$$\Lambda_{ij} = \sum_{n\neq 0} \frac{\langle \psi_0 | \hat{L}_i | \psi_n \rangle \langle \psi_n | \hat{L}_j | \psi_0 \rangle}{E_0 - E_n} \tag{2.11}$$

ψ_0 is the wave function of the electronic ground state with energy E_0 and ψ_n is the wave function of the n-th excited state with energy E_n. $\hat{L}_i$ is the i-th component of the angular momentum operator $\hat{\mathbf{L}}$. From this expression it can be deduced, that SOC with an unoccupied molecular orbital (MO) results in a negative shift of the g-factor compared to g_e ($E_0 - E_n < 0$), whereas SOC with an

occupied MO leads to a positive shift ($E_0 - E_n > 0$). By replacing the g-factor with the g-matrix in Equation 2.7, the orientation dependence of the Zeeman interaction can be included in the Hamiltonian.

$$\hat{\mathscr{H}}_{eZ} = \mu_B \mathbf{B} \mathbf{g} \hat{\mathbf{S}} \tag{2.12}$$

2.1.2.2 Nuclear-Zeeman interaction

Similar to electron-Zeeman interaction a nuclear-Zeeman interaction exists for nuclei with I≠0

$$\hat{\mathscr{H}}_{NZ} = -\mu_N \mathbf{B} \mathbf{g_N} \hat{\mathbf{I}} \tag{2.13}$$

with the nuclear spin operator $\hat{\mathbf{I}}$. This interaction is much smaller as compared to the electron-Zeeman interaction due to the smaller nuclear magneton μ_N (factor 1000). Thus, the anisotropy is small and can be neglected by replacing the $\mathbf{g_N}$ by a scalar g_N value. Nevertheless, the magnitude of this interaction is in the range of the hyperfine-interaction and must therefore be considered.

2.1.2.3 Nuclear hyperfine interaction

In paramagnetic species usually nuclei with nuclear spins I≠0 can be found, leading to hyperfine interaction. The nuclear hyperfine interaction arises from an interaction between the magnetic moment of a nucleus and the magnetic moment of the electron. This dipolar interaction is composed of two parts, the isotropic interaction (Fermi-contact part) and the anisotropic interaction. The full hf-tensor is then written as the sum of isotropic and anisotropic part.

$$\hat{\mathscr{H}}_{hfi} = \hat{\mathscr{H}}_{hfi,iso} + \hat{\mathscr{H}}_{hfi,dd} = \hat{\mathbf{S}} \mathbf{A} \hat{\mathbf{I}} \tag{2.14}$$

The isotropic hf-interaction is proportional to the probability density $|\psi(0)|^2$ of the unpaired electron at the nucleus.

$$\hat{\mathscr{H}}_{hfi,iso} = a_{iso} \hat{\mathbf{S}} \hat{\mathbf{I}} \tag{2.15}$$

$$a_{iso} = \frac{8\pi}{3} g_e \mu_B g_N \mu_N |\psi(0)|^2 \tag{2.16}$$

The electronic wavefunction $\psi(0)$ is only different from zero for an unpaired electron in a s-orbital. In transition metal complexes the unpaired electrons are usually located in the d-orbitals and in organic radicals in p-orbitals. For these systems isotropic interaction can be observed as well, which is based on the effect of spin polarization. The unpaired electron perturbs the paired electrons in the s-orbital leading to a certain amount of spin density in the s-orbitals.

The anisotropic part of the hf-interaction causes an orientation-dependent term in the Spin Hamiltonian.

$$\hat{\mathscr{H}}_{hfi,dd} = \frac{g_e \mu_B g_N \mu_N}{h} \left(\frac{3(\hat{\mathbf{S}}\mathbf{r})(\hat{\mathbf{I}}\mathbf{r})}{r^5} - \frac{\hat{\mathbf{S}}\hat{\mathbf{I}}}{r^3} \right) = \hat{\mathbf{S}}\mathbf{T}\hat{\mathbf{I}} \tag{2.17}$$

In the case of localized spins one can use the point-dipole approximation. Then the anisotropic part of the hf-interaction (in MHz) can be rewritten as

$$A(\theta) = A_0 \rho (3cos^2\theta - 1) \tag{2.18}$$

$$A_0 = \frac{g_e \mu_B g_N \mu_N}{h} \cdot \frac{1}{r^3} \tag{2.19}$$

θ is the angle between the magnetic field direction and the connection axis of electron and nuclear magnetic moments. When the spins are localized, it is not necessary to integrate over the spin density ρ. The dipolar hf-tensor is traceless with its principal values $2A_0$ ($\theta = 0°$) and $-A_0$ ($\theta = 90°$) and can be written as ($T_\perp$, $T_\perp$, $T_\parallel$). This relation is often used to estimate distances between the unpaired electron and nearby nuclei. However, it works only well for light elements (second row) and distances larger than 2.5 Å because in this case the spin density is assumed to be concentrated at the nucleus and the distance between the spins is larger than their spatial dimensions. [29]

2.1.2.4 Nuclear quadrupole interaction

Nuclei with a nuclear spin I≥1 carry a quadrupole moment. The interaction of the nuclear quadrupole moment with the electric field gradient, produced by the surrounding electrons, leads to an additional nuclear quadrupole interaction.

$$\hat{\mathscr{H}}_{NQ} = \hat{\mathbf{I}}\mathbf{P}\hat{\mathbf{I}} \tag{2.20}$$

The quadrupole tensor **P** is always traceless. The diagonal form of the tensor can be written with two parameters, which characterize the diagonal elements as follows (plus three angles that define the orientation)

$$\mathbf{P} = P \begin{pmatrix} (\eta - 1) & 0 & 0 \\ 0 & (-\eta - 1) & 0 \\ 0 & 0 & 2 \end{pmatrix} \tag{2.21}$$

η describes the symmetry of the tensor and has a value $0 \leq \eta \leq 1$ (η is zero for full axiality). The quantity P contains the z-component eq of the electric field-gradient and the scalar quadrupole moment Q.

$$P = \frac{e^2 q Q}{4I(2I-1)} \quad \text{and} \quad \eta = \frac{P_{xx} - P_{yy}}{P_{zz}} \tag{2.22}$$

The quadrupole interaction delivers information about the chemical environment of a nucleus such as protonation state, bonding situation and ligands. [33,34]

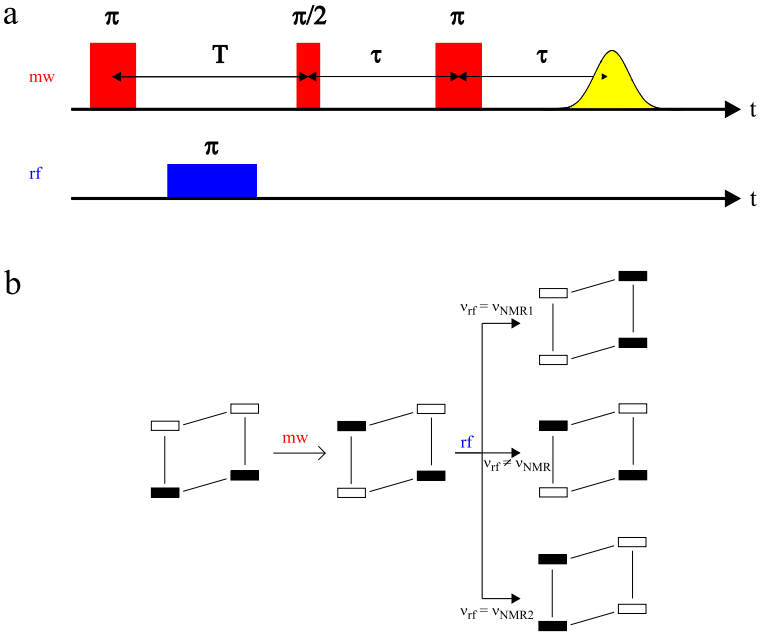

Figure 2.2: (a) Davies ENDOR pulse sequence with mw-pulses (red) and rf-pulse (blue). (b) Population changes of the energy levels of an S=1/2 I=1/2 spin system during the ENDOR experiment. The first π-pulse inverts the population of the EPR transition. The subsequent soft rf π-pulse can be either resonant (with one of the two NMR transitions) or non-resonant. In case of resonance the population difference vanishes and no spin echo is detected.

2.2 Pulsed EPR spectroscopy

The EPR spectra of transition metal complexes are usually broad because the unpaired electrons are located in the d-orbitals. Then the SOC contributions can be large, which leads to large *g*-anisotropy. However, important contributions such as hf-couplings are then often not clearly resolved in EPR spectra. Pulsed EPR is of advantage to detect such broad spectra and by applying techniques like ENDOR or ESEEM information about hf- and quadrupole-couplings can be obtained. With these advanced methods detailed information about the geometric structure of the paramagnetic centers can be derived.

2.2.1 ENDOR

Electron nuclear double resonance is a combined EPR and NMR experiment, which is of advantage to detect the hyperfine-couplings of nuclei that are coupled to the electron spin. In this work mainly Davies-ENDOR was applied.[35]

Figure 2.2 shows the Davies-ENDOR pulse sequence. The experiment starts with a selective π-pulse to invert the population of one EPR transition. Usually electronic T_1 relaxation times at low temperatures are in the range of a few hundred microseconds. For metal centers, as found in [NiFe]-hydrogenases, T_1 times are shorter (up to 100 microseconds). However, it is still possible to apply a selective rf π-pulse. When this pulse is in resonance with one of the NMR transitions, the polarization of the nuclear spins in one of the m_S-manifolds is inverted, which causes a decrease of the population difference. After this π-pulse the spin echo is detected with a $\pi/2-\tau-\pi$ Hahn-echo sequence. As a consequence the intensity of the spin echo is decreased or it vanishes completely in the ideal case.

ENDOR experiments have been successfully used to investigate the hf-couplings of the paramagnetic states of [NiFe]-hydrogenases such as Ni_r-B and Ni_a-C.[36–41]

2.2.2 ESEEM

Electron spin echo envelope modulation is a technique complementary to ENDOR.[42] It allows the observation especially of ^{14}N and ^{2}H nuclei at X-Band due to their small magnetogyric ratios.

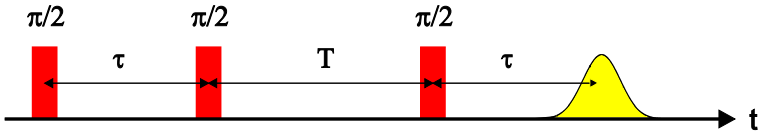

Figure 2.3: 3-pulse ESEEM sequence where T is incremented and the echo is detected at time τ after the last $\pi/2$-pulse.

Prerequisites for ESEEM are the simultaneously excitation of allowed and forbidden transitions and an anisotropic hf-interaction. Then the beating frequency between these transitions is detected in the experiment.

The pulse sequence for 3-pulse ESEEM is shown in Figure 2.3 and is based on the detection of a stimulated echo. The time T between the second and third $\pi/2$-pulse is incremented during echo detection. An echo with modulated intensity is then recorded. T can be in the range of T_1, which is important because the observed nuclear processes are slow. Unfortunately, the stimulated echo detection suffers from 'blind spots' due to the choice of τ. The modulation function, that describes the modulated echo, is zero when $cos(\omega_i\tau)$ becomes one.[42] ω_i is the frequency of one NMR transition. For this reason, τ is usually incremented in the second dimension and a 3-pulse vs. 2-pulse ESEEM is recorded. By plotting a skyline-projection (or sum projection) of this data set, a 'blind spot' free spectrum can be obtained.

For ^{14}N nuclei that are not directly coordinated to the spin center the case of 'exact cancellation' can be often observed (see Figure 2.4). [33,43]

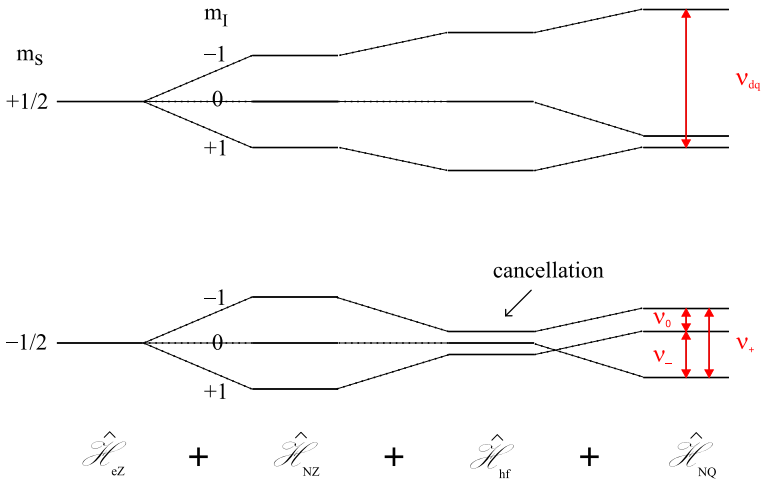

Figure 2.4: Energy level diagram for a ^{14}N nucleus with I=1 coupled to a S=1/2 electron spin in the case of almost exact cancellation ($2\nu_N \approx A$).

When the nuclear-Zeeman interaction matches about half the effective hf-interaction, these two interactions cancel each other in one spin-manifold. As a consequence the remaining interactions in this manifold are then dominated only by the electric quadrupole interaction of nuclei with I=1, and yield information about the charge distribution around this nucleus. [33,34,44] Three sharp lines can be observed and from the magnitude of these frequencies, the nuclear quadrupole constant e^2qQ and the asymmetry parameter η can be estimated according to. [42,45]

$$\nu_0 = 2K\eta,\ \nu_- = K(3-\eta),\ \nu_+ = K(3+\eta) \tag{2.23}$$

$$\text{with } K = \frac{e^2qQ}{4} \tag{2.24}$$

With knowledge of the quadrupole tensor one can obtain information about the chemical environment, which means information about the type of the involved amino acid. [33,34,44]

2.2.3 Orientation selection

In frozen solution spectra all orientations of a paramagnetic molecule are statistically distributed with respect to the external field and a powder spectrum is recorded. In spectra with a resolved g-

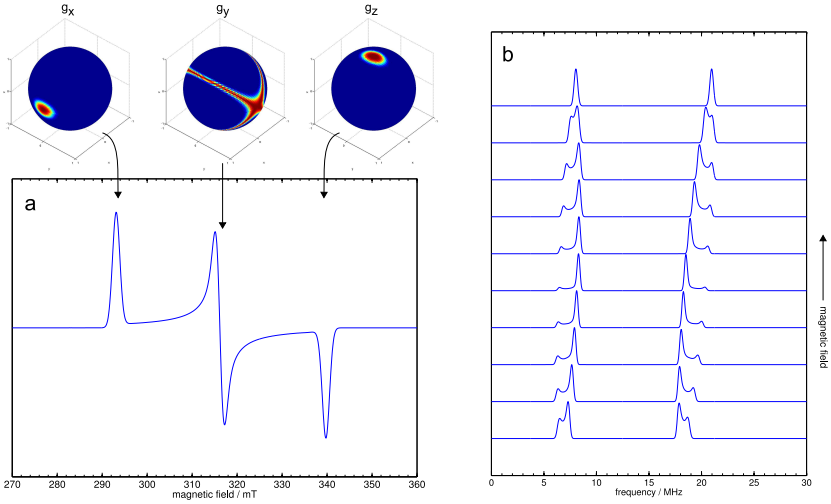

Figure 2.5: (a) Illustration of orientation selection in an EPR experiment with rhombic g-tensor. At the edges near g_x and g_z only few orientations contribute to the spectrum, which is shown at the top. (b) ENDOR simulation of a β-CH_2-proton, which can be found in [NiFe]-hydrogenases.

tensor anisotropy it is possible to select molecules with certain orientations by measuring at selected field positions. This is important for ENDOR and ESEEM experiments.

At the edges of the EPR spectrum in Figure 2.5 only molecules with their g_x or g_z axis parallel to the magnetic field contribute to the spectrum. At g_y position several molecular orientations with the same effective *g*-value contribute to the spectrum. By measuring at different magnetic field positions, the relative orientations between *g*- and each hf-tensor can be obtained by simulations, and hence information about the geometry of the system under investigation. [37,46]

2.3 FTIR spectroscopy

Since in [NiFe]-hydrogenases diatomic CO and CN^--ligands are coordinated to the Fe atom in their active sites, FTIR spectroscopy has been proven to be a valuable tool to investigate these proteins. [24,47–49] The absorption bands of the stretching vibrations of the ligands appear in a spectral window, where no other protein bands, such as amide I and amide II interfere.

The frequencies of the stretching modes reflect the electron density, delocalized within the active site. Changes are caused mainly due to alterations of the oxidation state of the Ni center, changes in the ligation or protein-cofactor interactions. [47] Thus, it is possible to identify the various redox states and follow their changes during the catalytic process.

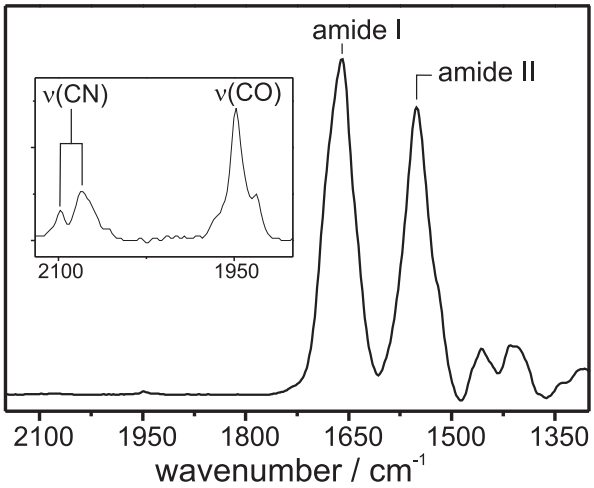

Figure 2.6: Typical SEIRA spectrum of a [NiFe]-hydrogenase with pronounced protein bands amide I and amide II.[50] The stretching modes of the inorganic ligands appear in a spectral window between 1900-2100 cm^{-1}.

A more advanced method is surface enhanced infrared absorption spectroscopy (SEIRA), where the protein is immobilized onto a biocompatibly coated gold surface. SEIRA has a much higher sensitivity as compared to conventional FTIR spectroscopy due to the coupling of the radiation field with the surface plasmons of the nanostructured metal, leading to an enhancement of ca. two orders of magnitude (Figure 2.6).[50] In addition, the experiment can be combined with electrochemistry and measurements can be carried out under potential control.

3 Experimental details

3.1 Purification of the *R. eutropha* hydrogenases

The MBH and SH were cultivated and purified in the laboratory of Prof. Friedrich at the Humboldt-Universität zu Berlin. The MBH was studied in membrane fragments, that contained overexpressed hydrogenase. For the purification of MBH a *Strep*-tag II was attached to the C-terminus of the small subunit HoxK by genetic engineering. With affinity chromatography a purity of $\sim$99% could be achieved according to analysis with SDS-Page and protein staining.[26,48]

The SH was studied in whole cells grown under hydrogenase-derepressing conditions.

3.2 Sample preparation

For X-Band EPR measurements the samples were filled in CFQ EPR tubes with 4 mm outer diameter (O.D.) (707-SQ-250, RototecSpintec, Biebesheim, Germany). A maximum sample volume of 100 μl was used. For Q-Band EPR measurements the samples were filled in CFQ EPR tubes with 3 mm O.D. (705-PQ-6.25, RototecSpintec, Biebesheim, Germany). A maximum sample volume of 35 μl was used.

The protein concentration for biological samples ranged from 50 μM to 1 mM. For experiments under anaerobic conditions, the samples were repeatedly degassed and gassed using a vacuum line and argon or hydrogen as exchange gases. Subsequently, they were transferred into an anaerobic glove box. Reduction by H_2 was carried out in an anaerobic tent (Coy Lab systems) with forming gas atmosphere (95% N_2, 5% H_2), in which the samples were flushed with 1 bar hydrogen in the EPR tube. Anaerobic sample treatment without hydrogen was performed in a glove box under 100% N_2 atmosphere (VAC).

3.3 Continuous-wave EPR experiments

All X-Band cw-EPR experiments have been performed on a Bruker ESP300E spectrometer. The spectrometer was equipped with a rectangular microwave cavity working in the TE_{102} mode. For low-temperature experiments the samples were placed in an Oxford ESR900 helium flow cryostat and the temperature was controlled with an Oxford ITC502 temperature controller. The exact microwave frequency was monitored with an EIP frequency counter (Microwave Inc., Milpitas, CA, USA). The magnetic field was calibrated using an external LiLiF standard for which the g-value is known with high accuracy of 2.002293 ± 0.000002.[51] Absolute spin-quantifications have been done by comparing the absolute integrated signal intensity with a $CuSO_4$ standard of known concentration and volume.

3.4 Pulsed EPR experiments

Pulsed EPR experiments at X-Band were carried out with a Bruker E580 ELEXSYS spectrometer equipped with a dielectric ring resonator (EN4118X-MD4) and a SuperX-FT microwave bridge. The microwave pulses were amplified using either a TWT (Applied Systems Engineering, Inc, Fort Worth, TX, USA) or the Bruker AmpX10 solid-state amplifier. Pulsed Q-Band measurements were performed on the same spectrometer using a home-built cylindrical Q-Band ENDOR resonator with a SuperQ-FT microwave bridge. Shortest π-pulses achieved with this setup were 40 ns and 20 μs for microwave and radiofrequency pulses, respectively. For ENDOR experiments the RF pulses were generated with a Bruker E560 ENDOR accessory and amplified with a RF amplifier (250 W, Amplifier Research, Model 250A250A).

3.5 Spectral simulations

The experimental EPR and ENDOR spectra were simulated using *EasySpin* (version 3.1.0),[52] which is a toolbox for MATLAB.[53] *EasySpin* is based on a full matrix-diagonalization of the spin Hamiltonian.

3.6 FTIR spectroscopy

FTIR spectra were recorded on a Bruker Tensor 27 spectrometer equipped with a liquid nitrogen-cooled MCT detector using a spectral resolution of 2 cm^{-1}. The sample compartment was purged with dried air, and the sample (0.2-0.5 mM isolated protein, $\sim$0.05 mM protein attached to the cytoplasmic membrane) was held in a temperature-controlled (10 °C) gas-tight IR-cell for liquid samples (volume $\sim$7 μl, path length = 50 μm) with CaF_2 windows. Spectra were baseline corrected by using a spline function implemented within OPUS 4.2 software of the spectrometer. Reduced protein samples were prepared through incubation with 1 bar H_2 or 0.05 bar H_2 in 1 bar gas mixture (95% nitrogen, 5% hydrogen) for 20-30 min at room temperature.

4 Hydrogenases

4.1 Structure of [NiFe]-hydrogenases

Hydrogenase structures for all three types, i.e. [NiFe]-, [FeFe]- and [Fe]-hydrogenase are available. The first crystal structure of a [NiFe]-hydrogenase has been solved for the sulfate-reducing bacterium *Desulfovibrio gigas* in 1995 with 2.85 Å resolution in its oxidized unready form (see Fig. 4.1).[11] This hydrogenase consists of a large subunit (60 kDa) that harbours the [NiFe] active site and a small subunit (30 kDa) which accomodates three iron-sulfur clusters (two [4Fe4S]- and one [3Fe4S]-cluster).

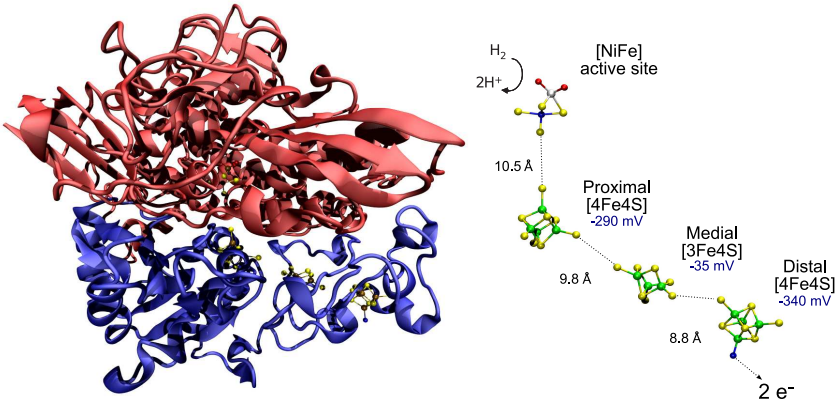

Figure 4.1: Crystal structure of the [NiFe]-hydrogenase from *D. gigas* (pdb 2FRV). The large subunit (red) with the [NiFe] center and the small subunit with the iron-sulfur clusters (blue) are shown. On the right side a schematic view of the cofactors with corresponding midpoint potentials and distances is displayed.

The amino acids around the active center are highly conserved in all [NiFe]-hydrogenases.[7] The Ni atom is coordinated by the sulfur atoms of four cysteine thiolate ligands. Two of them are located in a bridging position between the Ni and the Fe (Cys68 and Cys533) and the other two cysteines are terminal ligands of the Ni (Cys65 and Cys530). The Fe remains all the time in a low-spin Fe^{2+}

configuration (with S=0) due to the coordination by three diatomic ligands, one CO and two CN^-.[54] Depending on the respective redox state, an additional bridging ligand can be found between the Ni and the Fe.[39,55] In the oxidized form, usually a mixture of Ni_u-A and Ni_r-B states is detected with an oxo-species as additional bridging ligand. Upon activation[1] with hydrogen this additional oxygen-ligand is removed, which can be derived from the x-ray structure of the active state of *Dv* Miyazaki F hydrogenase.[56] HYSCORE experiments on D_2-treated hydrogenase from *Re* H16 and *Dv* Miyazaki F revealed, that the active state Ni_a-C contains a hydride in the bridging position.[39,40]

In all redox states (section 4.2) the Ni has a free coordination site. A gas channel ends at this position and therefore it is believed that the primary binding site for hydrogen is located at the Ni.[57,58] In addition, it has been shown that CO binds at this position and inhibits the protein.[59]

Standard hydrogenases usually contain one [3Fe4S]- and two [4Fe4S]-clusters. However, certain variations in the composition are found. The proximal [4Fe4S]-cluster is located in approximately 10 Å distance from the active site and coordinated by four cysteines. This cluster seems to be important for [NiFe]-hydrogenases because hydrogen oxidation is a two-electron process (n=2). H_2 reacts with Ni_a-C to form the Ni_a-SR states when the proximal FeS-cluster is oxidized.[60] Thus, it is important to mention that the [NiFe] site in the standard hydrogenase behaves as an one-electron redox entity (n=1). Hence, in the two-electron reaction with H_2, the redox states of the FeS-clusters must also be taken into consideration. The distal [4Fe4S]-cluster is modified insofar as one terminal cysteine is replaced by a histidin in all [NiFe]-hydrogenases that contain three FeS-clusters. This histidine is surrounded by acidic residues, which most likely interact with the natural redox partner, e.g. a cytochrome.[13]

The medial cluster is the [3Fe4S]-cluster. The distances between the different clusters are in a range of $\sim$12 Å , which suggests electron transfer can take place among them. The physiological function of the medial [3Fe4S]-cluster is yet unclear in view of its unusually high midpoint potential of -70 mV vs. SHE (in *D. gigas*,[61] see Figure 4.2). However, calculations have shown that the limiting factor for electron transfer is a distance smaller than 14 Å rather than the redox potential because the rate-limiting step is always the reaction of hydrogen at the active center.[62] This was proven by a mutation of the medial [3Fe4S]-cluster to a [4Fe4S]-cluster in the [NiFe]-hydrogenase from *D. fructosovorans*[63], where only a minor effect on the catalytic activity was observed.

4.2 Redox states observed in [NiFe]-hydrogenases

During catalysis the [NiFe] active site cycles through several redox states (see Figure 4.2). EPR spectroscopy was first used to observe the changes at the Ni atom. In all paramagnetic redox states the majority of the spin density is located on the Ni.[44,64–66] A signicant amount of spin density is present at one bridging sulfur as well.[37,41,66,67] In the oxidized form, at positive redox potentials, the hydrogenase remains in its catalytically inactive states Ni_u-A ('unready') and Ni_r-B ('ready'). Both states can be identified with EPR spectroscopy due to a S=1/2 ground state. The Ni is kept in an electronic ground state (low-spin $3d^7$) with a formal oxidation state of Ni^{3+}. The unpaired electron is located in the d_{z^2} orbital as derived from crystal-field theory, assuming a square-pyramidal ligand field (see Figure 4.3). The nature of the ligand-field was first elucidated from x-ray and EXAFS

[1] hydrogenases can be activated and reduced with H_2

data.[55,68] The Fe is kept in a low-spin Fe^{2+} state and carries virtually no spin density as shown by ^{57}Fe-ENDOR.[66,69] Thus, the Ni in the [NiFe]-center can be described as an uncoupled S=1/2 system.

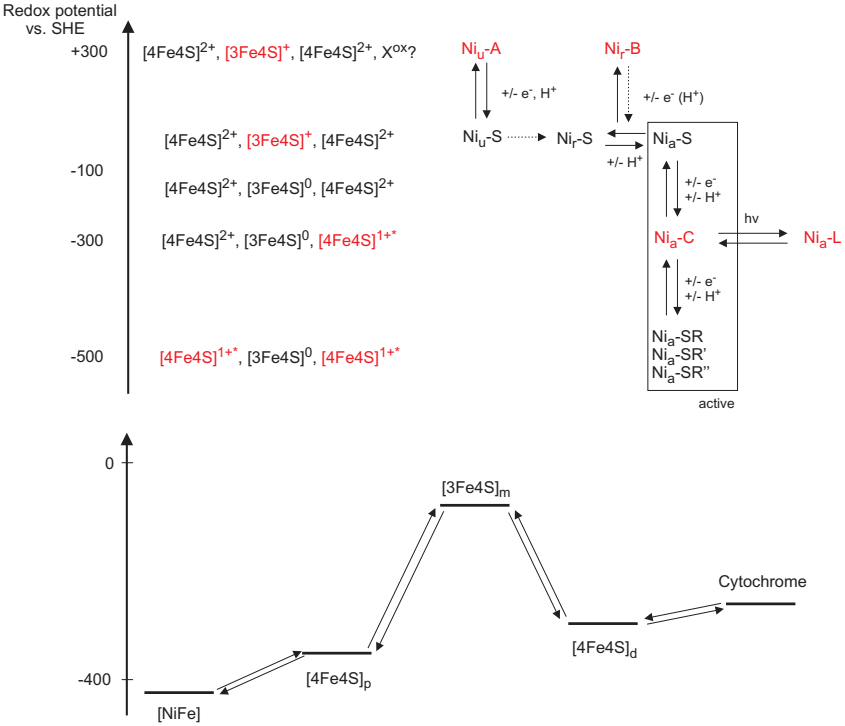

Figure 4.2: Redox states observed in standard [NiFe]-hydrogenases (adapted from[66,70]). All paramagnetic states of the [NiFe]-center and the different iron-sulfur clusters with a S=1/2 ground state are highlighted in red. The catalytically active redox states are Ni_a-S, Ni_a-C and the fully reduced Ni-SR states. The electron transfer pathway includes the [3Fe4S]-cluster with an unusual high redox potential.[61,62]

Ni_u-A shows signals at g-values of 2.32, 2.24 and 2.01 and Ni_r-B at 2.33, 2.16 and 2.01. In these states an additional oxygen-bridge between the Ni and the Fe is found. For the Ni_r-B state the oxo-species is most probably a hydroxide (OH^-) (Figure 4.3). This has been confirmed by single-crystal EPR and complementary DFT calculations[38] as well as with high resolution x-ray structures.[55,57] The nature of the bridging ligand in case of the Ni_u-A is not unambiguously clear. X-ray structures suggest the presence of a dioxo-species[55], whereas EPR spectroscopy favors a mono-oxo species.[66] The nature of this oxygen-species is quite important, because another major

difference between both states is the different activation behaviour with hydrogen. Ni_u-A requires a long time activation at elevated temperatures,[33,71] whereas the Ni_r-B state can be activated within seconds to minutes with hydrogen.[72] However, a few hydrogenases show no EPR detectable states in their oxidized form, e.g. the H_2-sensing hydrogenases from *R. eutropha* H16 and *Rhodobacter capsulatus*. Gas channel mutants proved, that the acessibility of their active sites for oxygen is inhibited and the Ni_u-A/Ni_r-B states cannot be formed.[73,74]

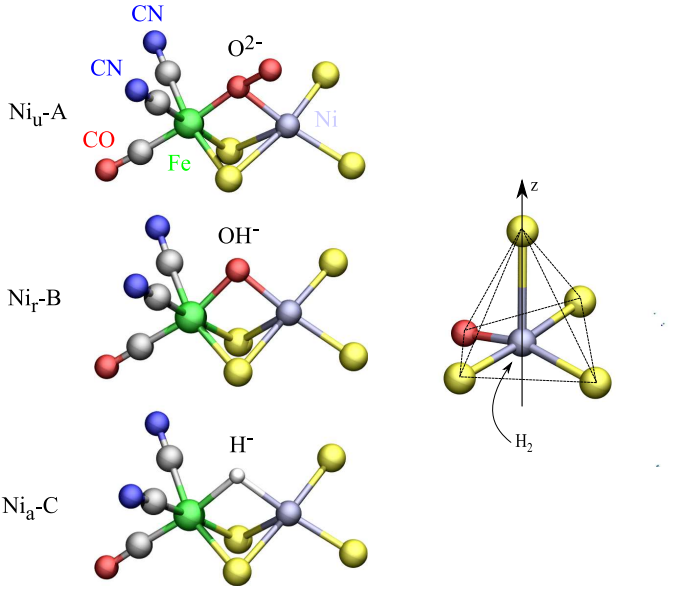

Figure 4.3: Structures of the [NiFe]-center in different paramagnetic redox states. The formal oxidation state is always Ni^{3+} but the additional bridging ligand is different. Ni_a-C carries a hydride and Ni_r-B a hydroxide. The nature of this ligand for the Ni_u-A state is still under discussion,[66] but it is thought to be an O^{2-} species.[55] The ligand-field at the Ni is square-pyramidal with an open coordination place for hydrogen.

Upon reductive activation with hydrogen, the bridging oxygen-ligand is released. The Ni is reduced to the so called Ni-S states[2] in a one-electron process and changes its oxidation state to Ni^{2+} (Figure 4.2). These states are EPR-silent and can be investigated using FTIR spectroscopy by monitoring the characteristic stretching modes of the diatomic ligands CO and CN^- of the Fe. It is still under discussion if the Ni^{2+} states are either in a high-spin or low-spin configuration.[75–77] Activation from the Ni_u-A state leads to the Ni_u-S state. Kinetic investigations have shown, that the rate-limiting step of activation is the conversion of Ni_u-S to the active states.[78] Upon activation

[2] S means EPR-silent

of Ni_r-B the [NiFe] center ends up in the Ni_r-S/Ni_a-S states, which are connected via a protonation/deprotonation process in a pH-dependent equilibrium.[47] The unprotonated form is Ni_r-S. Due to the changes in vibrational frequencies of the diatomic ligands it has been postulated that a terminal cysteine of the Ni is protonated leading to Ni_a-S.[47] Alternative models suggest a protonation of the OH^-.[79] No structures for the Ni-S states exist, only DFT calculations and activation studies with FTIR spectroscopy are available.

Ongoing reduction with hydrogen leads to another EPR detectable state with S=1/2 ground state, the so called Ni_a-C.[66] This state can be observed in all [NiFe]-hydrogenases by now (except the SH from *Re* H16) and is believed to be an intermediate during catalysis because its appearance is related to the catalytic activity of the protein.[80] It has a characteristic g-tensor with principal values of 2.20, 2.14 and 2.01. The x-ray structure of this state shows no additional bridging ligand. However, the presence of a hydride as bridging ligand has been found with HYSCORE experiments in the *Re* H16 RH and *Dv* Miyazaki F hydrogenases.[34,39,40,44] The electronic ground state is a d_{z^2} state with a formal Ni^{3+}. The Ni_a-C state was found to be light-sensitive and can be converted to the unphysiological Ni_a-L state.[81,82] The Ni_a-L state can be produced by illumination with white light at temperatures below 100 K. The highest conversion rate was determined between 550-700 nm with a maximum at 590 nm.[82] The reaction is a photodissociation where the bridging hydride is removed as a proton and leaves formally two electrons at the Ni (Ni^{1+}). A theoretical description of this state is rather difficult since crystal-field theory predicts the largest g-value along the z-axis. Thus, a mixture of d_{z^2} and $d_{x^2-y^2}$ ground state describes it adequately (subsection 4.2.1).[66] Additionally, the linewidth of Ni_a-L is smaller as compared to Ni_a-C, since the bridging hydride with a large hyperfine coupling is removed. Ni_a-L can be found in several substates (Ni_a-L1, Ni_a-L2, ...) with slightly different g_x-values, that describe slight changes in the geometry of the thiol bridges of the [NiFe] center.[34,66,82] The appearance of these substates depends on the illumination duration as well as on the respective temperature.[82,83] Annealing of the sample above 200 K in the dark leads to a complete reversion to Ni_a-C.[83]

In a further one-electron process the [NiFe] center is transformed to the fully reduced states, which are called Ni_a-SR, Ni_a-SR' and Ni_a-SR". Their relative populations are dependent on the pH and not all of them were observed in each standard [NiFe]-hydrogenase.

4.2.1 Electronic structure of the [NiFe] center in its paramagnetic redox states

With the knowledge of the crystal-field for a given complex it is possible to deduce the *g*-values by perturbaton-theoretical treatment.[84] From various crystal structures of [NiFe]-hydrogenases[11,55,56] it is known that the Ni atom is coordinated by five ligands in its oxidized states, four thiol groups from cysteines and one bridging oxygen-ligand (see Figure 4.3). The connection between the Ni and the bridging sulfur defines the z-axis. From this coordination a square-pyramidal ligand-field arises with a free coordination site for hydrogen at the Ni atom.

This ligand-field leads to a d-orbital splitting as shown in Figure 4.4. In the case of a d^7 system the unpaired electron is located in the d_{z^2} orbital. From single-crystal EPR measurements the *g*-tensor

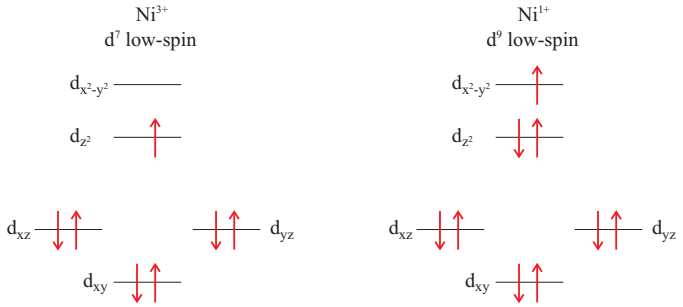

Figure 4.4: d-orbital splitting in a square-pyramidal crystal-field for a d^7 and d^9 system.[85]

axis orientation is known for the paramagnetic redox states Ni_u-A,[86] Ni_r-B,[86,87] Ni_a-C[88] and Ni_a-L.[88] For a formal Ni^{3+} state the three principal values of the g-tensor are defined in Equation 4.1 to Equation 4.3.

$$g_x = g_e - \rho \frac{6\lambda}{E_{d_{z^2}} - E_{d_{yz}}} \tag{4.1}$$

$$g_y = g_e - \rho \frac{6\lambda}{E_{d_{z^2}} - E_{d_{xz}}} \tag{4.2}$$

$$g_z = g_e \tag{4.3}$$

ρ is the spin density at the Ni, g_e the g-value of a free electron and λ the spin-orbit coupling parameter. For all paramagnetic states the g_z axis (smallest g-value) is colinear with the connection axis between the Ni and the bridging sulfur, which is in agreement with the calculated g-value in Equation 4.3 ($g_z \approx g_e$). For a formal Ni^{1+} oxidation state the unpaired electron is located in the $d_{x^2-y^2}$ orbital. The corresponding equations to estimate the g-values are given by

$$g_x = g_e - \rho \frac{2\lambda}{E_{d_{x^2-y^2}} - E_{d_{yz}}} \tag{4.4}$$

$$g_y = g_e - \rho \frac{2\lambda}{E_{d_{x^2-y^2}} - E_{d_{xz}}} \tag{4.5}$$

$$g_z = g_e - \rho \frac{6\lambda}{E_{d_{x^2-y^2}} - E_{d_{xy}}} \tag{4.6}$$

From crystal-field theory it can be concluded that the largest g-value would be expected for the g_z-component in the case of degenerated t_{2g} orbitals with $E_{d_{xy}} = E_{d_{xz}} = E_{d_{yz}}$. Unfortunately, this is in strong contrast to experimental results[88] where the g_z-value is the smallest. A solution is to

assume, that the electronic ground state as a mixture between d_{z^2} and $d_{x^2-y^2}$ ground state for the case of Ni^{1+}.[66]

4.3 The O_2-tolerant [NiFe]-hydrogenases from *Ralstonia eutropha* H16

In contrast to standard [NiFe]-hydrogenases from strictly anaerobic organisms, the hydrogenases from the β-proteobacterium *R. eutropha* H16 are able to oxidize hydrogen at ambient oxygen levels.[90] This is of interest for biotechnological applications, such as fuel cells and biosensors.[5] *R. eutropha* harbors three distinct [NiFe]-hydrogenases and their oxygen-tolerance is suggested to be based on different mechanisms.[25,91]

The best studied hydrogenase is the regulatory hydrogenase, which is located in the cytoplasm. The RH acts as a hydrogen sensor that monitors the H_2-level.[92] This sensor is catalytically inactive but regulates, via a kinase, gene-expression of the two other energy-generating hydrogenases MBH and SH. Hydrogen sensors have been found in *B. japonicum* and *R. capsulatus*, too.[74,93] Gas channel mutants revealed at least for the *Re* and *R. capsulatus* RH, that most probably a narrow gas channel prevents O_2 from accessing the [NiFe] center.

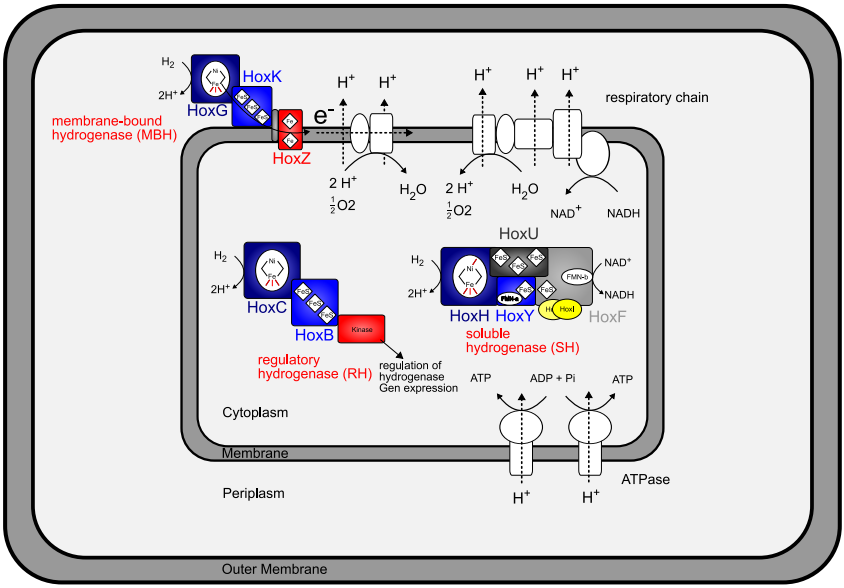

Figure 4.5: Schematic sketch, displaying the structures and physiological functions of the three [NiFe]-hydrogenases from *R. eutropha* H16.[89]

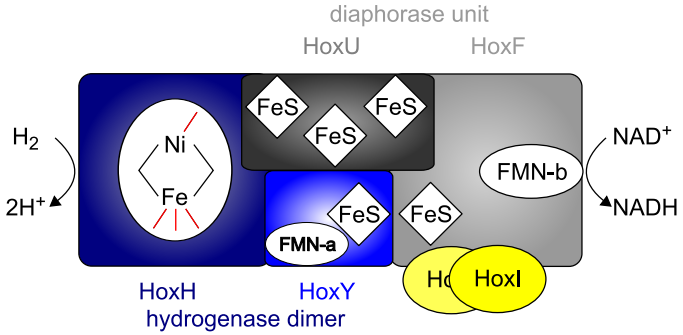

Figure 4.6: Cartoon of the SH in the heterohexameric form. The hydrogenase dimer is connected to the diaphorase unit. Two identical accessory proteins HoxI provide a $NADP^+$ binding site.

The soluble hydrogenase from *R. eutropha* H16 is also located in the cytoplasm and uses hydrogen to reduce NAD^+ to NADH. The NADH is used mainly for CO_2 fixation.[94]

The SH has a heterotetrameric structure and is composed of a hydrogenase heterodimer with a [NiFe] center and a diaphorase heterodimer where NAD^+ is converted.[91] The large subunit of the hydrogenase dimer, HoxH, contains four conserved cysteine residues, which provide binding sites for the [NiFe] center. The subunit HoxY (smaller version of HoxK from MBH) harbors presumably only one [4Fe4S]-cluster. The presence of a flavin (FMN-a) in HoxY was discovered recently because this cofactor could be released after prolonged reduction with NADH and detected based on its fluorescence.[95] After FMN-a is released, the NAD^+-reducing activity dramatically decreases, whereas benzylviologen activity at the Ni site is not influenced, suggesting a conformational change.[95] Due to its proposed proximity to the [NiFe] center, FMN-a is proposed to participate in hydride transfer.[96] The iron-sulfur cluster composition of the diaphorase heterodimer is similar to Complex I and at least two [4Fe4S] and one [2Fe2S] center are expected. Additionally, one flavin (FMN-b) is located in the HoxF subunit of the diaphorase unit.[95] The electrons derived from hydrogen-cleavage at the [NiFe] site are transferred via iron-sulfur clusters to FMN-b, where the NAD^+ binding site is located.[95] The SH can be purified in a heterohexameric form as well. Two additional identical subunits (HoxI) are docked to HoxF and the protein resides in its native conformation. This heterohexameric form ($HoxFUYHI_2$) can be activated with small amounts of NADPH, in contrast to the heterotetrameric form, indicating that HoxI provides a binding site for NADPH.[96]

The [NiFe] active site shows unusual FTIR spectra suggesting four CN^- and one CO ligand. It has thus been proposed that the ligation is different from that of standard hydrogenases. Four cyanide ligands were postulated, one of them directly coordinated to the Ni atom.[91,97–99] It was supposed, that the additional CN^--ligand shields the active site from oxygen and avoids Ni_u-A formation.[97,98,100] However, in some preparations significant amounts of a standard-like [NiFe]

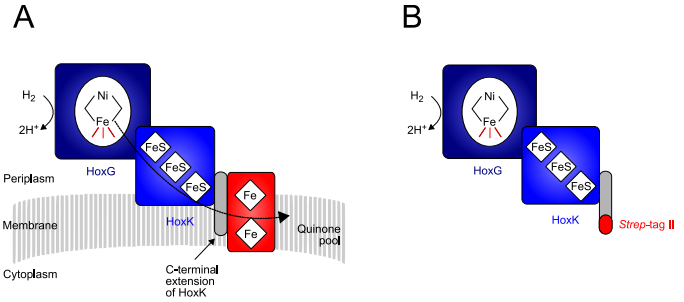

Figure 4.7: Cartoon of the MBH. (A) heterotrimeric form HoxGKZ (B) heterodimeric form HoxGK with *Strep*Tag II at the C-terminal extension of HoxK.

center have been found after reduction with an excess of NADH or dithionite (i.e. Ni_a-C and Ni_a-L states).[99,101]

The third hydrogenase is a membrane-bound hydrogenase (MBH), located in the cytoplasmic membrane. The MBH has a heterotrimeric structure HoxGKZ. The large subunit HoxG (67.1 kDa) embeds the [NiFe] center and the small subunit HoxK (34.6 kDa) accomodates three iron-sulfur clusters. The C-terminal extension of HoxK is connected to a membrane-integral cytochrome *b* HoxZ and anchored to the cytoplasmic membrane (see Figure 4.7).[102–105]

Electrons from the H_2-cleavage are transferred via the iron-sulfur clusters to the cytochrome *b* and finally to the respiratory chain.

The reason for the O_2-tolerance of the MBH is yet unclear. Recent electrochemical experiments have shown that the MBH has still 20% activity under atmospheric oxygen levels (21%) and is able to recover its full activity after oxygen is flushed out (see Figure 4.7).[90] In contrast to this, the MBH from *A. vinosum* is immediately inactivated under low levels of oxygen and does not recover after oxygen is flushed out unless the redox potential is shifted to low values.

It was found that the affinity towards hydrogen was much higher in *Re* H16 MBH as compared to standard hydrogenases.[26] Single site mutations in the vicinity of the [NiFe] center did not lead to an enhanced oxygen-sensitivity indicating that the mechanism of oxygen-tolerance is not based only on steric effects that hinder access of inhibiting gases but rather on a more complex mechanism.[26] It was also shown that the *Re* H16 MBH can be reactivated very rapidly at high potentials.[26]

Furthermore, the heterodimeric form including a *His*-tag was successfully immobilized onto a gold surface with a Ni-NTA monolayer and studied by SEIRA spectroscopy.[50] In principle, the advantage of this technique compared to classical electrochemical experiments is the additional structural information, which can be obtained by the combination of electrochemistry with FTIR spectroscopy.

A common feature of all three hydrogenases is the lack of the Ni_u-A state and it has been postulated earlier, that this might be a prerequisite for the O_2-tolerance.[20,23,48,106] Also in other hydrogenases Ni_u-A is missing and these hydrogenases have been postulated to be O_2-tolerant as well, e.g. the [NiFe]-hydrogenases from *Rm* CH34[107] or *A. aeolicus*.[108]

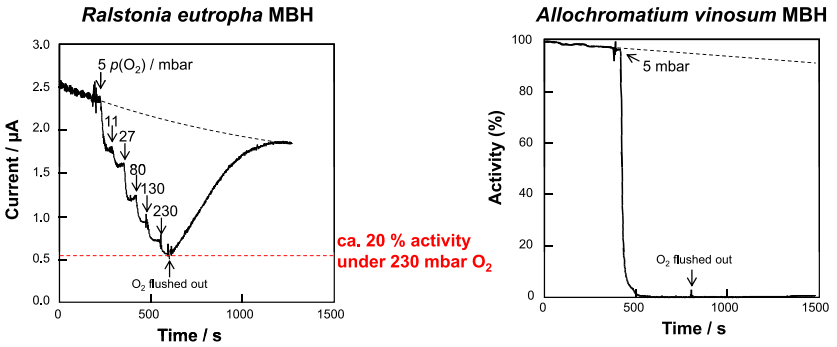

Figure 4.8: Protein filmvoltammetry of the aerobic MBH from *Re* H16 and the anaerobic hydrogenase from *A. vinosum* (adapted from [90]).

4.4 The bidirectional [NiFe]-hydrogenase from the cyanobacterium *Synechocystis* sp. PCC 6803

In principle, all hydrogenases are bidirectional enzymes, i.e. they can produce or consume hydrogen. However, their physiological function is usually limited to only one direction, depending in which environment the bacterium is found. [FeFe]-hydrogenases in strictly anaerobic organisms mainly produce hydrogen, whereas [NiFe]-hydrogenases mainly consume molecular hydrogen. *Synechocystis* PCC 6803 is a non-nitrogen fixing cyanobacterium and possesses a [NiFe]-hydrogenase, which works bidirectional under physiological conditions. Oxygenic photosynthetic microorganisms are a matter of high interest for the production of hydrogen by solar power. The bidirectional hydrogenase is the enzyme naturally involved in this process in cyanobacteria. [109–111]

The SH from *Synechocystis* PCC 6803 is a heteropentameric enzyme utilizing $NAD(P)^+$ as a substrate (Figure 4.9). HoxY and HoxH form the hydrogenase moiety and HoxE, HoxF and HoxU comprise the diaphorase unit. [112–115] Physiologically it has been shown that the hydrogenase functions as a valve for an excess of electrons. [109–111,116] It was suggested that cyclic electron transport, respiration via the NDH-1 complex and the bidirectional hydrogenase are competing for reducing equivalents. [116] Furthermore it has been proposed that the enzyme could be part of the respiratory complex I. [115] For a schematic representation of the proposed metabolic pathways see Figure 4.9. The bidirectional hydrogenase shows its highest activity (uptake and H_2 evolution) in cells with high photosynthetic activity and low respiration rates, [109] although it should be stressed that it is only active under anaerobic conditions. The Hox-genes are constitutively expressed in the presence of O_2. [109,117] The hydrogenase is inactive in the presence of oxygen but regains its activity under anaerobic conditions in less than a minute. [109,110] Crude extracts or the partially purified enzyme can be activated under anaerobic conditions within minutes by excess NADH or NADPH in the

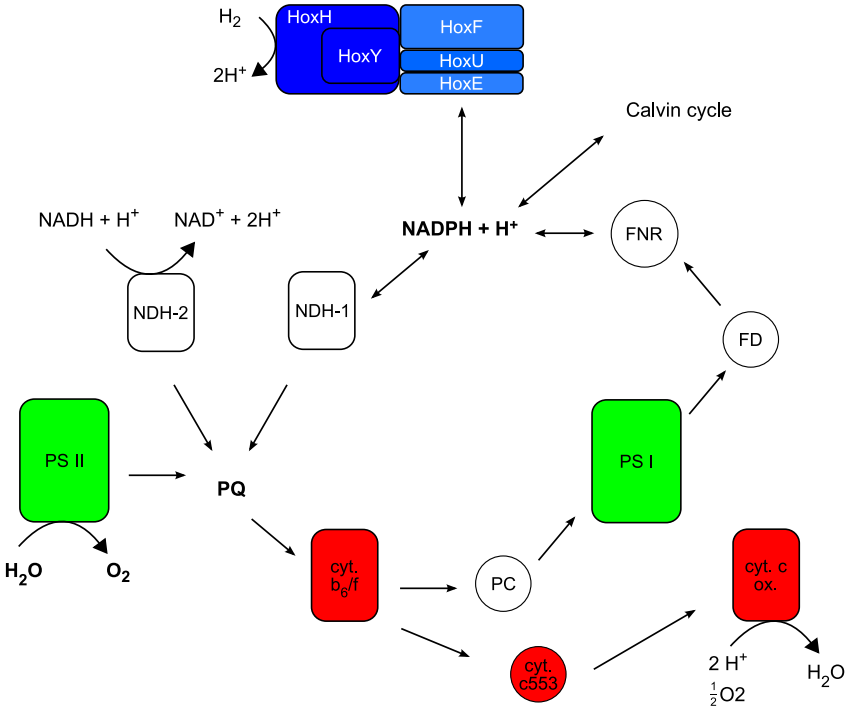

Figure 4.9: Physiological function of the bidirectional [NiFe]-hydrogenase from *Synechocystis* sp. PCC 6803.

absence of H_2.[111,118] Due to its high similarity to the SH from *Re* H16, the *Synechocystis* SH can be used for direct comparison of its spectroscopic properties (chapter 9).

4.5 Iron-sulfur clusters

Iron-sulfur clusters are found in a variety of proteins ranging from hydrogenases to molybdoenzymes of the xanthine oxidase (XO) family.[13,119] Usually they are part of electron transfer-chains but sometimes they are involved in direct catalysis, e.g. in isoprenoid biosynthesis.[120]

Different types of FeS-clusters have been identified. The most simple one consists of one iron atom coordinated by four sulfide-ligands (S^{2-}) with a tetrahedral geometry and is called rubredoxin (Figure 4.10).

In addition to this, clusters with higher complexity, consisting of more than one iron atom, are known and the theoretical description of these centers is far more complicated. Nevertheless, a few

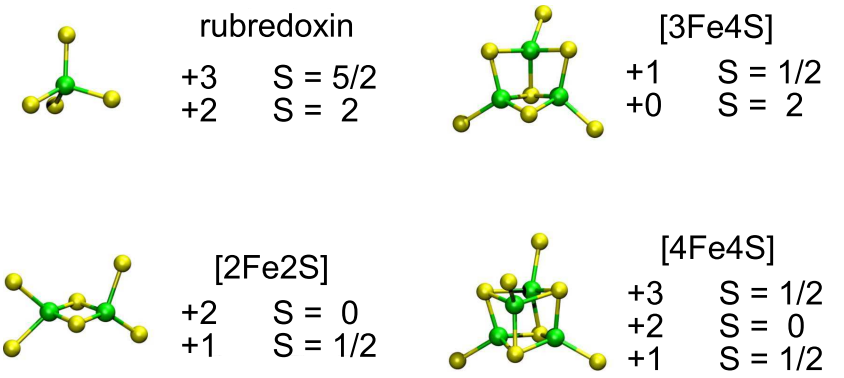

Figure 4.10: Different iron-sulfur clusters that can be found in proteins together with their oxidation/spin states. [121–123]

common characteristics for all iron-sulfur centers including their magnetic properties are known and reviewed in the literature. [121,122,124] The valence of each iron atom inside a cluster is either Fe^{2+} (ferrous) or Fe^{3+} (ferric). The spin states for both oxidation states are usually high-spin, i.e. S=2 for Fe^{2+} and S=5/2 for Fe^{3+}; only few examples are known with a low-spin iron. In systems with more iron atoms, e.g. [2Fe2S]-center, EPR spectroscopy does not reveal signals from S=5/2 or S=2 states. Usually, these systems are observed as a coupled system (Heisenberg exchange interaction), i.e. in [2Fe2S]-clusters both spins are coupled antiferromagnetically to an effective S=1/2 spin system for the reduced state, formally $Fe^{III}Fe^{II}$. A theoretical description of this case was first provided by Gibson. [125] Clusters with more than four iron atoms have been identified, e.g. the P-cluster in nitrogenase or the H-cluster in [FeFe]-hydrogenases, [13,66] but these cluster types represent special cases. Their redox potentials range between 400 mV and −500 mV indicating versatile electrochemical properties.

As described before, standard [NiFe]-hydrogenases contain three iron-sulfur clusters in their small subunit, the proximal [4Fe4S]-cluster, a medial [3Fe4S]-cluster and a distal [4Fe4S]-cluster. In the oxidized form, only the [3Fe4S]-cluster is paramagnetic with a S=1/2 ground state (see Figure 4.2). This cluster is located in a distance of about ∼24 Å from the Ni. [11,126] Thus there is no strong magnetic interaction between both centers, as confirmed with EPR spectroscopy. [126] However, some [NiFe]-hydrogenases show interactions between the Ni center and another paramagnetic center, possibly the [3Fe4S]-cluster, which result in complex EPR spectra, e.g. in *Rm* CH34, [107] *A. aeolicus* [127] and *A. vinosum*. [128] The origin of this interaction is not unambigiously resolved. For the *Rm* CH34 a direct coupling between the [3Fe4S] and the Ni has been postulated, [107] but for a few other hydrogenases an additional paramagnetic cofactor (X^{ox}, see Figure 4.2) has been postulated that might mediate spin-spin interaction. [65,128] This X^{ox} should be paramagnetic only in its oxidized form with a S=1/2 state and diamagnetic in its reduced form according to

$$[\mathrm{NiFe}]\cdots\mathrm{X}^{\mathrm{ox}}\cdots[\mathrm{3Fe4S}]^{+} \underset{\text{-e}}{\overset{\text{+e}}{\rightleftharpoons}} [\mathrm{NiFe}] \leftrightarrow \mathrm{X}^{\mathrm{red}} \leftrightarrow [\mathrm{3Fe4S}]^{+}$$

The cofactor X^{ox} was proposed to be either an additional iron, an overoxidized [4Fe4S]-cluster or a cystein radical.[65,128]

The *Re* H16 MBH investigated in this work shows a complex EPR spectrum in the oxidized form as well pointing to a similar structure as found in *Rm* CH34 or *A. aeolicus* (see chapter 5).[107,127]

In the reduced form both the proximal and distal [4Fe4S]-cluster are paramagnetic with a S=1/2 ground state. In standard hydrogenases this leads to the so called 'split' Ni_a-C or 'split' Ni_a-L states at low temperatures ($\leq$T=20 K), caused by a coupling between the [NiFe] center and the proximal [4Fe4S].[44,88,129]

Bibliography

[1] K. A. Vincent, A. Parkin, F. A. Armstrong, *Chem. Rev.* **2007**, *107*, 4366–4413.

[2] P. E. M. Siegbahn, J. W. Tye, M. B. Hall, *Chem. Rev.* **2007**, *107*, 4414–4435.

[3] R. Cammack, M. Frey, R. Robson, *Hydrogen as a fuel: learning from nature*, Taylor & Francis London, **2001**.

[4] A. K. Jones, E. Sillery, S. P. J. Albracht, F. A. Armstrong, *Chem. Commun.* **2002**, 866–867.

[5] K. A. Vincent, J. A. Cracknell, J. R. Clark, M. Ludwig, O. Lenz, B. Friedrich, F. A. Armstrong, *Chem. Commun.* **2006**, 5033–5035.

[6] M. Ihara, H. Nishihara, K. S. Yoon, O. Lenz, B. Friedrich, H. Nakamoto, K. Kojima, D. Honma, T. Kamachi, I. Okura, *Photochem. Photobiol.* **2006**, *82*, 676–682.

[7] P. M. Vignais, B. Billoud, *Chem. Rev.* **2007**, *107*, 4206–4272.

[8] A. I. Krasna, *Enzyme Microb. Technol.* **1979**, *1*, 165–172.

[9] J. W. Peters, W. N. Lanzilotta, B. J. Lemon, L. C. Seefeldt, *Science* **1998**, *282*, 1853–1858.

[10] S. Shima, O. Pilak, S. Vogt, M. Schick, M. S. Stagni, W. Meyer Klaucke, E. Warkentin, R. K. Thauer, U. Ermler, *Science* **2008**, *321*, 572–575.

[11] A. Volbeda, M. H. Charon, C. Piras, E. C. Hatchikian, M. Frey, J. C. Fontecilla Camps, *Nature* **1995**, *373*, 580–587.

[12] E. Garcin, X. Vernede, E. C. Hatchikian, A. Volbeda, M. Frey, J. C. Fontecilla Camps, *Structure* **1999**, *7*, 557–566.

[13] J. C. Fontecilla Camps, A. Volbeda, C. Cavazza, Y. Nicolet, *Chem. Rev.* **2007**, *107*, 4273–4303.

[14] M. W. Adams, *Biochim. Biophys. Acta* **1990**, *1020*, 115–145.

[15] E. J. Lyon, S. Shima, G. Buurman, S. Chowdhuri, A. Batschauer, K. Steinbach, R. K. Thauer, *Eur. J. Biochem.* **2004**, *271*, 195–204.

[16] S. Shima, R. K. Thauer, *Chem. Rec.* **2007**, *7*, 37–46.

[17] S. Shima, E. J. Lyon, M. Sordel Klippert, M. Kauss, J. Kahnt, R. K. Thauer, K. Steinbach, X. Xie, L. Verdier, C. Griesinger, *Angew. Chem. Int. Ed.* **2004**, *43*, 2547–2551.

[18] E. J. Lyon, S. Shima, R. Boecher, R. K. Thauer, F. W. Grevels, E. Bill, W. Roseboom, S. P. J. Albracht, *J. Am. Chem. Soc.* **2004**, *126*, 14239–14248.

[19] R. P. Happe, W. Roseboom, A. J. Pierik, S. P. Albracht, K. A. Bagley, *Nature* **1997**, *385*, 126.

[20] A. J. Pierik, M. Hulstein, W. R. Hagen, S. P. Albracht, *Eur. J. Biochem.* **1998**, *258*, 572–578.

[21] Y. Nicolet, B. J. Lemon, J. C. Fontecilla Camps, J. W. Peters, *Trends Biochem. Sci.* **2000**, *25*, 138–143.

[22] K. A. Vincent, A. Parkin, O. Lenz, S. P. J. Albracht, J. C. Fontecilla Camps, R. Cammack, B. Friedrich, F. A. Armstrong, *J. Am. Chem. Soc.* **2005**, *127*, 18179–18189.

[23] R. Cammack, V. M. Fernandez, K. Schneider, *Biochimie* **1986**, *68*, 85–91.

[24] B. Bleijlevens, F. A. van Broekhuizen, A. L. De Lacey, W. Roseboom, V. M. Fernandez, S. P. J. Albracht, *J. Biol. Inorg. Chem.* **2004**, *9*, 743–752.

[25] T. Buhrke, O. Lenz, N. Krauss, B. Friedrich, *J. Biol. Chem.* **2005**, *280*, 23791–23796.

[26] M. Ludwig, J. A. Cracknell, K. A. Vincent, F. A. Armstrong, O. Lenz, *J. Biol. Chem.* **2009**, *284*, 465–477.

[27] A. Abragam, B. Bleaney, *Electron Paramagnetic Resonance of Transition Ions*, Oxford University Press, **1970**.

[28] J. Weil, J. Bolton, J. Wertz, *Electron paramagnetic resonance, elementary theory and practical applications*, Wiley. New York, USA, **1994**.

[29] A. Schweiger, G. Jeschke, *Principles of Pulse Electron Paramagnetic Resonance*, Oxford University Press, USA, **2001**.

[30] N. Atherton, *Principles of electron spin resonance*, Ellis Horwood, **1993**.

[31] W. Gerlach, O. Stern, *Zeitschrift für Physik A Hadrons and Nuclei* **1922**, *9*, 349–352.

[32] A. Abragam, M. H. L. Pryce, *Proc. R. Soc. Lon. Ser.-A.* **1951**, *205*, 135–153.

[33] A. G. Agrawal, M. van Gastel, W. Gärtner, W. Lubitz, *J. Phys. Chem. B* **2006**, *110*, 8142–8150.

[34] M. T. J. Brecht, PhD thesis, TU Berlin, **2001**.

[35] E. R. Davies, *Phys. Lett. A* **1974**, *A 47*, 1–2.

[36] O. Trofantchouk, PhD thesis, TU Berlin, **2001**.

[37] C. Gessner, M. Stein, S. P. Albracht, W. Lubitz, *J. Biol. Inorg. Chem.* **1999**, *4*, 379–389.

[38] M. van Gastel, M. Stein, M. Brecht, O. Schröder, F. Lendzian, R. Bittl, H. Ogata, Y. Higuchi, W. Lubitz, *J. Biol. Inorg. Chem.* **2006**, *11*, 41–51.

[39] M. Brecht, M. van Gastel, T. Buhrke, B. Friedrich, W. Lubitz, *J. Am. Chem. Soc.* **2003**, *125*, 13075–13083.

[40] S. Foerster, M. van Gastel, M. Brecht, W. Lubitz, *J. Biol. Inorg. Chem.* **2005**, *10*, 51–62.

[41] M. Stein, PhD thesis, TU Berlin, **2001**.

[42] S. Dikanov, Y. Tsvetkov, *Electron spin echo envelope modulation (ESEEM) spectroscopy*, CRC press, **1992**.

[43] A. Chapman, R. Cammack, C. E. Hatchikian, J. McCracken, J. Peisach, *FEBS Lett.* **1988**, *242*, 134–138.

[44] S. A. E. Foerster, PhD thesis, TU Berlin, **2003**.

[45] W. B. Mims, J. Peisach, *J. Chem. Phys.* **1978**, *69*, 4921–4930.

[46] C. Gessner, PhD thesis, TU Berlin, **1996**.

[47] A. L. De Lacey, V. M. Fernandez, M. Rousset, R. Cammack, *Chem. Rev.* **2007**, *107*, 4304–4330.

[48] M. Saggu, I. Zebger, M. Ludwig, O. Lenz, B. Friedrich, P. Hildebrandt, F. Lendzian, *J. Biol. Chem.* **2009**, *284*, 16264–16276.

[49] C. Fichtner, C. Laurich, E. Bothe, W. Lubitz, *Biochemistry* **2006**, *45*, 9706–9716.

[50] N. Wisitruangsakul, O. Lenz, M. Ludwig, B. Friedrich, F. Lendzian, P. Hildebrandt, I. Zebger, *Angew. Chem. Int. Ed.* **2009**, *48*, 611–613.

[51] A. Stesmans, G. Vangorp, *Rev. Sci. Instrum.* **1989**, *60*, 2949–2952.

[52] S. Stoll, A. Schweiger, *J. Magn. Reson.* **2006**, *178*, 42–55.

[53] *MATLAB 7.6, Mathworks 2008*.

[54] A. J. Pierik, W. Roseboom, R. P. Happe, K. A. Bagley, S. P. Albracht, *J. Biol. Chem.* **1999**, *274*, 3331–3337.

[55] H. Ogata, S. Hirota, A. Nakahara, H. Komori, N. Shibata, T. Kato, K. Kano, Y. Higuchi, *Structure* **2005**, *13*, 1635–1642.

[56] Y. Higuchi, T. Yagi, N. Yasuoka, *Structure* **1997**, *5*, 1671–1680.

[57] A. Volbeda, J. C. Fontecilla Camps, *Dalton Trans.* **2003**, 4030–4038.

[58] Y. Montet, P. Amara, A. Volbeda, X. Vernede, E. C. Hatchikian, M. J. Field, M. Frey, J. C. Fontecilla Camps, *Nat. Struct. Biol.* **1997**, *4*, 523–526.

[59] H. Ogata, Y. Mizoguchi, N. Mizuno, K. Miki, S. Adachi, N. Yasuoka, T. Yagi, O. Yamauchi, S. Hirota, Y. Higuchi, *J. Am. Chem. Soc.* **2002**, *124*, 11628–11635.

[60] S. J. George, S. Kurkin, R. N. F. Thorneley, S. P. J. Albracht, *Biochemistry* **2004**, *43*, 6808–6819.

[61] M. Teixeira, I. Moura, A. V. Xavier, J. J. Moura, J. LeGall, D. V. DerVartanian, H. D. Peck, B. H. Huynh, *J. Biol. Chem.* **1989**, *264*, 16435–16450.

[62] C. C. Page, C. C. Moser, X. Chen, P. L. Dutton, *Nature* **1999**, *402*, 47–52.

[63] M. Rousset, Y. Montet, B. Guigliarelli, N. Forget, M. Asso, P. Bertrand, J. C. Fontecilla Camps, E. C. Hatchikian, *Proc. Natl. Acad. Sci. U. S. A.* **1998**, *95*, 11625–11630.

[64] S. P. J. Albracht, E. G. Graf, R. K. Thauer, *FEBS Lett.* **1982**, *140*, 311–313.

[65] S. P. J. Albracht, *Biochim. Biophys. Acta* **1994**, *1188*, 167–204.

[66] W. Lubitz, E. Reijerse, M. van Gastel, *Chem. Rev.* **2007**, *107*, 4331–4365.

[67] M. Stein, W. Lubitz, *Phys. Chem. Chem. Phys.* **2001**, *3*, 2668–2675.

[68] N. Baidya, M. M. Olmstead, J. P. Whitehead, C. Bagyinka, M. J. Maroney, P. K. Mascharak, *Inorg. Chem.* **1992**, *31*, 3612–3619.

[69] J. E. Huyett, M. Carepo, A. Pamplona, R. Franco, I. Moura, J. J. G. Moura, B. M. Hoffman, *J. Am. Chem. Soc.* **1997**, *119*, 9291–9292.

[70] S. Kurkin, S. J. George, R. N. F. Thorneley, S. P. J. Albracht, *Biochemistry* **2004**, *43*, 6820–6831.

[71] V. M. Fernandez, E. C. Hatchikian, R. Canmmack, *Biochim. Biophys. Acta* **1985**, *832*, 69–79.

[72] V. M. Fernandez, K. K. Rao, M. A. Fernandez, R. Cammack, *Biochimie* **1986**, *68*, 43–48.

[73] T. Buhrke, S. Löscher, O. Lenz, E. Schlodder, I. Zebger, L. K. Andersen, P. Hildebrandt, W. Meyer Klaucke, H. Dau, B. Friedrich, M. Haumann, *J. Biol. Chem.* **2005**, *280*, 19488–19495.

[74] O. Duché, S. Elsen, L. Cournac, A. Colbeau, *FEBS J.* **2005**, *272*, 3899–3908.

[75] F. Dole, A. Fournel, V. Magro, E. C. Hatchikian, P. Bertrand, B. Guigliarelli, *Biochemistry* **1997**, *36*, 7847–7854.

[76] H. J. Fan, M. B. Hall, *J. Am. Chem. Soc.* **2002**, *124*, 394–395.

[77] W. Gu, L. Jacquamet, D. S. Patil, H. X. Wang, D. J. Evans, M. C. Smith, M. Millar, S. Koch, D. M. Eichhorn, M. Latimer, S. P. Cramer, *J. Inorg. Biochem.* **2003**, *93*, 41–51.

[78] A. L. D. Lacey, E. C. Hatchikian, A. Volbeda, M. Frey, J. C. FontecillaCamps, V. M. Fernandez, *J. Am. Chem. Soc.* **1997**, *119*, 7181–7189.

[79] F. A. Armstrong, S. P. J. Albracht, *Phil. Trans. R. Soc. A* **2005**, *363*, 937–54; discussion 1035–40.

[80] M. Teixeira, I. Moura, A. V. Xavier, B. H. Huynh, D. V. DerVartanian, H. D. Peck, J. LeGall, J. J. Moura, *J. Biol. Chem.* **1985**, *260*, 8942–8950.

[81] J. W. van der Zwaan, S. P. Albracht, R. D. Fontijn, E. C. Slater, *FEBS Lett.* **1985**, *179*, 271–277.

[82] C. Fichtner, M. van Gastel, W. Lubitz, *Phys. Chem. Chem. Phys.* **2003**, *5*, 5507–5513.

[83] M. Medina, R. Williams, R. Cammack, E. C. Hatchikian, *J. Chem. Soc. Faraday. T.* **1994**, *90*, 2921–2924.

[84] J. Pilbrow, *Transition Ion Electron Paramagnetic Resonance*, Clarendon Press Oxford, **1990**.

[85] E. I. Solomon, E. G. Pavel, K. E. Loeb, C. Campochiaro, *Coord. Chem. Rev.* **1995**, *144*, 369–460.

[86] O. Trofanchuk, M. Stein, C. Gessner, F. Lendzian, Y. Higuchi, W. Lubitz, *J. Biol. Inorg. Chem.* **2000**, *5*, 36–44.

[87] C. Gessner, O. Trofanchuk, K. Kawagoe, Y. Higuchi, N. Yasuoka, W. Lubitz, *Chem. Phys. Lett.* **1996**, *256*, 518–524.

[88] S. Foerster, M. Stein, M. Brecht, H. Ogata, Y. Higuchi, W. Lubitz, *J. Am. Chem. Soc.* **2003**, *125*, 83–93.

[89] T. Burgdorf, O. Lenz, T. Buhrke, E. van der Linden, A. K. Jones, S. P. J. Albracht, B. Friedrich, *J. Mol. Microbiol. Biotechnol.* **2005**, *10*, 181–196.

[90] K. A. Vincent, J. A. Cracknell, O. Lenz, I. Zebger, B. Friedrich, F. A. Armstrong, *Proc. Natl. Acad. Sci. U. S. A.* **2005**, *102*, 16951–16954.

[91] T. Burgdorf, S. Löscher, P. Liebisch, E. van der Linden, M. Galander, F. Lendzian, W. Meyer Klaucke, S. P. J. Albracht, B. Friedrich, H. Dau, M. Haumann, *J. Am. Chem. Soc.* **2005**, *127*, 576–592.

[92] M. Bernhard, T. Buhrke, B. Bleijlevens, A. L. De Lacey, V. M. Fernandez, S. P. Albracht, B. Friedrich, *J. Biol. Chem.* **2001**, *276*, 15592–15597.

[93] L. K. Black, C. Fu, R. J. Maier, *J. Bacteriol.* **1994**, *176*, 7102–7106.

[94] K. Schneider, H. G. Schlegel, *Biochim. Biophys. Acta* **1976**, *452*, 66–80.

[95] E. van der Linden, B. W. Faber, B. Bleijlevens, T. Burgdorf, M. Bernhard, B. Friedrich, S. P. J. Albracht, *Eur. J. Biochem.* **2004**, *271*, 801–808.

[96] T. Burgdorf, E. van der Linden, M. Bernhard, Q. Yuan Yin, J. W. Back, A. F. Hartog, A. O. Muijsers, C. G. de Koster, S. P. J. Albracht, B. Friedrich, *J. Bacteriol.* **2005**, *187*, 3122–3132.

[97] E. van der Linden, T. Burgdorf, M. Bernhard, B. Bleijlevens, B. Friedrich, S. P. J. Albracht, *J. Biol. Inorg. Chem.* **2004**, *9*, 616–626.

[98] J. P. van der Linden, PhD thesis, Universiteit van Amsterdam, **2005**.

[99] E. van der Linden, T. Burgdorf, A. L. de Lacey, T. Buhrke, M. Scholte, V. M. Fernandez, B. Friedrich, S. P. J. Albracht, *J. Biol. Inorg. Chem.* **2006**, *11*, 247–260.

[100] B. Bleijlevens, T. Buhrke, E. van der Linden, B. Friedrich, S. P. J. Albracht, *J. Biol. Chem.* **2004**, *279*, 46686–46691.

[101] A. Erkens, K. Schneider, A. Müller, *J. Biol. Inorg. Chem.* **1996**, *1*, 99–110.

[102] B. Schink, H. G. Schlegel, *Biochim. Biophys. Acta* **1979**, *567*, 315–324.

[103] M. Bernhard, E. Schwartz, J. Rietdorf, B. Friedrich, *J. Bacteriol.* **1996**, *178*, 4522–4529.

[104] C. Kortlüke, B. Friedrich, *J. Bacteriol.* **1992**, *174*, 6290–6293.

[105] C. Kortlüke, K. Horstmann, E. Schwartz, M. Rohde, R. Binsack, B. Friedrich, *J. Bacteriol.* **1992**, *174*, 6277–6289.

[106] R. P. Happe, W. Roseboom, G. Egert, C. G. Friedrich, C. Massanz, B. Friedrich, S. P. Albracht, *FEBS Lett.* **2000**, *466*, 259–263.

[107] K. Knüttel, K. Schneider, A. Erkens, W. Plass, A. Müller, E. Bill, A. X. Trautwein, *B. Pol. Acad. Sci.-Chem.* **1994**, *42*, 495–511.

[108] M. Brugna Guiral, P. Tron, W. Nitschke, K. O. Stetter, B. Burlat, B. Guigliarelli, M. Bruschi, M. T. Giudici Orticoni, *Extremophiles* **2003**, *7*, 145–157.

[109] J. Appel, S. Phunpruch, K. Steinmüller, R. Schulz, *Arch. Microbiol.* **2000**, *173*, 333–338.

[110] L. Cournac, F. Mus, L. Bernard, G. Guedeney, P. Vignais, G. Peltier, *Int. J. Hydrogen Energy* **2002**, *27*, 1229–1237.

[111] L. Cournac, G. Guedeney, G. Peltier, P. M. Vignais, *J. Bacteriol.* **2004**, *186*, 1737–1746.

[112] J. Appel, R. Schulz, *J. Photochem. Photobiol.* **1998**, *47*, 1–11.

[113] O. Schmitz, G. Boison, R. Hilscher, B. Hundeshagen, W. Zimmer, F. Lottspeich, H. Bothe, *Eur. J. Biochem.* **1995**, *233*, 266–276.

[114] O. Schmitz, G. Boison, H. Salzmann, H. Bothe, K. Schütz, S. Wang, T. Happe, *Biochim. Biophys. Acta* **2002**, *1554*, 66–74.

[115] J. Appel, R. Schulz, *Biochim. Biophys. Acta* **1996**, *1298*, 141–147.

[116] F. Gutthann, M. Egert, A. Marques, J. Appel, *Biochim. Biophys. Acta* **2007**, *1767*, 161–169.

[117] K. Gutekunst, S. Phunpruch, C. Schwarz, S. Schuchardt, R. Schulz Friedrich, J. Appel, *Mol. Microbiol.* **2005**, *58*, 810–823.

[118] P. Vignais, L. Cournac, E. Hatchikian, S. Elsen, L. Serebryakova, N. Zorin, B. Dimon, *Int. J. Hydrogen Energy* **2002**, *27*, 1441–1448.

[119] R. Hille, *Chem. Rev.* **1996**, *96*, 2757–2816.

[120] Y. Xiao, P. Liu, *Angew. Chem. Int. Ed.* **2008**, *47*, 9722–9725.

[121] W. R. Hagen, *Adv. Inorg. Chem.* **1992**, *38*, 165–222.

[122] B. Guigliarelli, P. Bertrand, *Adv. Inorg. Chem.* **1999**, *47*, 421–497.

[123] H. Beinert, *FASEB J.* **1990**, *4*, 2483–2491.

[124] A. Hoff, *Advanced EPR: Applications in Biology and Biochemistry*, Elsevier Science, **1989**.

[125] J. F. Gibson, D. O. Hall, J. H. Thornley, F. R. Whatley, *Proc. Natl. Acad. Sci. U. S. A.* **1966**, *56*, 987–990.

[126] C. Elsässer, M. Brecht, R. Bittl, *J. Am. Chem. Soc.* **2002**, *124*, 12606–12611.

[127] K. Schneider, D. S. Patil, R. Cammack, *Biochim. Biophys. Acta* **1983**, *748*, 353–361.

[128] K. K. Surerus, M. Chen, J. W. van der Zwaan, F. M. Rusnak, M. Kolk, E. C. Duin, S. P. Albracht, E. Münck, *Biochemistry* **1994**, *33*, 4980–4993.

[129] B. Guigliarelli, C. More, A. Fournel, M. Asso, E. C. Hatchikian, R. Williams, R. Cammack, P. Bertrand, *Biochemistry* **1995**, *34*, 4781–4790.

5 Spectroscopic insights into the oxygen-tolerant membrane-associated [NiFe]-hydrogenase of *Ralstonia eutropha* H16

M. Saggu, I. Zebger, M. Ludwig, O. Lenz, B. Friedrich, P. Hildebrandt and F. Lendzian

published in *J. Biol. Chem.* (**2009**), *284*, 16264-16276

THE JOURNAL OF BIOLOGICAL CHEMISTRY VOL. 284, NO. 24, pp. 16264–16276, June 12, 2009

Spectroscopic Insights into the Oxygen-tolerant Membrane-associated [NiFe] Hydrogenase of *Ralstonia eutropha* H16*[S]

Received for publication, July 24, 2008, and in revised form, March 19, 2009 Published, JBC Papers in Press, March 20, 2009, DOI 10.1074/jbc.M805690200

Miguel Saggu[‡], Ingo Zebger[‡1], Marcus Ludwig[§], Oliver Lenz[§], Bärbel Friedrich[§], Peter Hildebrandt[‡], and Friedhelm Lendzian[‡2]

From the [‡]Institut für Chemie, Technische Universität Berlin, PC14, Strasse des 17. Juni 135, D-10623 Berlin and the [§]Institute of Biology, Department of Microbiology, Humboldt-Universität zu Berlin, Chausseestrasse 117, D-10115 Berlin, Germany

This study provides the first spectroscopic characterization of the membrane-bound oxygen-tolerant [NiFe] hydrogenase (MBH) from *Ralstonia eutropha* H16 in its natural environment, the cytoplasmic membrane. The H_2-converting MBH is composed of a large subunit, harboring the [NiFe] active site, and a small subunit, capable in coordinating one [3Fe4S] and two [4Fe4S] clusters. The hydrogenase dimer is electronically connected to a membrane-integral cytochrome *b*. EPR and Fourier transform infrared spectroscopy revealed a strong similarity of the MBH active site with known [NiFe] centers from strictly anaerobic hydrogenases. Most redox states characteristic for anaerobic [NiFe] hydrogenases were identified except for one remarkable difference. The formation of the oxygen-inhibited Ni_u-A state was never observed. Furthermore, EPR data showed the presence of an additional paramagnetic center at high redox potential (+290 mV), which couples magnetically to the [3Fe4S] center and indicates a structural and/or redox modification at or near the proximal [4Fe4S] cluster. Additionally, significant differences regarding the magnetic coupling between the Ni_a-C state and [4Fe4S] clusters were observed in the reduced form of the MBH. The spectroscopic properties are discussed with regard to the unusual oxygen tolerance of this hydrogenase and in comparison with those of the solubilized, dimeric form of the MBH.

Hydrogenases are metalloenzymes that catalyze the reversible cleavage of H_2 into protons and electrons and play a pivotal role in the energy metabolism of many microorganisms (1). They are grouped into three phylogenetically distinct classes as follows: the di-iron [FeFe], nickel-iron [NiFe], and iron-sulfur cluster-free [Fe] hydrogenases (2–6). The basic module of [NiFe] hydrogenases consists of two subunits, a large subunit that contains the [NiFe] active site and a small subunit that accommodates one to three electron-transferring iron-sulfur clusters (2, 7, 8). The active site nickel is coordinated to the protein via the thiol groups of four invariant cysteine residues, two of which serve as bridging ligands to the iron. The active site iron carries three additional diatomic ligands, two cyanides (CN^-) and one carbon monoxide (CO) (9, 10).

In addition to H_2, the active sites of the vast majority of [FeFe] and [NiFe] hydrogenases react with dioxygen. In case of the [FeFe] hydrogenases, this usually leads to an irreversible destruction of the active site (11, 12). Most [NiFe] hydrogenases, however, are reversibly inactivated by molecular oxygen (13, 14). Under electron-rich conditions in the presence of O_2 a mono-oxo species, most probably a hydroxide, is formed in the bridging position between nickel and iron (15–17). On the basis of EPR spectroscopy, this paramagnetic "ready inactive" state has been designated as Ni_r-B. Incubation of the enzyme with O_2 under electron-poor conditions results in the so-called "unready inactive" Ni_u-A state. It is anticipated that a di-oxo species (*e.g.* hydroperoxide) binds in the bridging position (16, 17). However, the nature of this ligand is still a matter of debate (18). The Ni_u-A and Ni_r-B states differ significantly in their reactivation kinetics. H_2-mediated reductive activation of the Ni_u-A state is a long term process and requires hours until the oxygen species is completely removed from the active site. In contrast, only seconds of incubation with H_2 are required to convert the Ni_r-B state into the catalytically active, EPR-detectable Ni_a-C state in which a hydride occupies the bridging position between nickel and iron (19, 20). An overview of the different redox states of the [NiFe] active site is shown in Fig. 1*A* (18, 21).

Formation of the Ni_u-A state prevents most of the [NiFe] hydrogenases, predominantly those from anaerobic microorganisms, from being catalytically active even in the presence of traces of O_2. However, the so-called Knallgasbacteria contain [NiFe] hydrogenases that enable these microorganisms to gain energy from H_2 oxidation even in the presence of atmospheric oxygen concentrations (22–24). Prominent examples are β-proteobacteria of the genus *Ralstonia,* including the well studied chemolithoautotrophic model organism *Ralstonia eutropha* H16. *R. eutropha* harbors three distinct [NiFe] hydrogenases that catalyze H_2 oxidation in the presence of ambient oxygen concentrations (11, 25–27). Their O_2 tolerance is based on at least two molecular mechanisms. For the cytoplasmic, hexameric NAD^+-reducing hydrogenase, a modified composition of the active site nickel has been described. It is proposed

* This work was supported by Deutsche Forschungsgemeinschaft Grants SFB 498 TP C1, TP C9 and by Cluster of Excellence "Unifying Concepts in Catalysis," and by the Federal Ministry of Education and Research (BMBF, project "Bio-H2").
[S] The on-line version of this article (available at http://www.jbc.org) contains supplemental Tables S1 and S2 and Figs. S1–S4.
[1] To whom correspondence may be addressed: Tel.: 49-30-314-26727; Fax: 49-30-314-21122; E-mail: ingo.zebger@tu-berlin.de.
[2] To whom correspondence may be addressed. Tel.: 49-30-314-22489; Fax: 49-30-314-21122; E-mail: f.lendzian@tu-berlin.de.

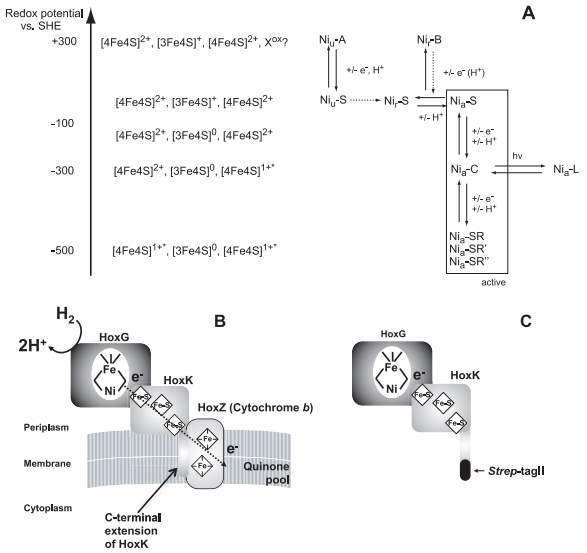

FIGURE 1. *A*, different redox states of the [NiFe] active site and the [FeS] clusters in oxygen-sensitive standard [NiFe] hydrogenases (adapted from Refs. 18, 21). See text for further details. No Ni_u-A is observed for the *R. eutropha* MBH. *B*, schematic of MBH of *R. eutropha* attached to the membrane via the cytochrome *b*. *C*, schematic of solubilized dimeric *R. eutropha* MBH harboring a *Strep* affinity tag at the C-terminal end of the small subunit.

that an extra CN^- ligand bound to the nickel protects the enzyme from O_2 inactivation (25, 28, 29). O_2 resistance of the H_2-sensing regulatory [NiFe] hydrogenases from *R. eutropha* (27) and *Rhodobacter capsulatus* (30) is likely based on a narrow gas channel that prevents access of O_2 to the active site.

The third H_2-converting catalyst in *R. eutropha* is a membrane-bound [NiFe] hydrogenase (MBH)[3] composed of the large subunit HoxG (67.1 kDa) and the small subunit HoxK (34.6 kDa) (31), which are anchored to the membrane-integral *b*-type cytochrome HoxZ via the hydrophobic C terminus of HoxK (Fig. 1*B*) (31–33). Electrochemical experiments revealed that the isolated MBH dimer (Fig. 1*C*), attached to a graphite electrode, retains more than 20% of its H_2-oxidizing activity in the presence of 0.21 bar O_2, compared with the activity under completely anaerobic conditions (26, 34). This result impressively demonstrates that O_2 reacts with the MBH active site in a way that still allows the catalytic conversion of H_2. FTIR and EPR spectroscopy are valuable techniques to get insights into the composition and redox state of cofactors as well as on structure-function relationships even if a crystal structure of the enzyme is not yet available (for recent reviews see Refs. 18, 35). Earlier data obtained by Fourier transform infrared (FTIR) spectroscopy indicate that the active site iron exhibits the standard set of diatomic ligands, two CN^- and one CO (26).

EPR allows the detection of redox-dependent changes of the electronic structure of both the [NiFe] active site in the large subunit and the Fe-S clusters in the small subunit. However, only paramagnetic metal species can be traced by EPR, whereas divalent nickel species that are constituents of the hydrogenase catalytic cycle are invisible by this technique.

The dimeric form of the MBH has been used successfully as a constituent in enzymatic fuel cells and for light-driven H_2 production (36, 37). These applications crucially depend on oxygen-tolerant hydrogen catalysts. A very recent biochemical and electrochemical study revealed that O_2 tolerance of the *R. eutropha* MBH is ultimately linked to a high affinity for hydrogen with a concomitant extremely low affinity for oxygen (34). To get insights into the electronic structure of the active site and the iron-sulfur clusters, which underlies the oxygen tolerance, we have re-investigated the spectroscopic properties of the MBH. In addition to earlier studies (38, 39), which are discussed below and which employed solely EPR spectroscopy, we have also used FTIR spectroscopy that probes the intra-ligand stretching modes of the diatomic active site ligands CO and CN^-. The frequencies of these modes are known to be sensitive to the electron density distribution in the catalytic center and thus can be used to monitor redox transitions (35, 40). The CO stretching frequency has been shown to respond also to changes in the amino acid composition of the protein backbone in the vicinity of the active site (21, 41, 42). Importantly, FTIR spectroscopy does not only rely on paramagnetic states of metal centers and, hence, is a useful tool to investigate all O_2-mediated noncatalytic states as well as all redox states involved in H_2 conversion. In this study we show that the MBH was never found in the oxygen-inactivated Ni-A state, which is in perfect agreement with recent electrochemical studies that revealed an extremely fast reactivation of the MBH dimer after treatment with dioxygen (34). However, our studies also present evidence that a significant portion of the MBH dimer that has been removed from the cytoplasmic membrane resided in a catalytically inactive form. Therefore, we investigated for the first time the spectroscopic properties of the trimeric form of the MBH, including HoxZ, tightly bound to the

[3] The abbreviations used are: MBH, membrane-bound hydrogenase; FTIR, Fourier transform infrared; ICP-OES, inductive coupled plasma optical emission spectroscopy; mT, millitesla.

cytoplasmic membrane (Fig. 1*B*). The trimeric MBH turned out to form only the Ni_r-B state and a small amount of ready or unready Ni-S states upon oxidation, which both reacted completely and reversibly with H_2. The spectroscopic properties of the MBH are discussed with regard to the O_2 tolerance of this unusual catalyst.

MATERIALS AND METHODS

Preparation of the Cytoplasmic Membrane—The *R. eutropha* MBH was overexpressed in a nontagged version using plasmid pLO6, harboring the complete MBH operon, in *R. eutropha* strain HF631, a megaplasmid-free derivative of *R. eutropha* (43). The cytoplasmic membrane was separated by osmotic shock to remove the outer membrane according to a modified protocol of Witholt *et al.* (44).

Cells were cultivated lithoautotrophically in mineral salts medium (45) under an atmosphere of 75% H_2, 15% O_2, and 10% CO_2 at 30 °C and continuous shaking at 120 rpm. Cells from 0.5 liter of culture volume were harvested at an A_{436} of 18–20 (centrifugation at 5000 × *g* at 4 °C for 20 min) and resuspended in 1 liter of 50 mM Tris/HCl buffer at pH 7.8. The cells were collected by centrifugation (5000 × *g*, 20 min, 4 °C) and resuspended in 400 ml of sucrose buffer (192 g of sucrose, 50 mM Tris/HCl buffer at pH 7.8 in 500 ml, 1 mM EDTA) and incubated at room temperature for 5 min. Subsequently, the suspension was again centrifuged (32,000 × *g*, 20 min, 4 °C), and the cells were exposed to osmotic shock by resuspending the pellet in 200 ml of deionized H_2O. The resulting spheroplasts were collected by centrifugation (4000 × *g*, 20 min, 4 °C), resuspended in 100 ml of 50 mM K-PO_4 buffer (pH 7.0), and subsequently disrupted using a French pressure cell (Constant Cell Disruption Systems) and ultrasonication (2 min, level 2.5, 75%) (Branson Sonifier). The cell extract was subjected to ultracentrifugation (100,000 × *g*, 60 min 4 °C), and the membrane fraction was isolated by removing the upper brownish part of the pellet with a spatula. The cytoplasmic membrane was homogenized in an appropriate volume of 50 mM K-PO_4 buffer (pH 7.0), ultracentrifuged (100,000 × *g*, 30 min, 4 °C), and finally homogenized in about 1 ml of 50 mM K-PO_4 buffer (pH 7.0).

Enzyme Purification—For purification of the MBH, a derivative carrying a *Strep*Tag II at the C terminus of the small subunit (HoxK) encoded on plasmid pGE636 in *R. eutropha* strain HF631 was used (46). The cells were grown lithoautotrophically in a fermentor (type NLF 22, Bioengineering, Wald, Switzerland) in mineral salts medium (45) under an atmosphere of 75% H_2, 15% O_2, and 10% CO_2 at 30 °C. The cells were harvested by centrifugation (5000 × *g*, 20 min 4 °C) at an A_{436} of about 20. The cell pellet was washed with an appropriate amount of phosphate buffer (90 g liter^{-1} Na_2HPO_4 × 12 H_2O, 15 g liter^{-1} KH_2PO_4), frozen in liquid nitrogen, and stored at −80 °C. The MBH dimer was purified as described previously (34). The protein was concentrated using centrifugal filter devices (Amicon Ultra15 (PL-30), Amicon Microcon (YM-30), Millipore) to volumes with protein concentrations (200–500 μM) appropriate for IR and EPR spectroscopy. The protein concentration was determined by the Bradford method (47) using bovine serum albumin as standard. The purity of the samples was examined by SDS-PAGE (48).

Enzyme Assay—Hydrogenase assays were performed as described previously (32) in 50 mM K-PO_4 buffer at pH 7.0 for membrane-attached MBH and at pH 5.5 for solubilized MBH. Methylene blue was used as artificial electron acceptor, and its absorption was measured photometrically at 570 nm.

EPR Spectroscopy—9.5 GHz X-band EPR spectroscopy has been carried out using a Bruker ESP300E spectrometer equipped with a rectangular microwave cavity in the TE_{102} mode. For low temperature measurements the sample was kept in an Oxford ESR 900 helium flow cryostat that allows for temperature control between 6 and 100 K (Oxford ITC4). The microwave frequency was detected with an EIP frequency counter (Microwave Inc.). For determination of *g* values, the magnetic field was calibrated with an external Li/LiF standard with a known *g* value of 2.002293 (49). Spin quantifications have been performed by comparing the double integrated signal with the signal of a $CuSO_4$ standard of known concentration. Base-line corrections, if required, were performed by subtracting a background spectrum, obtained under the same experimental conditions from a sample containing only a buffer solution. Simulations of the EPR spectra have been performed with the program EasySpin (50) that diagonalizes the Spin-Hamiltonian and calculates transition probabilities.

Fourier Transform Infrared Spectroscopy—FTIR spectra were recorded on a Bruker Tensor 27 spectrometer equipped with a liquid nitrogen-cooled MCT detector with a spectral resolution of 2 cm^{-1}. The sample compartment was purged with dried air, and the sample (0.2–0.5 mM isolated protein, ~0.05 mM protein attached to the cytoplasmic membrane) was held in a temperature-controlled (10 °C) gas-tight IR-cell for liquid samples (volume ~7 μl, path length = 50 μm) with CaF_2 windows. Spectra were base-line corrected by using a spline function implemented within OPUS 4.2 software of the spectrometer. Reduced protein samples were prepared through incubation under 1 bar H_2 or under 0.05 bar H_2 in 1 bar gas mixture (95% nitrogen, 5% hydrogen) atmosphere for 20–30 min at room temperature.

Metal and Cyanide Determination—The iron and nickel contents of solubilized dimeric *R. eutropha* MBH preparations were quantified by ICP-OES analysis with an Optima 2100 DV from PerkinElmer Life Sciences. The multiple element standard solution XVI (Merck) was used as reference. The cyanide content was determined chemically by distillation and subsequent UV/visible spectroscopic quantification of the formed polymethine according to Ref. 10.

Potential Measurements—The redox potentials of bulk protein samples in the "as-isolated" state or after different chemical treatments were measured in a homemade, low volume cell by means of a miniaturized Pt/Ag/AgCl "single-rod" redox electrode (Pt5900, Schott) at room temperature. All potentials cited in the text refer to the standard hydrogen electrode.

RESULTS

Determination of the Nickel, Iron, and Cyanide Content

The MBH dimer was solubilized from the membrane and purified by affinity chromatography as described previously (34). According to SDS-PAGE and subsequent protein staining,

the purity of the MBH subunits was estimated to be ~99%. Metal analysis using ICP-OES revealed a nickel content of 0.7 nickel per protein molecule and an iron content of about 10 ± 2 iron. This is in good agreement with the results of an earlier study (38) and consistent with the composition of one [NiFe], one [3Fe4S], and two [4Fe4S] as found in oxygen-sensitive standard [NiFe] hydrogenases, *e.g.* that from *Desulfovibrio vulgaris* (18, 41). The metal content reflects an occupancy of 70% for all metal cofactors. Nevertheless, the ratio of iron and nickel meets the expectation. Determination of the cyanide content in the purified MBH revealed 1.8 CN^- per protein molecule indicating a standard-like coordination of the iron in the active site, as observed by FTIR spectroscopy, *i.e.* two cyanides and one CO.

EPR Spectroscopic Analysis of the Solubilized MBH Dimer

Fig. 2 shows 9.5 GHz EPR spectra obtained for the solubilized, dimeric MBH in its oxidized (as isolated) and reduced forms. The spectra taken at 20 K from samples buffered at pH 5.5 and pH 7.0 (Fig. 2, *traces b* and *d*) exhibit a complex line shape. The prominent signal at $g = 2.0$ results from an oxidized $[3Fe\text{-}4S]^+$ cluster with an $S = 1/2$ ground state. The signal consists of a narrow component, similar to that observed for standard [NiFe] hydrogenases (see Fig. 2, *trace a*), and a superimposed complex broad "split" component (labeled by ▽). The intensity of this broad signal varied between different enzyme preparations, and in some samples, it even exceeded that of the narrow signal. It is interesting to note that the broad signal component was never observed in the spectra of most well studied periplasmic standard hydrogenases such as that from *D. vulgaris* Miyazaki F (Fig. 2, *trace a*).

Upon mild reduction of the as-isolated MBH dimer sample with 5 mM β-mercaptoethanol, the redox potential decreased to +40 mV resulting in a transformation of the complex broad and split EPR signal into a narrow signal, as it is usually observed for an uncoupled $[3Fe4S]^+$ cluster (see supplemental Fig. S1). This narrow signal at $g = 2.0$ is very similar to that found for the $[3Fe4S]^+$ center in the *D. vulgaris* Miyazaki F standard [NiFe] hydrogenase (Fig. 2, *trace a*).

At pH 7.0 signals of a Ni(III) species in the active site of the oxidized MBH dimer were detected. The g_x and g_y values (2.30 and 2.17) agree with those of the Ni_r-B state observed for standard [NiFe] hydrogenases (Fig. 2, *traces a* and *b*) (51–54). The Ni_r-B signals were broadened in protein samples at pH 5.5 (Fig. 2, *trace d*). This result indicates heterogeneity of the underlying species, hampering a reliable quantification at this low pH. Relative quantification of the integrated EPR signal intensities for a variety of samples at pH 7.0 showed that the amount of the Ni_r-B relative to the $[3Fe4S]^+$ signal was about 30%. Absolute quantification of the $[3Fe4S]^+$ signal (narrow signal component, Fig. 2, *traces b* and *d*) using a $CuSO_4$ standard sample revealed ~1 spin per protein indicating that the oxidized $[3Fe4S]^+$ cluster is present in essentially 100% of the protein. Notably, in samples with a high contribution of the $[3Fe4S]^+$ split component, spin quantification yielded up to 1.8 spins per protein for this signal (see supplemental Table S1).

EPR signals attributable to the Ni_u-A state were not observed in any *R. eutropha* MBH preparations, neither at high redox potential in as-isolated samples nor in samples reoxidized after previous treatment with H_2. This is in sharp contrast to the situation in standard [NiFe] hydrogenases, where usually a mixture of Ni_u-A and Ni_r-B states is observed in the as-isolated enzyme (18, 41).

Upon incubation with 1 bar H_2, the signal of the $[3Fe4S]^+$ cluster disappeared, whereas a complex spectrum of reduced $[4Fe4S]^+$ clusters emerged (g value range 2.0 to 1.82, see Fig. 2, *trace c*). Absolute quantification of the broad EPR signal, using a $CuSO_4$ spin standard sample, revealed 0.5–0.8 spins per protein for the reduced iron-sulfur centers. This value corresponds to one reduced [4Fe4S] center in only 50–80% of the isolated MBH protein. The shape of the spectrum indicates coupling to another paramagnetic center, which could be, according to an

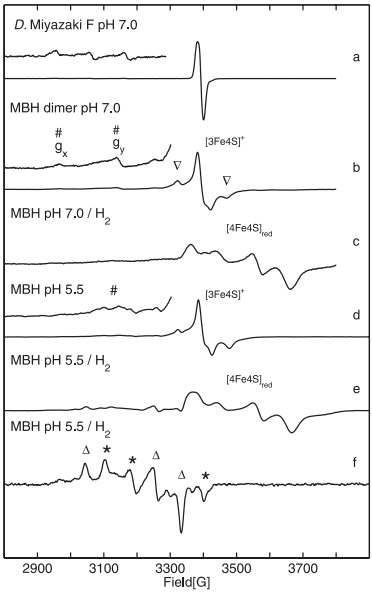

FIGURE 2. **EPR spectra of solubilized MBH dimer showing signals from the [NiFe] and [FeS] centers.** The enhanced traces of the spectra show the range of nickel signals with five times increased amplification. Definition of symbols is as follows: #, Ni_r-B; Δ, Ni_s-L; *, Ni_s-C; ▽, split signal from $[3Fe4S]^+$. *Trace a,* oxidized (as isolated) *D. vulgaris* Miyazaki F hydrogenase. The enhanced trace shows signals from superimposed g_x and g_y components of Ni_u-A and Ni_r-B. *Trace b,* oxidized (as isolated) *R. eutropha* MBH protein solution at pH 7.0 saturated with air, showing signals of the $[3Fe4S]^+$ cluster and Ni_r-B state. *Trace c,* H_2-reduced (1 bar H_2) *R. eutropha* MBH sample (pH 7.0) displaying signals from reduced [4Fe4S] centers. *Trace d,* oxidized (as isolated), and *trace e,* H_2-reduced (1 bar H_2) *R. eutropha* MBH samples at pH 5.5. *f,* H_2-reduced (1 bar H_2) *R. eutropha* MBH at $T = 80$ K, showing a superposition of signals from the Ni_s-C and Ni_s-L states. Experimental conditions for spectra (*traces a–e*) $T =$ 20 K, (*f*) $T = 80$K; 1 milliwatt microwave power; microwave frequency 9.56 GHz; 1 mT modulation amplitude, 12.5 kHz modulation frequency.

earlier proposal (38), the reduced [3Fe4S]^0 cluster with a spin S = 2.

EPR spectra of H_2-reduced samples at pH 5.5 display signals at lower field that are in the range expected for Ni_a-C and Ni_a-L (Fig. 2, *trace e*). At higher temperature (T = 80 K), the reduced iron-sulfur centers are broadened beyond detection, and the Ni_a-C/Ni_a-L signals became narrow and well resolved (Fig. 2, *trace f*). The g values obtained by simulations (Table 1) are in good agreement with those of Ni_a-C and Ni_a-L from standard [NiFe] hydrogenases (51). The spectra clearly show a superposition of nearly equal amounts of Ni_a-C and Ni_a-L. It should be emphasized that this Ni_a-L signal is observed without any extra illumination of the samples, except normal light conditions in the laboratory. It appears to be that Ni_a-L is easily formed in the isolated dimeric *R. eutropha* MBH, which is in contrast to standard [NiFe] hydrogenases, where prolonged illumination at low temperature is required to induce the transition from Ni_a-C to Ni_a-L. Contrary to the latter, the Ni_a-L state of the solubilized MBH dimer was stable under normal daylight conditions and did not convert to the Ni_a-C state at elevated temperature in the dark (20, 55), as observed in standard [NiFe] hydrogenases. This finding indicates that the catalytic active part of the solubilized enzyme shows a functional modification compared with standard [NiFe] hydrogenases.

TABLE 1

***g*-tensor principal values observed for the various redox states of the [NiFe] center of *R. eutropha* H16 MBH obtained by simulation compared with literature data for the *D. vulgaris* Miyazaki F hydrogenase**

	Redox state	g_x	g_y	g_z	Line width/ mT	Refs.
R. eutropha H16 dimer	Ni_a-B	2.30	2.17	2.01	[a]	This work and Ref. 38
	Ni_a-C	2.20	2.14	2.01	2.2	This work
	Ni_a-L	2.25	2.10	2.05	1.8	This work
R. eutropha H16 trimer	Ni_a-B	2.30	2.17	2.01	2.0	This work
	Ni_a-C	2.20	2.14	2.01	1.8	This work
	Ni_a-L1	2.30	2.11	2.05	1.5	This work
	Ni_a-L2	2.27	2.11	2.05	1.5	This work
	Ni_a-L3	2.24	2.11	2.05	1.4	This work
D. vulgaris Miyazaki F	Ni_a-B	2.33	2.16	2.01	1.9	This work and Ref. 59
	Ni_a-C	2.198	2.142	2.012		52
	Ni_a-L1	2.26	2.11	2.05		60
	Ni_a-L2	2.298	2.116	2.045		52
R. metallidurans CH34	Ni_a-B	2.30	2.17	2.01		39
	Ni_a-C	2.20	2.16	2.01		39
	Ni_a-L	2.31	2.12	2.05		39

[a] Line widths of spectra at 20 K are typically broad and range from 2 to 3 mT.

The total amount of the Ni_a-C and Ni_a-L mixture was estimated to be up to 20%. We consider the occurrence of Ni_a-L in the solubilized MBH dimer without illumination as nonphysiological (see below). It is likely that this unusual property results from a non-native structure and/or heterogeneity of the protein in the solubilized state.

The finding that much more Ni_a-C/Ni_a-L is formed at pH 5.5 than at pH 7.0 can be interpreted in terms of the pH dependence of the redox potential in the H_2-saturated protein solutions. Based on Nernst equation, redox potentials are expected to be about −320 and −410 mV at pH 5.5 and 7.0, respectively. Measurements of protein solutions at pH 7.0 using a platinum redox electrode revealed a potential at −380 mV. These findings are consistent with the results of an earlier study on the MBH from *Ralstonia metallidurans* CH34, which is closely related to *R. eutropha* H16. In that investigation, redox titration experiments have revealed a maximum amount of Ni_a-C at −301 mV, whereas only a small amount of Ni_a-C signal was observed at −420 mV (39). To investigate a possible coupling between Ni_a-C and the reduced [4Fe4S] cluster, the temperature dependence of the EPR spectra of H_2-reduced MBH samples was studied (see Fig. 3*A*).

Between 10 and 40 K, the spectra of Ni_a-C and reduced [4Fe4S] remained unchanged in MBH samples. At 60 K, however, the signal of the reduced iron-sulfur cluster was significantly broadened because of spin relaxation. This behavior is an inherent property of reduced [4Fe4S] clusters. At 80 K the [4Fe4S]$^+$ signal vanished completely, and only Ni_a-C/Ni_a-L signals were observed. This observation shows that a magnetic coupling between the Ni_a-C site and a reduced [4Fe4S] center is either absent or very different from that observed in standard [NiFe] hydrogenases (20, 55, 56). For comparison, Fig. 3*B* shows the temperature-dependent EPR spectra of the *D. vulgaris* Miyazaki F hydrogenase obtained after 3 h of incubation under 1 bar H_2 at 37 °C. At temperatures between 25 and 80 K, the well resolved signal of Ni_a-C signal was visible, but below 15 K a complex spectrum was obtained that had been attributed to magnetic cou-

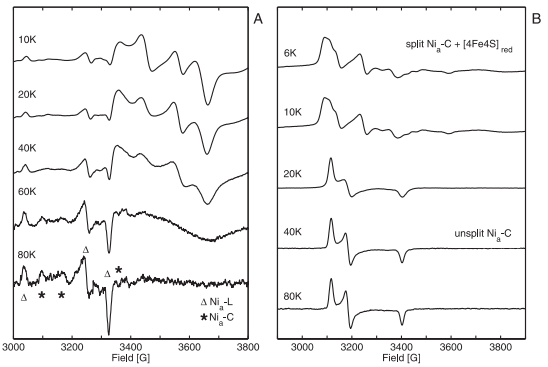

FIGURE 3. **Temperature-dependent EPR spectra of H_2-reduced hydrogenase.** *A*, signals of Ni_a-C, Ni_a-L, and reduced [4Fe4S] centers in *R. eutropha* MBH. *B*, signals of the coupled Ni_a-C and reduced [4Fe4S] centers in *D. vulgaris* Miyazaki F hydrogenase. Experimental conditions are as follows: 1 milliwatt microwave power; microwave frequency 9.56 GHz; 1 mT modulation amplitude, 12.5 kHz modulation frequency.

pling between the Ni_a-C and the reduced proximal [4Fe4S] cluster (20, 55, 56).

Our results from EPR spectroscopy are generally in good agreement with previous EPR studies on *Ralstonia* MBH (38, 39), where a different method has been used to prepare the enzyme in its solubilized dimeric form (32, 57) consisting of the small HoxK subunit with the iron-sulfur clusters and the large HoxG subunit harboring the [NiFe] active site (Fig. 1*C*). At high redox potential, an EPR signal of Ni(III) was observed. The *g* values were in agreement with those subsequently assigned to Ni_r-B (Fig. 1*A*). The Ni(III) signal of the oxidized MBH was reported to correspond to 0.15 spins per protein, and we found up to 30% Ni_r-B. In our study we found generally less Ni_r-B in samples that exhibited a larger fraction of inactive enzyme, as determined by FTIR (see below). Furthermore, a complex and split EPR signal was also found in Ref. 38, which was assigned to a $[3Fe4S]^+$ cluster, coupled to a yet unknown paramagnetic species. This species was reported to have a midpoint potential of +160 mV, where the EPR signal was converted to a narrow line shape, typically representing an uncoupled $[3Fe4S]^+$ cluster. Upon reduction with H_2 or dithionite, another EPR signal was observed that was attributed to two coupled $[4Fe4S]^+$ clusters. The redox potential of the transition $[4Fe4S]^{2+/1+}$ was determined to be −90 mV, which is unusually high for common [4Fe4S] clusters. Our EPR results confirm these findings. The dimeric MBH of *R. metallidurans* CH34, which is closely related to the *R. eutropha* MBH, was investigated in a later EPR and redox study (39). In addition to the EPR species found for the *R. eutropha* MBH another Ni-derived EPR signal, the so called Ni_a-C was observed, which is known as a catalytic intermediate in anaerobic [NiFe] standard hydrogenases (41, 52). We observed the Ni_a-C state also in *R. eutropha* MBH, underlining the close similarity of the hydrogenases of both species.

Our findings for the different paramagnetic states of the redox active centers in *R. eutropha* MBH and their proposed interactions are compared with those from the earlier studies (38, 39) in supplemental Table S2 and are discussed below.

FTIR Spectroscopy on the Solubilized MBH Dimer

The potential of FTIR spectroscopy for probing redox transitions and the intermolecular interactions within the catalytic center have been demonstrated for the standard [NiFe] hydrogenases from *Allochromatium vinosum* (14), *Desulfovibrio gigas* (9, 42), and *D. vulgaris* (41). The results obtained from these studies guided the assignment of the IR spectra of the *R. eutropha* MBH presented in this work (Table 2). This approach minimized the uncertainty in the interpretation of spectra caused by unavoidable variations of the sample preparation. Additional information on the assignment of bands was obtained from time-resolved H_2 reduction and reoxidation experiments by FTIR (data not shown) and studies of the trimeric MBH complex (see below).

Oxidized MBH—Fig. 4 displays the spectra of the oxidized enzyme recorded at pH 5.5 and 7.0 (*traces a* and *d*). The Ni_r-B state was identified based on the bands observed at 2098 and 2080 cm^{-1} (CN stretching bands) and 1948 cm^{-1} (CO stretching) by comparison with the respective bands of anaerobic standard hydrogenases (Table 2). Taking the integrated relative

TABLE 2

Wave-numbers of the CN^- and CO stretching modes of the *R. eutropha* H16 MBH compared with oxygen-sensitive standard [NiFe] hydrogenases (4, 9, 14, 41, 58)

(Redox) state	Enzyme	CO [cm^{-1}]	CN1 [cm^{-1}]	CN2 [cm^{-1}]
Ni_u-S	*R. eutropha* H16 MBH	**1943**[a]	**2082**	**2104**
	A. vinosum MBH	1950	2089	2099
	D. gigas	1950	2089	2099
	D. vulgaris Miyazaki F	1958	2089	2100
Ni_u-A	*R. eutropha* H16 MBH	ND[b]	ND	ND
	A. vinosum MBH	1945	2083	2093
	D. gigas	1947	2083	2093
	D. vulgaris Miyazaki F	1956	2084	2094
Ni_r-B	*R. eutropha* H16 MBH	**1948**	**2081**	**2098**
	A. vinosum MBH	1944	2079	2090
	D. gigas	1946	2079	2090
	D. vulgaris Miyazaki F	1955	2081	2090
Ni_r-S	*R. eutropha* H16 MBH	**1910**	**2055**	**2063**
		1936	**2075**	**2093**
	A. vinosum MBH	1911	2053	2067
		1932	2074	2086
	D. gigas	1914	2055	2067
	D. vulgaris Miyazaki F	1922	2056	2070
Ni_a-S	*R. eutropha* H16 MBH	**1936**	**2075**	**2093**
	A. vinosum MBH	1932	2074	2086
	D. gigas	1934	2075	2087
	D. vulgaris Miyazaki F	1943	2075	2086
Ni_a-C	*R. eutropha* H16 MBH	**1957**	**2075**	**2097**
	A. vinosum MBH	1950	2074	2087
	D. gigas	1952	2073	2086
	D. vulgaris Miyazaki F	1961	2074	2085
Ni_a-L	*R. eutropha* H16 MBH	**1899**	**2040**	**2065**
	A. vinosum MBH	1898	2043	2058
Ni_a-SR	*R. eutropha* H16 MBH	**1948**	**2068**	**2087**
	A. vinosum MBH	1936	2059	2073
	D. gigas	1940	2059	2073
	D. vulgaris Miyazaki F	1948	2061	2074
Ni_a-SR′	*R. eutropha* H16 MBH	**1926**	**2049**	**2075**
	A. vinosum MBH	1921	2048	2064
	D. gigas	1923	—	—
	D. vulgaris Miyazaki F	1933	—	—
Ni_a-SR″	*R. eutropha* H16 MBH	**1919**	**2046**	**2071**
	A. vinosum MBH	1913	2043	2058
	D. vulgaris Miyazaki F	1919	—	—
Ni_u-S	*R. eutropha* H16 MBH	**1930**	**2060**	**2076**
	D. gigas	1936	2063	2070

[a] Boldface numbers indicate this work.
[b] ND, not detected; —, not assigned.

CO band intensities as a direct measure for the relative amounts of nickel states, the Ni_r-B was estimated to be 10–40% of the total MBH sample, the actual amount being dependent on the pH value and to some degree on the preparation. Generally, an increase of the amount of Ni_r-B was observed for lower pH values as compared with pH 8.0 used in Ref. 26; however, heterogeneity also increased toward lower pH. At pH 7.0 about 20% Ni_r-B was observed in the FTIR spectra, which is in agreement with the value estimated from EPR spectroscopy. An additional species with bands at wave-numbers of 1943 (CO) and 2104 cm^{-1} (CN^-) corresponds to a small amount of another oxidized EPR-silent state, which might be either attributed to the so-called Ni_u-S (unready, silent) state (see Table 2) (14, 41, 42), which shows, in contrast to anaerobic standard [NiFe] hydrogenases, a rather fast H_2-mediated re-activation within minutes instead of hours. Alternatively, these bands may originate from another "ready" state, derived from Ni_r-B, which has been recently observed in the *D. vulgaris* Miyazaki F enzyme.[4] Because of the large number of overlapping bands in the CN stretching region, the second CN stretching mode of

[4] W. Lubitz and M. Pandelia, personal communication.

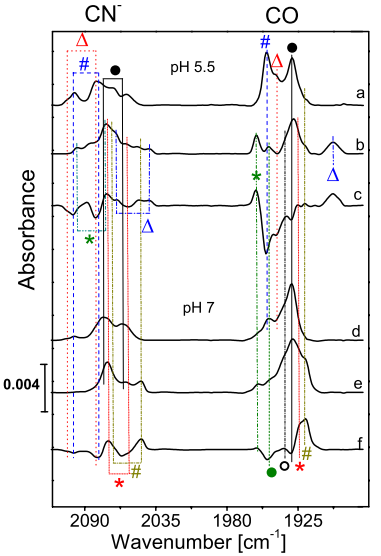

FIGURE 4. **FTIR spectra of the *R. eutropha* MBH, oxidized (as isolated) enzyme (*traces a* and *d*), the H_2-reduced (1 bar H_2) samples (*traces b* and *e*), and the corresponding difference spectra (H_2-reduced minus oxidized, *traces c* and *f*) at different pH values: pH 5. 5, *traces a–c;* pH 7.0, *traces d–f*.** Definition of the symbols is as follows: Δ (*red*), $Ni_{u/r}$-S; # (*blue*), Ni_r-B; ○, Ni_{ia}-S; ●, Ni_{ia}-S (only 20% active); Δ (*blue*), Ni_a-L; * (*green*), Ni_a-C; ● (*green*), Ni_a-SR; * (*red*), Ni_a-SR′; # (*dark yellow*), Ni_a-SR″.

this species could not be identified unambiguously for the solubilized MBH dimer (HoxKG, Fig. 1*C*). However, this CN band position could be resolved in the FTIR spectra of the membrane-attached trimeric MBH (HoxKGZ, see below) and was identified at 2082 cm^{-1} (Table 2).

At pH 8.0 only one dominant species was observed in more than 80% of the enzyme preparations (see supplemental Fig. S3). This nickel state showed IR bands at 2076, 2060, and 1930 cm^{-1} and included only a small fraction of about 15% that could be activated. The major portion, however, did not react with H_2 and was therefore attributed to an irreversibly inactive state, designated as Ni(inactive)-S (Ni_{ia}-S). In this state, solubilized, dimeric MBH could not be activated, even after prolonged incubation with H_2. This inactive state is also present in MBH samples at pH 5.5 and pH 7.0, although with smaller amounts ranging between 40 and 60%. A similar inactive state was found in some cases for the *D. gigas* hydrogenase.[5] The Ni_{ia}-S state was not detectable in the spectra of the HoxKGZ trimer in the cytoplasmic membrane (see below). Therefore, we suggest that Ni_{ia}-S is a non-native state.

[5] A. L. De Lacey, personal communication.

As solubilization of the MBH dimer is associated with a downshift of the optimum pH for H_2-oxidizing activity, one may rationalize the higher content of the Ni_r-B ready state and the lower amount of the inactive Ni_{ia}-S in the solubilized heterodimer at lower pH values. Even though the Ni_r-B state was clearly detectable, FTIR signals attributable to the Ni_u-A state were not observed. This is in agreement with the EPR spectroscopic results.

Reduced MBH—FTIR spectra were recorded for *dimeric* MBH samples at different pH values (5.5 and 7.0) after incubation under an atmosphere of 1 bar H_2 (Fig. 4, *traces b* and *e*). At pH 5.5 and a redox potential of −320 mV, IR bands corresponding to Ni_a-C (2097, 2075, and 1957 cm^{-1}) and Ni_a-L (2065, 2040, and 1899 cm^{-1}) were observed (Table 2). Contrary to standard [NiFe] hydrogenases Ni_a-L was found even at ambient temperature (10 °C). The Ni_a-C and Ni_a-L state mixture constituted each about 10% of the enzyme, which is in agreement with the data obtained by EPR spectroscopy. Because of the contributions of active Ni_a-SR and inactive Ni_{ia}-S (about 50%) states, specifically the spectral cogent CN^- stretching region is difficult to disentangle. However, comparison with the spectra of the reduced trimeric, membrane-attached enzyme (see below) allows for an assignment of the bands at 1948, 1926, and 1919 cm^{-1} in the CO stretching region and at 2068/2087, 2049/2075, and 2046/2071 cm^{-1} in the CN^- stretching region. These frequencies are characteristic for the EPR-silent fully reduced states Ni_a-SR, Ni_a-SR′, and Ni_a-SR″ (Table 2). As described above, the pronounced CO absorption band at 1930 cm^{-1} did barely change upon incubation with H_2 and was therefore assigned to the inactive Ni(inactive)-S state.

At 1 bar H_2 and pH 7.0, no Ni_a-C nor Ni_a-L but only the fully reduced states Ni_a-SR, Ni_a-SR′, Ni_a-SR″ were observed and assigned on the basis of their characteristic band positions (Fig. 4 and Table 2).

To highlight the fraction of redox active enzyme, the "H_2-reduced" minus "oxidized (as isolated)" difference spectra obtained for MBH samples buffered at different pH values are shown Fig. 4 (*traces c* and *f*). Bands originating from reduced and oxidized species appear as positive and negative signals, respectively. The difference spectra show that the main redox active species in the solubilized, dimeric MBH was Ni_r-B in addition to a small amount of "unready" or ready Ni-S state (see above). The large fraction of the EPR-silent Ni_{ia}-S species, which increased at higher pH values, remained inactive and is therefore not visible in the IR-difference spectra.

The relative contributions of the reduced Ni_a-SR, Ni_a-SR′, and Ni_a-SR″ subspecies depend on the pH (see Fig. 4 and data related to the trimeric species, described below). This behavior has also been observed for the *A. vinosum* MBH enzyme (14) and suggests the involvement of protonable groups in the equilibria between these states.

EPR Spectroscopic Characterization of the MBH Protein as a Constituent of the Cytoplasmic Membrane

Preparations of the solubilized dimeric *R. eutropha* MBH contained a large protein fraction (up to 80%) that did not react with hydrogen, hence being catalytically inactive. Also the active fraction itself showed peculiar properties such as the

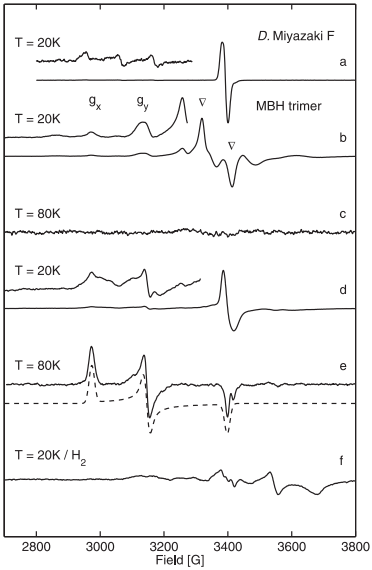

FIGURE 5. **EPR spectra of *R. eutropha* MBH attached to the membrane (*traces b–f*) and oxidized (as isolated) *D. vulgaris* Miyazaki F hydrogenase (*trace a*).** The enhanced (*trace a*) shows signals from superimposed g_x and g_y components of Ni_a-A and Ni_a-B. Experimental conditions are as follows: 1 milliwatt microwave power; 1 mT modulation amplitude, 12.5 kHz modulation frequency. *Trace b,* EPR spectra of oxidized (as isolated or reoxidized) MBH from a preparation of the cytoplasmic membrane at $T = 20$ K (redox potential +290 mV) showing signals from Ni_r-B and split signal from $[3Fe4S]^{+}$. *Trace c,* oxidized (as isolated) from cytoplasmic membrane preparations at $T = 80$ K. *Trace d,* MBH, partially reduced with 5 mM β-mercaptoethanol (+40 mV), recorded at $T = 20$ K (the complex split [3Fe4S] signal has disappeared, and a narrow signal arises at a redox potential of +40 mV), Enhanced trace, Ni_r-B. *Trace e,* MBH partially reduced with 5 mM β-mercaptoethanol (+40 mV), recorded at $T = 80$ K; the *dashed line* represents the simulated spectrum of Ni_r-B. *Trace f,* H_2-reduced samples from cytoplasmic membrane preparation (redox potential −390 mV). Experimental conditions for spectra (*traces b–f*) are as follows: 10 milliwatt microwave power; microwave frequency 9.56 GHz; 1 mT modulation amplitude, 12.5 kHz modulation frequency.

appearance of Ni_a-L in nonilluminated samples. These findings indicate structural and functional rearrangements because of the detachment of the enzyme from the membrane. Thus, the spectroscopic studies were expanded to entire membrane fragments containing the native trimeric form of the *R. eutropha* MBH.

MBH at Positive Redox Potentials—Fig. 5 shows the EPR spectra of the *R. eutropha* cytoplasmic membrane. The spectrum of the oxidized (as isolated) membrane at 20 K and pH 7.0 (*trace b*) exhibited a complex line shape with a superposition of several paramagnetic species. In the air-saturated membrane sample at a redox potential of approximately +290 mV, the prominent contribution was represented by the complex broad and split EPR signal (Fig. 5, labeled by ▽), which results from the coupling of a $[3Fe4S]^{+}$ complex with another paramagnetic center. The broad signal component is not present in the spectra of periplasmic anaerobic standard hydrogenases, such as that of *D. vulgaris* Miyazaki F (see Fig. 5, *trace a*). To test whether the complex spectrum is because of MBH-derived paramagnetic centers, membrane preparations of the *R. eutropha* mutant strain HF359, which carries a deletion in the MBH large subunit gene *hoxG,* have been investigated by EPR spectroscopy (supplemental Fig. S2). It has been shown previously that this strain does not possess HoxG as well as the mature subunit HoxK in the membrane (46). The spectral features attributable to the coupled $[3Fe4S]^{+}$ cluster were only visible in MBH-containing wild-type membranes but were absent in the Δ*hoxG* mutant. Only a weak signal of negligible intensity was found at $g = 2$, the origin of which is unknown (supplemental Fig. S2).

The membrane-attached enzyme also showed signals attributable to a Ni(III) center. The respective g_x and g_y values (2.30 and 2.17) agree with the Ni_r-B state observed in standard hydrogenases (51–54). The g_z component is superimposed by the complex split signal of the [3Fe4S] cluster. Compared with the EPR signal of $[3Fe4S]^{1+}$, the relative intensity of the double-integrated Ni(III) signal is ~40%. Because FTIR spectroscopy indicates >80% Ni_r-B in these samples (see below), we conclude that approximately two spins per protein contribute to the split $[3Fe4S]^{+}$ signal (see also results from dimeric MBH).

At 80 K, and a redox potential of +290 mV, the EPR signals attributed to Ni_r-B are no longer visible (Fig. 5, *trace c*). This indicates that at redox potentials, at which the complex $[3Fe4S]^{+}$ signal is visible, the relaxation behavior of Ni_r-B in the *R. eutropha* hydrogenase is different from that observed in standard [NiFe] hydrogenases. Thus, both the Ni_r-B and the $[3Fe-4S]^{+}$ center seem to be magnetically coupled to another paramagnetic center.

Upon mild reduction of the as-isolated membrane sample with 5 mM β-mercaptoethanol, the redox potential decreased to +40 mV resulting in a transformation of the complex broad and split EPR signal into a narrow signal, as it is usually observed for an uncoupled $[3Fe4S]^{+}$ cluster (Fig. 5, *trace d*). This narrow signal at $g = 2.0$ is very similar to that found for the $[3Fe4S]^{+}$ center in the *D. vulgaris* Miyazaki F standard [NiFe] hydrogenase (Fig. 5, *trace a*).

At 20 K and +40 mV the spectrum of Ni_r-B showed a broadening of each *g* component (Fig. 5, *trace d*). However, at higher temperatures (80 K) the EPR signals from Ni_r-B were strong and now well resolved, and the spectrum could be readily simulated, yielding all three *g* values (Table 1 and Fig. 5, *trace e*). This result indicates that the magnetic coupling to another paramagnetic state is no longer present at +40 mV. The absence of the paramagnetic species inducing a splitting of the $[3Fe4S]^{+}$ signal at +290 mV also changed the relaxation behavior of the Ni_r-B in such a way that it can be observed at 80 K, a temperature where the EPR signal of the uncoupled $[3Fe4S]^{+}$ cluster is no longer present.

Comparison of the second integrals of the broad and narrow EPR signals derived from the $[3Fe4S]^{+}$ cluster at +290 and +40 mV showed that the intensity of the narrow signal was less than

50% of the broad and split signal. This is consistent with one spin per protein for the $[3Fe4S]^{+}$ cluster. The total integral of the broad and split signal observed at a redox potential of +290 mV *versus* standard hydrogen electrode in the membrane corresponds to two spins per protein indicating the occurrence of an additional yet unknown high potential paramagnetic center coupling to $[3Fe4S]^{1+}$.

It is important to note that signals attributable to the Ni_u-A state were not observed under any conditions. Traces of Ni_u-A below the detection limit (<2%) cannot be excluded.

Reduced MBH—To analyze the catalytically relevant reduced states of the MBH, the membrane samples were incubated under anaerobic conditions at pH 7.0 in the presence of 1 bar H_2. The Ni_r-B and the $[3Fe4S]^{+}$ signals disappeared, and weak broad EPR spectral features emerged in the low field range between 3100 and 3300 G, where the signals of the reduced Ni_a-C and Ni_a-L states are expected (Fig. 5, *trace f*). However, these broad features could also reflect superpositions of signals from other membrane proteins harboring paramagnetic metal species. On the high field side, between 3350 and 3700 G, a broad EPR spectrum emerged, displaying more than three spectral components in the *g* value range from 2.0 to 1.82. These signals cannot be attributed to only one reduced $[4Fe4S]^{+}$ species. For anaerobic standard hydrogenases, two coupled $[4Fe4S]^{+}$ centers have been proposed. For *R. eutropha* MBH, the signals may be attributed to a single $[4Fe4S]^{+}$ center, which is coupled to the reduced $[3Fe4S]^{0}$ cluster with a spin S = 2. This is supported by the relative quantification of the double-integrated signals of the broad $[4Fe4S]^{+}$ signal in H_2-reduced MBH compared with the split $[3Fe4S]^{+}$ signal in oxidized samples (Fig. 5, *trace b*), which was attributed to two coupled paramagnetic species, each having a spin S = 1/2. The calculation revealed only one-half of the intensity for the $[4Fe4S]^{+}$ signals in H_2-reduced samples indicating that only one spin per protein (S = 1/2) is present, *i.e.* only one of the two $[4Fe4S]^{+}$ clusters is reduced.

Re-oxidation of the membrane samples under air led to the same EPR signals of Ni_r-B and the $[3Fe4S]^{+}$ center as observed previously in the untreated, as-isolated MBH (Fig. 5, *trace b*). This observation clearly indicates that the H_2-mediated reduction is completely reversible when the MBH is associated with the cytoplasmic membrane.

Reduction with 1 bar H_2 at pH 5.5 led to the same broad EPR signals of reduced $[4Fe4S]^{+}$ on the high field side as at pH 7.0 (Fig. 5, *trace f*). At higher temperature (80 K) the background signals from paramagnetic metal centers became weaker, and a well resolved EPR spectrum of Ni_a-C appeared. Upon illumination by white light for 25 min at 80 K, the Ni_a-C was converted completely to Ni_a-L, which appeared in three sub-species, with slightly different g_x values (Table 1 and Fig. 6). The experimental "dark-minus-light" difference spectrum is shown together with its simulation in Fig. 6, *trace b*. Simulated spectra of the pure Ni_a-C and Ni_a-L states, the latter with negative intensity, are given in Fig. 6 (*traces a* and *c*). The integrated intensities of the Ni_a-C and Ni_a-L spectra are identical within the experimental error showing the complete conversion from Ni_a-C to Ni_a-L. The respective *g* values are very similar to those from standard hydrogenases (Table 1). When the membrane sample was kept in the dark for 15 min at 200 K, the Ni_a-L state was completely back-converted to the Ni_a-C state. Hence, the [NiFe] active site of the trimeric MBH shows the same light-induced Ni_a-C/Ni_a-L inter-conversion as reported for anaerobic standard [NiFe] hydrogenases (20, 60).

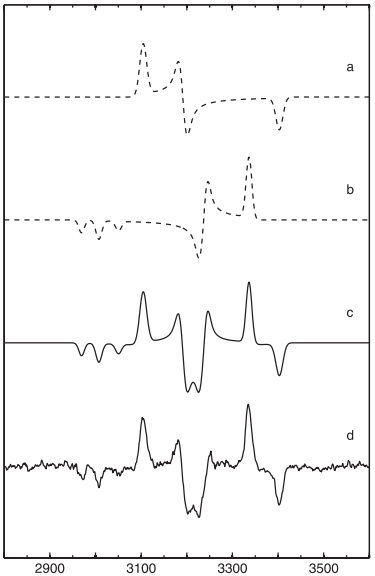

FIGURE 6. **Experimental and simulated EPR spectra of reduced, membrane-attached *R. eutropha* MBH pH 5. 5 at *T* = 80 K (for *g* values see Table 1).** *Trace a,* simulation of Ni_a-C spectrum. *Trace b,* simulation of the spectrum of superimposed Ni_a-L states (inverted intensities) showing three different g_x values. *Trace c,* sum of simulated Ni_a-C and Ni_a-L (inverted intensities) spectra. *Trace d,* experimental EPR difference spectrum (dark minus light) of H_2-reduced cytoplasmic membrane at *T* = 80 K, Experimental conditions are as follows: 10 milliwatt microwave power; microwave frequency 9.56 GHz; 1 mT modulation amplitude, 12.5 kHz modulation frequency.

FTIR Spectroscopic Characterization of the MBH Protein as a Constituent of the Cytoplasmic Membrane

Oxidized MBH—The FTIR spectra of oxidized, membrane-attached MBH at pH 7.0 and at potentials between +250 and +300 mV displayed the characteristic band signature of an almost pure (up to 90%) Ni_r-B state (Fig. 7, *trace a*). The characteristic CN^{-} stretching modes at 2098 and 2081 cm^{-1} and a CO stretching at 1948 cm^{-1} were in agreement with those of the Ni_r-B state of standard [NiFe] hydrogenases from *D. gigas* and *D. vulgaris* Miyazaki F (Table 2) (21, 41, 42). Only relatively small contributions (less than 20%) to the spectrum might originate from an EPR-silent oxidized form, which was also observed to a larger extent in the isolated MBH dimer. Signals

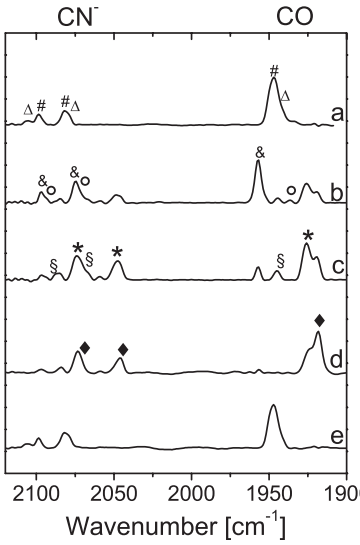

FIGURE 7. **FTIR spectra of the membrane-attached *R. eutropha* MBH from cytoplasmic membrane preparations as follows: oxidized (as isolated, +250 to +300 mV) at pH 7.0 (*trace a*), reduced at pH 5.5 with 0.05 bar H_2 in N_2 (−280 mV) (*trace b*), reduced at pH 5.5 with 1 bar H_2 in N_2 (−320 mV) (*trace c*), reduced at pH 7.0 with 1 bar H_2 in N_2 (−410 mV) (*trace d*), and re-oxidized with air (+250 to +300 mV) (*trace e*).** Definition of the symbols is as follows: Δ, $Ni_{u/r}$-S; #, Ni_r-B; ○, $Ni_{r/a}$-S; &, Ni_a-C; §, Ni_a-SR; *, Ni_a-SR′; ♦, Ni_a-SR″.

attributable to the Ni_u-A state, if present at all, did not exceed the detection limit (<2%).

Reduced MBH—Upon exposure to 1 bar H_2 at pH 7.0, which results in a redox potential of −410 mV, the bands of the Ni_r-B state disappeared, and new bands were observed at lower wave numbers. According to previous data on standard [NiFe] hydrogenases (21), these bands are assigned to the fully reduced Ni_a-SR states. The most prominent stretching vibrations are located at 1926 and 1919 cm^{-1} in the CO region and some broader CN^- stretchings at 2071 and 2046 cm^{-1} (Fig. 7, *trace d*). These band pairs can be attributed to the Ni_a-SR′ and Ni_a-SR″ sub-states. Their band positions and relative intensities slightly change as a function of the pH. Re-oxidation of the reduced membrane sample in air or argon resulted in an FTIR spectrum identical to that obtained prior to H_2 reduction, irrespective of the pH value (Fig. 7, *trace e*). These findings clearly show that almost 100% of the membrane-attached MBH is reversibly redox-active.

Fig. 7 (*traces b* and *c*) illustrates the FTIR spectra of membrane samples at pH 5.5 reduced by applying different concentrations of H_2 in a nitrogen atmosphere. The spectrum of the aerobic as-isolated sample shows predominantly Ni_r-B and a small amount of another oxidized EPR-silent state, *e.g.* Ni_u-S, as observed at pH 7.0 (data not shown). Reduction with H_2 at 0.05 bar leads to the formation of a considerable amount of Ni_a-C (*trace b*), which was not observed at pH 7.0. Only small amounts of the Ni_a-SR′ and SR″ states were observed, probably because of the more positive redox potential (approximately −280 mV at pH 5.5). The observation of Ni_a-C with a characteristic CO stretching at 1957 cm^{-1} and corresponding CN stretching frequencies at 2075 and 2097 cm^{-1} is in agreement with the EPR spectra obtained from the same material at pH 5.5. Additionally, small amounts of the (Ni_r-S) Ni_a-S were found corresponding to the positions of the CO band at 1936 cm^{-1} and the CN^- bands at 2075 and 2093 cm^{-1}. This transitional state was also detectable in a time-resolved gas-exchange experiment (data not shown).

At a redox potential of −320 mV, which was achieved in the presence of 1 bar H_2 at pH 5.5, the relative amount of Ni_a-C is considerably lower (Fig. 7, *trace c*). Interestingly, all three substates of the fully reduced form are visible, *i.e.* Ni_a-SR, Ni_a-SR′, and Ni_a-SR″. The two CO bands assigned to the Ni_a-SR′ and SR″ states show different relative intensities as compared with the spectrum taken at pH 7.0. Also, the two dominant bands of the CN^- stretching modes are slightly shifted (2049 and 2075 cm^{-1}) and broadened and show different relative intensities compared with the spectrum at pH 7 (2046 and 2071 cm^{-1}). This comparison allows for a more reliable assignment of these bands to Ni_a-SR′ (1926, 2049, and 2075 cm^{-1}) and Ni_a-SR″ (1919, 2046, and 2071 cm^{-1}) (Table 2). Furthermore, Ni_a-SR is detectable with bands at 1946 (CO), 2068 (CN^-), and 2087 (CN^-) cm^{-1}.

DISCUSSION

The heterodimeric membrane-bound hydrogenase of *R. eutropha* H16 is composed of a large subunit containing the [NiFe] active site and a small subunit presumably harboring one [3Fe4S] and two [4Fe4S] clusters. This basic composition, including the specific cofactors, is similar to that of the well studied anaerobic standard [NiFe] hydrogenases. By applying FTIR spectroscopy and chemical quantification of the cyanide content, we present evidence that the catalytic center of the *R. eutropha* MBH is equipped with one CO and two CN^- ligands (see also Ref. 26).

In its native environment, the MBH has a trimeric structure, *i.e.* it is tightly bound to its primary electron acceptor, a membrane-integral cytochrome *b*. The treatment with detergent results in the detachment of MBH dimer from the membrane. The resulting solubilized MBH dimer has been repeatedly demonstrated to be suitable for electrochemical and electrocatalytic studies (11, 26). Because protein film voltammetry solely probes the electroactive protein, the inactive protein fraction does not influence the results in those experiments. The present EPR and FTIR results reveal that the solubilized dimeric MBH contains considerable amounts of the irreversibly inactive Ni_{ia}-S state, even after fast and mild purification by affinity chromatography. Nevertheless, the catalytic site active fraction of the solubilized MBH dimer exhibited the redox states known from oxygen-sensitive standard [NiFe] hydrogenases. Notably, the Ni_{ia}-S state within the MBH dimer could be detected and quantified only by FTIR spectroscopy, because this particular state is

EPR-silent. In EPR spectroscopic experiments, the heterogeneity of the solubilized enzyme samples just results in a lower net yield of EPR-visible signals. Therefore, we are not able to draw conclusions about the state composition of the catalytic site from the earlier studies on MBH dimer preparations, where FTIR spectroscopy was not applied (38, 39).

Because the spectroscopic experiments of solubilized dimeric MBH were hampered by the inactive enzyme fraction, a new approach focused on the preparation of an MBH sample in its native trimeric state. Thus, we performed FTIR and EPR studies on isolated cytoplasmic membrane fractions containing overproduced trimeric MBH, including the *b*-type cytochrome. To our knowledge, this is the first spectroscopic study on a membrane-bound [NiFe] hydrogenase in its native environment. Only the trimeric MBH preparation was found to be 100% reducible by H_2 and re-oxidizable to full extent with argon or air.

The integrated spectroscopic analysis by EPR and FTIR revealed that almost all functional [NiFe] states, which have been characterized in the standard [NiFe] hydrogenases of anaerobic bacteria, were also found in the MBH albeit with one remarkable exception. There was no indication for the presence of the oxygen-inactivated Ni_u-A state under any conditions. Ni_u-A represents a state in which an oxygen species, presumably a peroxo ligand (16, 17), blocks the active site. The resulting unready, inactive enzyme requires a long term reactivation with H_2 to acquire a catalytically active conformation. Two other hydrogenases in *R. eutropha*, the soluble, hexameric NAD^+-reducing hydrogenase and the cytoplasmic H_2-sensing hydrogenase, share the exceptional ability of being quickly reactivated after exposure to oxygen, and for none of them have Ni_u-A signals been detected (25, 61).

The prevention of forming the Ni_u-A state appears to be a prerequisite for H_2 catalysis in the presence of O_2 and represents a fundamental feature of the so-called oxygen-tolerant [NiFe] hydrogenases. This conclusion is strongly supported by the spectroscopic analysis of the O_2-tolerant hydrogenases from *R. metallidurans* CH34 (39), *A. aeolicus* (62), and *A. ferrooxidans* (51), all of which do not exhibit the Ni_u-A state.

In view of the close structural similarity of the *R. eutropha* MBH and other O_2-tolerant membrane-bound hydrogenases from *R. metallidurans* and *A. aeolicus* with anaerobic standard [NiFe] hydrogenases, the following question arises. What is the structural and/or functional basis for the observed O_2 tolerance?

FTIR spectroscopy on the different redox states of the [NiFe] active site shows that the trimeric membrane-attached oxidized form of the MBH mainly resides in the Ni_r-B state with a minor contribution of an unready and/or ready EPR silent state ($Ni_{u/r}$-S). Both states were found to react completely with H_2 and exhibit similar EPR and FTIR parameters as observed for anaerobic standard [NiFe] hydrogenases (21).[4] Upon reduction with H_2, the reduced Ni_a-C and Ni_a-L states, the fully reduced Ni_a-SR species as well as reduced $[4Fe4S]^+$ clusters were identified. During reduction and re-oxidation of the samples, the Ni_r-S/Ni_a-S states also were observed as intermediates. The redox-dependent stretching mode frequencies of the CO and CN^- ligands were in good agreement to those observed in standard [NiFe] hydrogenases. Only minor shifts of $\pm 5\ cm^{-1}$ were noted. A larger shift of up to $+10\ cm^{-1}$ was observed only for one CN^- stretching mode, indicating differences in the protein environment of one of the CN ligands. However, the generally small frequency deviations compared with the respective IR bands in standard [NiFe] hydrogenases allowed the identification of all functional redox states. This observation is in accordance with the notion that, apart from Ni_u-A, the active site of the trimeric MBH is very similar to that of standard hydrogenases.

In addition to the lack of Ni_u-A, another feature of the trimeric MBH was intriguing, namely the complex and split EPR signal attributed to the $[3Fe4S]^+$ cluster. A similar complex EPR spectrum of the $[3Fe4S]^+$ cluster has been observed previously for the solubilized membrane-bound hydrogenases of *R. metallidurans* (39) and *A. aeolicus* (62) as well as for the enzyme of *A. vinosum* (7, 63–65). In all three cases this signal has been attributed to a $[3Fe\text{-}4S]^+$ cluster magnetically coupled to another paramagnetic center (for an overview see supplemental Table S2). In the case of the *A. vinosum* MBH, it was proposed that the additional paramagnetic center could be either the Ni(III) in the Ni_r-B state of the active site (7, 63–65), or a cofactor X^{ox} that is only paramagnetic in its oxidized form and mediates a magnetic coupling between the Ni_r-B and the $[3Fe4S]^+$ cluster. This X^{ox} center was proposed to be either an additional Fe^{3+} species located between the [NiFe] site and the medial cluster, *i.e.* close to the proximal Fe-S cluster (7, 64, 66) or, alternatively, the proximal [4Fe4S] cluster itself in a high potential $[4Fe4S]^{3+}$ form (65).

Based on the present data only the two latter interpretations are plausible explanations for the unusual EPR signal of the $[3Fe4S]^+$ cluster in the *R. eutropha* MBH. A direct coupling between the Ni_r-B and the medial $[3Fe4S]^+$ cluster would require an exchange of the cluster positions resulting in a proximal $[3Fe4S]^+$ cluster and a medial [4Fe4S] cluster (39). Such a cluster exchange would explain the split signal of the oxidized $[3Fe4S]^{1+}$. However, the amino acid composition at the binding sites of the Fe-S clusters does not support this hypothesis, because the medial Fe-S cluster is coordinated by only three cysteine ligands, which is not sufficient for the coordination in a [4Fe4S] center (see supplemental Fig. S4). Moreover, we observed that in β-mercaptoethanol-treated samples of trimeric MBH (redox potential +40 mV), the split $[3Fe4S]^+$ EPR signal is converted completely into the narrow signal of an uncoupled $[3Fe4S]^+$. This conversion had no major effect on the Ni_r-B signal (except for a modified relaxation behavior) indicating that the $[3Fe4S]^+$ split EPR signal does not result from a direct magnetic coupling between $[3Fe4S]^+$ and Ni_r-B. This is supported by the observation that the FTIR bands related to the Ni_r-B state did not change upon mild reduction by β-mercaptoethanol (data not shown).

The $[3Fe4S]^+$ EPR spectra of *R. eutropha* H16 MBH are similar to those reported for the purified dimeric MBH of the closely related strain *R. metallidurans* CH34 that displayed the complex EPR signal only at high redox potentials (+323 mV) (39). This indicates that the splitting of the EPR signal is associated with the oxidation of the postulated cofactor X (X^{ox}). Such a cofactor is in full agreement with the observation that the *R. eutropha* H16 MBH exhibits the complex $[3Fe4S]^+$ EPR

split signal at a redox potential of +290 mV, which transforms to a narrow signal at lower redox potential of +40 mV (Fig. 4). The latter signal is generally indicative for an uncoupled $[3Fe4S]^+$ center (7, 62, 64, 66).

Notably, the relaxation behavior of Ni_r-B in *R. eutropha* MBH was found to be different from that of standard hydrogenases. At high redox potential (+290 mV), the Ni_r-B signals vanished at temperatures above 60 K. This demonstrates that the proposed high potential paramagnetic species that causes the split EPR signal of $[3Fe4S]^+$ leads, by weak magnetic interaction, also to enhanced spin relaxation of Ni_r-B. This indicates a close proximity to the medial [3Fe4S] cluster and also a proximity to the active site nickel. The proposed high potential species is therefore consistent with the presence of an additional iron close to the position of the proximal [4Fe4S] cluster or, alternatively, with the presence of an oxidized high potential $[4Fe4S]^{3+}$ at the proximal position.

The presence of an additional metal ion at medium distance to the [Ni-Fe] active site is known for some [NiFe] hydrogenases, whose structures have been solved. In case of *Desulfomicrobium baculatum* (67) and *Desulfovibrio desulfuricans* (58) iron and magnesium were identified, respectively. Such an additional metal species (as X^{ox}) has not yet been found in the *R. eutropha* H16 MBH.

Further indication for an additional high potential paramagnetic species with $S = 1/2$ is based on the integral signal intensity of the complex split $[3Fe\text{-}4S]^+$ EPR signal, corresponding to more than one spin per protein (supplemental Table S1), whereas the narrow $[3Fe\text{-}4S]^+$ EPR signal corresponds to one spin per protein.

Significant differences as compared with anaerobic standard hydrogenases were also found in the EPR spectra of the reduced [NiFe] and [4Fe4S] states. In the case of anaerobic standard [NiFe] hydrogenases, a strong coupling is observed between Ni-C and the reduced proximal [4Fe4S] cluster. The temperature-dependent EPR spectra of the MBH, incubated with H_2 showed, however, no indication for a magnetic coupling between Ni_a-C/Ni_a-L and reduced [4Fe4S]. This finding indicates that the electron, which is released by the heterolytic cleavage of H_2 resulting in the Ni_a-C state, is transferred all the way to the terminal [4Fe4S] cluster of the MBH. This cluster, however, is too far away from the catalytic site to induce coupled EPR signals of Ni_a-C/Ni_a-L. Moreover, relative spin quantification of the MBH for the reduced signal showed only 50% of the intensity as compared with the split signal indicating only one reduced [4Fe4S] cluster per protein after incubation with 1 bar H_2. This again indicates a unique redox behavior of the proximal Fe-S cluster in *R. eutropha* MBH.

The peculiar spectroscopic features of the *R. eutropha* MBH point to a modification at or near the proximal Fe-S cluster, whereas the active [NiFe] site seems to have a highly similar structure as compared with anaerobic standard [NiFe] hydrogenases. This is supported by the results of a recent biochemical and electrochemical investigation of the MBH (34). The exchange of amino acids close to the active site, which are unique in the MBH and closely related O_2-tolerant hydrogenases, revealed mutant proteins with a significantly lowered K_i toward oxygen. However, these MBH variants still showed a considerable O_2 tolerance, which was still orders of magnitude higher that that of O_2-sensitive standard [NiFe] hydrogenases (34). These results indicate that the reason for O_2 tolerance may not be intimately related to the unique amino acid composition in the first coordination shell of the MBH active site. The oxygen tolerance could be explained by an alteration of the proximal Fe-S cluster being functional in preventing the formation of the oxygen-inhibited Ni_u-A state. Remarkably, there are two additional cysteine residues in close vicinity to the proximal [4Fe4S] cluster that are absent in oxygen-sensitive standard [NiFe] hydrogenases (see supplemental Fig. S4). These two additional cysteines may play a crucial role in the unusual redox potential dependent splitting of the $[3Fe4S]^+$ EPR signal and might provide additional binding sites for an unusual proximal cluster, of higher complexity than a standard-type cubane. Interestingly, these two additional cysteines are only conserved in other membrane-bound hydrogenases, like those from *R. metallidurans* (39) and *A. aeolicus* (62), which have been shown to be or are proposed to be O_2-tolerant (supplemental Fig. S4).

Further studies, including the construction of *R. eutropha* MBH mutant proteins with altered coordination of the proximal and medial iron-sulfur clusters, are envisaged to explore their detailed structure and their potential role in the unusual oxygen tolerance of the membrane-bound hydrogenases from aerobic H_2-oxidizing bacteria.

Acknowledgments—We are grateful to Wolfgang Lubitz and Maria Pandelia (Max Plank Institute) for providing a hydrogenase sample from D. vulgaris Miyazaki F and for helpful discussions. Robert Bittl is gratefully acknowledged for helpful discussions. Metal analyses have been performed with the help of Silke Leimkühler and Meina Neumann using ICP-OES (University of Potsdam).

REFERENCES

1. Cammack, R., Frey, M., and Robson, R. (eds) (2001) *Hydrogen As a Fuel: Learning from Nature*, Taylor and Francis Ltd., London
2. Volbeda, A., Charon, M. H., Piras, C., Hatchikian, E. C., Frey, M., and Fontecilla-Camps, J. C. (1995) *Nature* **373,** 580–587
3. Higuchi, Y., Yagi, T., and Yasuoka, N. (1997) *Structure* **5,** 1671–1680
4. Peters, J. W., Lanzilotta, W. N., Lemon, B. J., and Seefeldt, L. C. (1998) *Science* **282,** 1853–1858
5. Nicolet, Y., Piras, C., Legrand, P., Hatchikian, C. E., and Fontecilla-Camps, J. C. (1999) *Struct. Fold. Design* **7,** 13–23
6. Pilak, O., Mamat, B., Vogt, S., Hagemeier, C. H., Thauer, R. K., Shima, S., Vonrhein, C., Warkentin, E., and Ermler, U. (2006) *J. Mol. Biol.* **358,** 798–809
7. Surerus, K. K., Chen, M., van der Zwaan, J. W., Rusnak, F. M., Kolk, M., Duin, E. C., Albracht, S. P., and Münck, E. (1994) *Biochemistry* **33,** 4980–4993
8. Albracht, S. P. (1994) *Biochim. Biophys. Acta* **1188,** 167–204
9. Volbeda, A., Garcia, E., Piras, C., de Lacey, A. L., Fernandez, V. M., Hatchikian, E. C., Frey, M., and Fontecilla-Camps, J. C. (1996) *J. Am. Chem. Soc.* **118,** 12989–12996
10. Pierik, A. J., Roseboom, W., Happe, R. P., Bagley, K. A., and Albracht, S. P. (1999) *J. Biol. Chem.* **274,** 3331–3337
11. Vincent, K. A., Parkin, A., Lenz, O., Albracht, S. P., Fontecilla-Camps, J. C., Cammack, R., Friedrich, B., and Armstrong, F. A. (2005) *J. Am. Chem. Soc.* **127,** 18179–18189
12. Adams, M. W. (1990) *Biochim. Biophys. Acta* **1020,** 115–145
13. Cammack, R., Fernandez, V. M., and Schneider, K. (1986) *Biochimie* **68,** 85–91

14. Bleijlevens, B., van Broekhuizen, F. A., De Lacey, A. L., Roseboom, W., Fernandez, V. M., and Albracht, S. P. (2004) *J. Biol. Inorg. Chem.* **9,** 743–752
15. Lamle, S. E., Albracht, S. P., and Armstrong, F. A. (2004) *J. Am Chem. Soc.* **126,** 14899–14909
16. Ogata, H., Hirota, S., Nakahara, A., Komori, H., Shibata, N., Kato, T., Kano, K., and Higuchi, Y. (2005) *Structure* **13,** 1635–1642
17. Volbeda, A., Martin, L., Cavazza, C., Matho, M., Faber, B. W., Roseboom, W., Albracht, S. P., Garcin, E., Rousset, M., and Fontecilla-Camps, J. C. (2005) *J. Biol. Inorg. Chem.* **10,** 239–249
18. Lubitz, W., Reijerse, E., and van Gastel, M. (2007) *Chem. Rev.* **107,** 4331–4365
19. Fernandez, V. M., Hatchikian, E. C., and Cammack, R. (1985) *Biochim. Biophys. Acta* **832,** 69–79
20. Brecht, M., van Gastel, M., Buhrke, T., Friedrich, B., and Lubitz, W. (2003) *J. Am. Chem. Soc.* **125,** 13075–13083
21. Kurkin, S., George, S. J., Thorneley, R. N., and Albracht, S. P. (2004) *Biochemistry* **43,** 6820–6831
22. Aragno, M., and Schlegel, H. G. (1992) in *The Prokaryotes* (Balows, H. G., Trüper, H. G., Dworkin, M., Harder, W., and Schleifer, K. H., eds) pp. 344–384, Springer-Verlag Inc., New York
23. Friedrich, B., and Schwartz, E. (1993) *Annu. Rev. Microbiol.* **47,** 351–383
24. Vignais, P. M., and Billoud, B. (2007) *Chem. Rev.* **107,** 4206–4272
25. Burgdorf, T., Löscher, S., Liebisch, P., Van der Linden, E., Galander, M., Lendzian, F., Meyer-Klaucke, W., Albracht, S. P., Friedrich, B., Dau, H., and Haumann, M. (2005) *J. Am. Chem. Soc.* **127,** 576–592
26. Vincent, K. A., Cracknell, J. A., Lenz, O., Zebger, I., Friedrich, B., and Armstrong, F. A. (2005) *Proc. Natl. Acad. Sci. U. S. A.* **102,** 16951–16954
27. Buhrke, T., Lenz, O., Krauss, N., and Friedrich, B. (2005) *J. Biol. Chem.* **280,** 23791–23796
28. Van der Linden, E., Burgdorf, T., Bernhard, M., Bleijlevens, B., Friedrich, B., and Albracht, S. P. (2004) *J. Biol. Inorg. Chem.* **9,** 616–626
29. Happe, R. P., Roseboom, W., Egert, G., Friedrich, C. G., Massanz, C., Friedrich, B., and Albracht, S. P. (2000) *FEBS Lett.* **466,** 259–263
30. Duché, O., Elsen, S., Cournac, L., and Colbeau, A. (2005) *FEBS J.* **272,** 3899–3908
31. Bernhard, M., Benelli, B., Hochkoeppler, A., Zannoni, D., and Friedrich, B. (1997) *Eur. J. Biochem.* **248,** 179–186
32. Schink, B., and Schlegel, H. G. (1979) *Biochim. Biophys. Acta* **567,** 315–324
33. Kortlüke, C., Horstmann, K., Schwartz, E., Rohde, M., Binsack, R., and Friedrich, B. (1992) *J. Bacteriol.* **174,** 6277–6289
34. Ludwig, M., Cracknell, J. A., Vincent, K. A., Armstrong, F. A., and Lenz, O. (2009) *J. Biol. Chem.* **284,** 465–477
35. De Lacey, A. L., Fernandez, V. M., Rousset, M., and Cammack, R. (2007) *Chem. Rev.* **107,** 4304–4330
36. Vincent, K. A., Cracknell, J. A., Clark, J. R., Ludwig, M., Lenz, O., Friedrich, B., and Armstrong, F. A. (2006) *Chem. Commun.* **28,** 5033–5035
37. Ihara, M., Nishihara, H., Yoon, K. S., Lenz, O., Friedrich, B., Nakamoto, H., Kojima, K., Honma, D., Kamachi, T., and Okura, I. (2006) *Photochem. Photobiol.* **82,** 676–682
38. Schneider, K., Patil, D. S., and Cammack, R. (1983) *Biochim. Biophys. Acta* **748,** 353–361
39. Knüttel, K., Schneider, K., Erkens, A., Plass, W., Müller, A., Bill, E., and Trautwein, A. X. (1994) *Bull. Pol. Acad. Sci. Chem.* **42,** 495–511
40. Bagley, K. A., Duin, E. C., Roseboom, W., Albracht, S. P., and Woodruff, W. H. (1995) *Biochemistry* **34,** 5527–5535
41. Fichtner, C., Laurich, C., Bothe, E., and Lubitz, W. (2006) *Biochemistry* **45,** 9706–9716
42. De Lacey, A. L., Hatchikian, E. C., Volbeda, A., Frey, M., Fontecilla-Camps, J. C., and Fernandez, V. M. (1997) *J. Am. Chem. Soc.* **119,** 7181–7189
43. Lenz, O., Gleiche, A., Strack, A., and Friedrich, B. (2005) *J. Bacteriol.* **187,** 6590–6595
44. Witholt, B., Boekhout, M., Brock, M., Kingma, J., van Heerikhuizen, H., and Leij, L. D. (1976) *Anal. Biochem.* **74,** 160–170
45. Schwartz, E., Gerischer, U., and Friedrich, B. (1998) *J. Bacteriol.* **180,** 3197–3204
46. Schubert, T., Lenz, O., Krause, E., Volkmer, R., and Friedrich, B. (2007) *Mol. Microbiol.* **66,** 453–467
47. Bradford, M. M. (1976) *Anal. Biochem.* **72,** 248–254
48. Laemmli, U. K. (1970) *Nature* **227,** 680–685
49. Stesmans, A., and Vangorp, G. (1989) *Rev. Sci. Instrum.* **60,** 2949–2952
50. Stoll, S., and Schweiger, A. (2006) *J. Magn. Res.* **178,** 42–55
51. Schröder, O., Bleijlevens, B., de Jongh, T. E., Chen, Z., Li, T., Fischer, J., Förster, J., Friedrich, C. G., Bagley, K. A., Albracht, S. P., and Lubitz, W. (2007) *J. Biol. Inorg. Chem.* **12,** 212–233
52. Foerster, S., Stein, M., Brecht, M., Ogata, H., Higuchi, Y., and Lubitz, W. (2003) *J. Am. Chem. Soc.* **125,** 83–93
53. Trofanchuk, O., Stein, M., Gessner, C., Lendzian, F., Higuchi, Y., and Lubitz, W. (2000) *J. Biol. Inorg. Chem.* **5,** 36–44
54. van Gastel, M., Stein, M., Brecht, M., Schröder, O., Lendzian, F., Bittl, R., Ogata, H., Higuchi, Y., and Lubitz, W. (2006) *J. Biol. Inorg. Chem.* **11,** 41–51
55. Foerster, S., van Gastel, M., Brecht, M., and Lubitz, W. (2005) *J. Biol. Inorg. Chem.* **10,** 51–62
56. Dole, F., Medina, M., More, C., Cammack, R., Bertrand, P., and Guigliarelli, B. (1996) *Biochemistry* **35,** 16399–16406
57. Podzuweit, H. G., Schneider, K., and Knüttel, H. (1987) *Biochim. Biophys. Acta* **905,** 435–446
58. Rousset, M., Montet, Y., Guigliarelli, B., Forget, N., Asso, M., Bertrand, P., Fontecilla-Camps, J. C., and Hatchikian, E. C. (1998) *Proc. Natl. Acad. Sci. U. S. A.* **95,** 11625–11630
59. Agrawal, A. G., van Gastel, M., Gärtner, W., and Lubitz, W. (2006) *J. Phys. Chem. B.* **110,** 8142–8150
60. Fichtner, C., van Gastel, M., and Lubitz, W. (2003) *Phys. Chem. Chem. Phys.* **5,** 5507–5513
61. Buhrke, T., Löscher, S., Lenz, O., Schlodder, E., Zebger, I., Andersen, L. K., Hildebrandt, P., Meyer-Klaucke, W., Dau, H., Friedrich, B., and Haumann, M. (2005) *J. Biol. Chem.* **280,** 19488–19495
62. Brugna-Guiral, M., Tron, P., Nitschke, W., Stetter, K. O., Burlat, B., Guigliarelli, B., Bruschi, M., and Giudici-Orticoni, M. T. (2003) *Extremophiles* **7,** 145–157
63. Albracht, S. P., Albrechtellmer, K. J., Schmedding, D. J., and Slater, E. C. (1982) *Biochim. Biophys. Acta* **681,** 330–334
64. Albracht, S. P., Vanderzwaan, J. W., and Fontijn, R. D. (1984) *Biochim. Biophys. Acta* **766,** 245–258
65. Albracht, S. P., Kalkman, M. L., and Slater, E. C. (1983) *Biochim. Biophys. Acta* **724,** 309–316
66. Coremans, J. M., van der Zwaan, J. W., and Albracht, S. P. (1992) *Biochim. Biophys. Acta* **1119,** 157–168
67. Garcin, E., Vernede, X., Hatchikian, E. C., Volbeda, A., Frey, M., and Fontecilla-Camps, J. C. (1999) *Structure* **7,** 557–566

6 Comparative investigation of the ready oxidized state of the membrane bound [NiFe]-hydrogenases from *Ralstonia eutropha* H16 and *D. vulgaris* Miyazaki F by pulsed EPR spectroscopy

M. Saggu, C. Teutloff, M. Ludwig, M. Brecht, M. Pandelia, B. Friedrich, W. Lubitz, P. Hildebrandt, F. Lendzian and R. Bittl

Phys. Chem. Chem. Phys., in press

Comparative investigation of the oxidized ready state of the membrane-bound [NiFe] hydrogenases from *R. eutropha* H16 and *D. vulgaris* Miyazaki F by pulsed EPR spectroscopy†

Miguel Saggu,[a] Christian Teutloff,[b] Marcus Ludwig,[c] Marc Brecht,[b] Maria-Eirini Pandelia,[d] Oliver Lenz,[c] Bärbel Friedrich,[c] Wolfgang Lubitz,[a] Peter Hildebrandt,[a] Friedhelm Lendzian[a] and Robert Bittl*[b]

Received 23rd October 2009, Accepted 7th December 2009
First published as an Advance Article on the web
DOI: 10.1039/b922236g

The geometric and electronic structures of the active sites in the oxidized Ni_r–B state of the [NiFe] hydrogenases from *Ralstonia eutropha* H16 and *Desulfovibrio vulgaris* Miyazaki F were investigated in pulsed EPR and ENDOR experiments at two different microwave frequencies (X- and Q-band). Two hyperfine-couplings were clearly resolved in the frozen solution spectra arising from the β-protons of the nickel-coordinating cysteine residues Cys549 and Cys586 from the *Desulfovibrio vulgaris* and *Ralstonia eutropha* hydrogenase, respectively. ESEEM spectroscopic experiments indicated the presence of a histidine in the second coordination sphere of the Ni. The spectroscopic data indicate that the electronic structures of the [NiFe] centers in both hydrogenases are identical in the Ni_r–B state. However, additional spin couplings of the active site to further paramagnetic centers were identified for the *Ralstonia eutropha* hydrogenase. The respective couplings could be clearly resolved and simulated. The results from this study are discussed in view of the exceptional O_2-tolerance of *Ralstonia eutropha* hydrogenase.

Introduction

Hydrogenases catalyze the reversible cleavage of H_2 into two protons and two electrons ($H_2 \rightleftharpoons 2H^+ + 2e^-$) and play an important role in the energy metabolism of a variety of microorganisms.[1]

Hydrogenases are metalloenzymes that are classified according to their metal content into the three distinct classes of di-iron [FeFe]-, nickel-iron [NiFe]- and mono-iron [Fe]-hydrogenases.[2–6] The basic module of [NiFe]-hydrogenases consists of two polypeptides, a large subunit which harbors the [NiFe] active site, and a small subunit which binds one to three electron-transferring iron–sulfur clusters.[2,7,8] The active site Ni is coordinated to the protein *via* four thiol groups originating from conserved cysteine residues. Two of these cysteines serve as bridging ligands to the Fe in the active site. The Fe atom in the active site carries three additional inorganic ligands, two CN^- and one CO, which keep the iron in a low-spin state.[9,10] In addition to H_2, the active sites of anaerobic [FeFe]- and [NiFe]-hydrogenases react with dioxygen. In the case of the [FeFe]-hydrogenases, this usually leads to an irreversible destruction of the active site.[11,12] [NiFe]-hydrogenases, however, are in most cases reversibly inactivated by molecular oxygen.[13,14] Under electron-rich conditions in the presence of O_2 a mono-oxo species, most probably a hydroxide, is formed in the bridging position between Ni and Fe.[15–18] This 'ready inactive' Ni_r–B state is characterized by a paramagnetic EPR signal with characteristic g-values of 2.33, 2.16 and 2.01 (see Scheme 1). Incubation of the enzyme with O_2 under electron-poor conditions results in the so-called 'unready inactive' Ni_u-A state. X-Ray crystallography provides evidence that a di-oxo species (hydro-peroxide) binds in the bridging position.[16,17] However, a hydro-peroxide as bridging ligand is still a matter of debate.[19] The Ni_u-A and Ni_r–B states differ significantly in their reactivation kinetics. H_2-mediated reductive activation of the Ni_u-A state is a long-term process that requires hours until the oxygen species is completely removed from the active site. In contrast, only seconds of incubation with H_2 are necessary to convert the Ni_r–B state into the catalytically active EPR-detectable Ni_a–C state in which a hydride occupies the bridging position between Ni and Fe.[20,21] The formation of the Ni_u-A state prevents the standard [NiFe]-hydrogenases from being catalytically active under aerobic conditions.

However, the so-called 'Knallgasbacteria' contain [NiFe]-hydrogenases, which enable these microorganisms to gain energy from H_2 oxidation at ambient O_2 levels.[22–24] A prominent example is the chemolithoautotrophic model organism *Ralstonia eutropha* H16 (*Re*), which harbors three distinct [NiFe] hydrogenases catalyzing H_2 oxidation in the presence of ambient oxygen concentrations.[11,25,26] It has been demonstrated previously that the O_2-tolerance of the *Re* hydrogenases is based on at least two different molecular mechanisms. A modified active site has been proposed for the cytoplasmic,

[a] *Technische Universität Berlin, Strasse des 17. Juni 135, 10623 Berlin*
[b] *Freie Universität Berlin, Arnimallee 14, 14195 Berlin. E-mail: Robert.Bittl@FU-Berlin.DE*
[c] *Humboldt-Universität zu Berlin, Chausseestrasse 117, 10115 Berlin*
[d] *Max-Planck-Institut für Bioanorganische Chemie, Stiftstr. 34-36, 45470 Mülheim an der Ruhr*

† Electronic supplementary information (ESI) available: X-Band cw-EPR spectra of reoxidized hydrogenase from *D. vulgaris* Miyazaki F. See DOI: 10.1039/b922236g

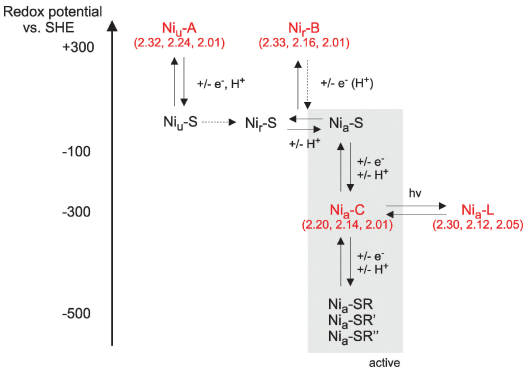

Scheme 1 Redox states observed in standard [NiFe]-hydrogenases.[19,33] Paramagnetic states with S = 1/2 ground state are shown in red. The g-values are taken from the *Dv* H_2ase (numbers in parentheses).[48,57]

NAD^+-reducing soluble hydrogenase (SH). An extra CN^- ligand is postulated to be bound to the Ni to protect the enzyme from assuming the oxidized Ni_u-A state.[25,27,28] In case of the regulatory hydrogenase (RH) from *Re*, which acts as a hydrogen sensor, O_2 resistance is probably based on a narrow gas tunnel that completely prevents access of O_2 to the active site and thereby avoids the formation of the oxidized Ni_u-A and Ni_r–B states.[29] The third H_2-cycling enzyme in *Re* is a membrane-bound [NiFe]-hydrogenase (MBH), consisting of the large subunit HoxG (67.1 kDa) and the small subunit HoxK (34.6 kDa).[30] A hydrophobic peptide located at the C-terminus of HoxK anchors the MBH to the membrane integral *b*-type cytochrome HoxZ.[30–32] FTIR spectroscopy revealed that the active site iron is coordinated with a standard set of diatomic ligands, two CN^- and one CO. Furthermore, all redox states known from anaerobic standard [NiFe]-hydrogenases were found for the MBH, except for the most oxidized Ni_u-A state.[26,33] Previous mutagenesis studies revealed that single amino acids unique in the second coordination shell of the MBH active site cannot be accounted for the O_2-tolerance of the MBH enzyme. Also, the O_2-tolerance was not enhanced narrowing the proposed gas tunnel.[34] These results point to the existence of a diverse mechanism for O_2-tolerance in the MBH that is different to those in SH and RH.

EPR spectroscopy is a valuable tool for providing information on the composition of cofactors and dynamic structure/function relationships even if a crystal structure of the enzyme is not yet available.[19] In the case of [NiFe]-hydrogenases, EPR allows the detection of redox-dependent electronic structures of the [NiFe] active site and the electron-transferring FeS clusters in all states that are paramagnetic (see Scheme 1). Diamagnetic redox species, which occur in the hydrogenases catalytic cycle, are invisible by this technique.

Earlier EPR measurements on MBH protein solubilized from the membrane and MBH embedded within the cytoplasmic membranes led to the identification of three iron–sulfur clusters in the small subunit HoxK, two [4Fe–4S] clusters and one [3Fe–4S] cluster. The Ni_r–B, Ni_a–C and Ni_a-L states of the MBH active site were deduced from their characteristic g-values (see Scheme 1). Their relative amounts, however, varied significantly depending on the preparation method.[13,33,35]

Pulsed EPR is of advantage to probe broad spectra which are usually found in hydrogenases.[19] The unpaired electron is usually located in the d-orbitals of the metal center, which leads to strong deviation from the g-factor of the free electron and large g-anisotropy. To directly detect hydrogen atoms in paramagnetic metal centers, *e.g.* the [NiFe] active site, electron nuclear double resonance (ENDOR) is a valuable tool.[18,36] A complementary technique to ENDOR that monitors the nuclei-induced electron spin-echo modulations (ESEEM) is of advantage to detect nuclei with small magnetogyric ratios such as ^{14}N or ^2H.[37]

In order to obtain insights into the mechanism of O_2-tolerance, we have undertaken a detailed characterization of the [NiFe] active site of the *Re* MBH. In this respect, the oxidized Ni_r–B state is of particular interest because it is clearly different from O_2-sensitive standard hydrogenases due to additional couplings and an additional paramagnetic center of unknown origin.[33] In this work we analyzed the ready state Ni_r–B of the *Re* MBH using pulsed EPR spectroscopy and compared our results to the O_2-sensitive standard [NiFe]-hydrogenase from *D. vulgaris* Miyazaki F (*Dv*), which has been thoroughly investigated by multiple EPR techniques and for which a crystal structure at high-resolution is available.[3,16] Owing to the fact that the *Re* MBH solubilized from the membrane contains a large amount of an irreversible inactive state (diamagnetic Ni^{2+} state), we used in our experiments exclusively membrane fragments that harbored overproduced MBH.[33] The catalytic site of oxidized MBH embedded in the cytoplasmic membrane persists in an almost pure Ni_r–B state (80%). The remaining 20% of the protein are

in the diamagnetic Ni_u–S state and do not contribute to the EPR signal.[33]

Experimental

Preparation of cytoplasmic membranes containing *Re* MBH

The *Re* MBH was over-produced using plasmid pLO6 in *R. eutropha* strain HF631.[38] Cells were cultivated and the cytoplasmic membrane was prepared as described by Saggu *et al.*[33]

Preparation of the D. *vulgaris* Miyazaki F wild-type hydrogenase

The [NiFe] hydrogenase from *D. vulgaris* Miyazaki F was isolated and purified from 50 L cultures as described previously.[39] The purified enzyme was kept in pH 7.4 Tris-HCl buffer for all experiments.

Sample treatment

The [NiFe]-hydrogenase from *D. vulgaris* Miyazaki F contains in the as-isolated form a mixture of Ni_u-A and Ni_r–B. To obtain a maximum amount of Ni_r–B, the sample was treated as described by Agrawal *et al.*[40] After 2 h of incubation under hydrogen at 37 °C in an EPR tube, the sample was reoxidized in air for 5 min. This procedure resulted in almost 85% Ni_r–B and 15% Ni_u-A, respectively

For ENDOR experiments the sample of *Re* MBH was repeatedly exchanged with D_2O buffer and incubated for 2 d. Subsequently, the sample was centrifuged into the Q-band EPR tube.

Experimental setup

9.5 GHz X-band cw-EPR spectroscopy has been carried out on a Bruker ESP300E spectrometer equipped with a rectangular microwave cavity working in the TE_{102} mode. For low temperature measurements the sample was kept in an Oxford ESR 900 helium flow cryostat controlled by an Oxford ITC502 temperature controller. The microwave frequency was measured with an EIP frequency counter (Microwave Inc.). For determination of g-values the magnetic field was calibrated with an external LiLiF standard with a known g-value of 2.002293.[41]

X-Band pulsed EPR studies were performed on a Bruker E580 ELEXSYS spectrometer equipped with a dielectric ring resonator (EN4118X-MD4) and a SuperX-FT microwave bridge. The temperature was controlled with an Oxford ITC503 temperature controller and cryogenic temperatures were reached with an Oxford CF935 flow cryostat. The microwave was amplified either with a Bruker AmpX10 solid-state or a TWT (ASE 117X, 1kW) microwave amplifier.

Q-Band EPR/ENDOR experiments were performed on the same spectrometer using a home-built Q-band ENDOR resonator and a SuperQ-FT microwave bridge. The minimal achieved π_{mw}-pulse duration is 40 ns and the minimal π_{rf}-pulse duration 20 μs. Low temperatures were reached with an Oxford CF935 flow cryostat. Davies-ENDOR experiments were recorded in stochastic acquisition mode using a Bruker E560 DICE ENDOR accessory and an Amplifier Research 250A250A RF amplifier.

Pulse EPR methods and evaluation of spectra

X-Band EPR spectra were recorded at a microwave frequency of 9.7 GHz using a Hahn-echo pulse sequence ($\pi/2 - \tau - \pi - \tau$ – echo). The length for the microwave π pulse was 128 ns for the *Dv* H_2ase and the partially reduced *Re* MBH and 40 ns for the isolated *Re* H16 MBH.

Q-Band field-swept echos were obtained at a microwave frequency of 34 GHz with the same pulse sequence as used for X-band experiments. The used microwave π pulse had a length of 160 ns for the *Dv* H_2ase and 128 ns for the *Re* MBH. For the simulations of the *Re* MBH EPR spectra the first derivative was used, which was obtained by pseudomodulation of the spectra.[42]

ENDOR-spectra ($\pi_{mw} - \pi_{rf} - \pi/2_{mw} - \tau - \pi_{mw} - \tau$ – echo) for reoxidized *Dv* H_2ase and partially reduced *Re* MBH were recorded at $T = 10$ K where the best signal/noise ratio could be achieved. The used π_{rf} pulse had a length of 20 μs, the π_{mw} pulse length was 160 ns for *Dv* H_2ase and 128 ns for *Re* MBH. The ENDOR and EPR spectra were simulated using the MATLAB[43] toolbox *EasySpin* (version 3.0.0).[44] For simulations the method of full matrix-diagonalization of the Spin-Hamiltonian was used.

3pulse *vs.* 2pulse X-band ESEEM ($\pi/2 - \tau - \pi/2 - T - \pi/2 - \tau$ – echo) spectra were recorded at 8 K at the g_y position of Ni_r–B ($g = 2.16$ for *Dv* H_2ase, $g = 2.17$ for *Re* MBH) with 256 × 32 data points (*Dv* H_2ase) and 512 × 32 data points (*Re* MBH). The spectra were obtained using a $\pi/2$ pulse of 16 ns length for *Dv* H_2ase and 8 ns for *Re* MBH. A 4-step phase cycle was used to get rid of unwanted echos.[45] The time traces were baseline corrected using a polynomial function of 3rd order. Then the spectra were treated with a hamming apodization function and the number of points was increased by zero-filling to 512 × 32 (*Dv* H_2ase) and 1024 × 32 (*Re* MBH). After Fourier transformation the skyline-projection of the absolute spectra was plotted to minimize blind spots.

For ^{14}N nuclei that are not directly coordinated to the spin center the case of 'exact cancellation' in ESEEM can often be observed, *e.g.* in [NiFe]-hydrogenases.[40,46] When the nuclear Zeeman interaction is equal to half the effective hyperfine coupling ($\nu_N \approx |A|/2$), hyperfine and nuclear Zeeman interaction 'cancel' each other in one spin manifold. The remaining interactions in this manifold are then due to quadrupole interactions of nuclei with $I \geq 1$, and yield information on the charge distribution around this nucleus. From the charge distribution one can get information on the type of bonding such as protonation state, the chemical environment and the type of the involved amino acid.[37] Three sharp lines at low frequencies can be observed in the ESEEM spectrum (ν_0, ν_-, ν_+). From the magnitude of these frequencies, the nuclear quadrupole coupling constant e^2qQ/h and the asymmetry parameter η can be estimated according to:[37,47]

$$\nu_0 = 2\ \mathrm{K}\eta,\ \nu_- = K(3 - \eta),\ \nu_+ = K(3 + \eta) \qquad (1)$$

$$\text{with}\ \ K = \frac{e^2qQ}{4h}\ \ \text{and}\ \ \eta = \frac{q_{xx} - q_{yy}}{q_{zz}} \qquad (2)$$

These two parameters are dependent on the size and symmetry

of the nuclear quadrupole interaction and directly related to the traceless quadrupole tensor $\boldsymbol{P}$.

$$\boldsymbol{P} = K[(\eta - 1), (-\eta - 1), 2] \quad (3)$$

Q is the scalar nuclear quadrupole moment and the q_{ii} are the principal components of the electric field gradient at the nucleus.

In the spectrum an additional weak band can be observed due to a double-quantum transition ($\Delta m_I = 2$) in the non-cancelled second spin manifold. From this transition an effective hf-coupling can be estimated occurring at a frequency of:[37]

$$\nu_{\mathrm{dq}}^{\pm} = 2\left[\left(\frac{A}{2} \pm \nu_N\right)^2 + K^2(3 + \eta^2)\right]^{1/2} \quad (4)$$

The isotropic and anisotropic parts of the hf-coupling contribute to A.

Results

EPR

Pulsed EPR experiments on the oxidized Ni_r–B states of the standard [NiFe]-hydrogenase from *Desulfovibrio vulgaris* Miyazaki F (*Dv* H_2ase) and the membrane-bound [NiFe]-hydrogenase from *Ralstonia eutropha* H16 (*Re* MBH) were carried out at two different microwave frequencies (X- and Q-band). Thus it is possible to disentangle field-dependent (Zeeman) and field-independent interactions (hyperfine, quadrupole) of the Spin-Hamiltonian.

In order to maximize the Ni_r–B content in the *Dv* H_2ase, the protein samples were treated as described in the Experimental section. This resulted in a relative amount of about 85% Ni_r–B and 15% Ni_u-A (ESI†) as shown in previous experiments.[40] The Ni_r–B state already dominates in *Re* MBH residing in aerobically isolated cytoplasmic membranes.[33] Fig. 1A shows the X-band field-swept echo-detected spectra of the *Dv* H_2ase (trace a) and *Re* MBH (traces b and c). In the spectrum of *Dv* H_2ase (trace a), a sharp signal at $g = 2$ arises from an oxidized $[3Fe4S]^+$-cluster with S = 1/2 ground state. In the expanded view in the low-field region, the signals from the [NiFe] center are visible. The superposition of Ni_u-A (g-values 2.32, 2.24, 2.01) and Ni_r–B (g-values 2.33, 2.16, 2.01) both with a formal Ni(III) oxidation state can be clearly distinguished using EPR spectroscopy due to their characteristic g-values.[16,18,48]

In contrast to the *Dv* H_2ase, the *Re* MBH (trace b) shows a very complex EPR spectrum. Around $g = 2.0$, where the signal of the $[3Fe4S]^+$-cluster is expected, a broad and highly structured signal appears that cannot be attributed to a single $[3Fe4S]^+$-cluster. In previous studies this signal was attributed to a $[3Fe4S]^+$-cluster coupled to an unknown paramagnetic center.[33] The signal intensity corresponds to two spins/protein, indicating that the unknown center is a S = 1/2 system, which was estimated earlier (see discussion).[33] In the region where the Ni-signals are expected, no clearly resolved g-tensor of Ni_r–B or Ni_u-A can be observed.[33] The Ni-signals are broadened and partially overlapping with the complex FeS-signal.

After partial reduction by the addition of β-mercaptoethanol ($E = +40$ mV), the spectrum of the *Re* MBH becomes similar to a 'standard hydrogenase' (trace c). A rhombic tensor is visible in the Ni region which can be attributed to one single Ni species. The g_x- and g_y-values are 2.30 and 2.17, which is in agreement with Ni_r–B in standard [NiFe]-hydrogenases.[19,33]

To obtain a higher spectral resolution, all samples were measured in Q-band as well. The corresponding Q-band field-swept echo spectra are displayed in Fig. 1B. Trace a shows the field-swept echo-detected EPR spectrum of the reoxidized *Dv* H_2ase with well resolved g_x- and g_y-signals of Ni_r–B (2.333 and 2.162) and a small g_y-signal of Ni_u-A ($g = 2.24$). Also the g-anisotropy of the $[3Fe4S]^+$-cluster is now fully resolved. The deduced g-values of 2.026, 2.017 and 2.012 (g_x, g_y and g_z, respectively) are in good agreement with those found by W-band EPR for *Dv* H_2ase.[49]

For the *Re* MBH the structure of the EPR spectrum changes upon transition from X- to Q-band frequency. The signal in the iron–sulfur cluster region is broadened and less structured as compared to the X-band spectrum (trace b). However, the width of the FeS signal does not scale linear with the frequency (factor of 3.5) indicating that the major part of the X-band FeS signal broadening and splitting is caused by couplings and not by g-anisotropy. The signals in the Ni region are visible and more structured in the Q-band spectrum. Additional splittings on each g-component become obvious, that are not clearly resolved in X-band experiments (trace b).

Trace c shows the spectrum of *Re* MBH buffered in D_2O and partially reduced by β-mercaptoethanol. The g_x and g_y principal components of the g-tensor are now clearly resolved (2.300, 2.173) and the $[3Fe4S]^+$-cluster is uncoupled. The shape of the uncoupled [3Fe4S] signal can be mainly ascribed to g-anisotropy and g-strain.

A detailed analysis of the spin couplings in the as-isolated spectra of the *Re* MBH is given in the Discussion section.

ENDOR

In order to resolve the hyperfine structure of the protons in the Ni_r–B state, orientation-selective Q-band ^{1}H-ENDOR spectra of frozen-solution samples were recorded at a variety of field-positions for both the *Re* MBH and the *Dv* H_2ase at $T = 10$ K (see Fig. 2). Orientation-selective ENDOR allows the complete determination of the hf-tensors and their relative orientations with regard to the g-tensor axes can be obtained. Due to the superposition by the strong signal of the $[3Fe4S]^+$ cluster, ENDOR spectra at the exact position of g_z (2.01) could not be recorded. However, spectra close to g_z were obtained by measuring at $g = 2.05$ where the orientation-selection should be sufficient to get all information about the hf-tensor. The ENDOR spectra of Ni_r–B from *Dv* H_2ase recorded at different field positions (indicated in the EPR spectrum, top panel) are shown in Fig. 2A. In the spectrum measured close to the g_x-position (1044 mT), where only few orientations contribute to the spectrum, hf-couplings from two protons ($\sim$15 MHz and 12 MHz) are clearly resolved from the proton matrix (top trace). The couplings of these two protons show only a small relative field-dependence when measured over a broad field-range indicating that the hf-couplings are

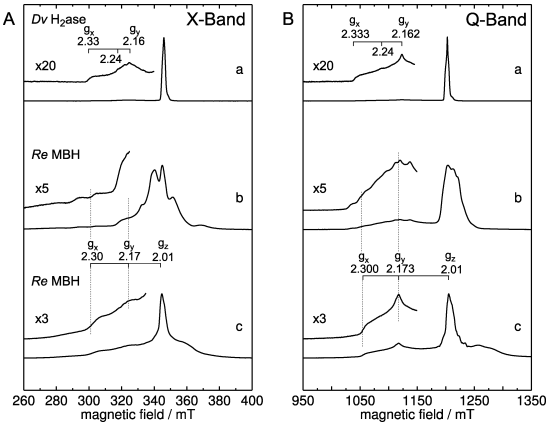

Fig. 1 Pulsed EPR spectra of [NiFe]-hydrogenases from *D. vulgaris* Miyazaki F and *Re* MBH. (A) X-Band two-pulse field-swept echo detected EPR spectra. (a) Reoxidized *Dv* H_2ase (pH 7.4) at $T = 10$ K showing signals from Ni_r–B (and minor amounts of Ni_u-A) and oxidized $[3Fe4S]^+$-cluster. (b) *Re* MBH (pH 7.0) at $T = 8$ K as-isolated showing complex FeS signal. (c) *Re* MBH (pH 7.0) at $T = 10$ K in D_2O-buffer partially reduced with β-mercaptoethanol. (B) Q-Band two-pulse field-swept echo detected EPR spectra. (a) Reoxidized *Dv* H_2ase (pH 7.4) at $T = 10$ K. (b) *Re* MBH (pH 7.0) at $T = 8$ K as-isolated. (c) *Re* MBH (pH 7.0) at $T = 10$ K in D_2O-buffer reduced by β-mercaptoethanol.

mostly of isotropic nature. In earlier EPR and ENDOR studies on single crystals from *Dv* H_2ase combined with DFT calculations, these protons were assigned to two *β*-protons of one bridging cysteine (Cys549).[18] The isotropic hf-coupling a_{iso} has a value of 13.0 MHz for *β*-H1 and 11.5 MHz for *β*-H2 due to the high spin-density at one bridging cysteine-sulfur (Table 1).[18,50] The direction cosines and principal values of each hf-tensor were investigated in the single-crystal work as well.[18] Trofanchuk *et al.*[48] and Gessner *et al.*[51] already investigated the g-tensor orientation with respect to the crystal-axis system. These single-crystal data for the g- and A-tensors were used as starting reference for the simulation of the ENDOR spectra in frozen solution. An overall good agreement could be achieved by modifications of the Euler angles in the range of ±15° (see Table 1).

It is known that deuterium influences the relaxation properties of the electron spin, leading to higher ENDOR intensities. To obtain ENDOR spectra with satisfactory S N^{-1} ratio for the Ni_r–B from *Re* MBH, the sample was buffered in D_2O. Fig. 2B shows the orientation-dependent ENDOR spectra from the partially reduced *Re* H16 (redox potential +40 mV). The spectra are very similar as compared to those derived from the *Dv* H_2ase. Two large hf-couplings are found, which show a comparable magnitude as well as a similar field-dependence. These two hf-couplings could be simulated using the same parameters as for the *Dv* H_2ase (see Table 1) indicating that the spin density distribution of Ni_r–B in both hydrogenases is very similar.

The EPR spectra of as-isolated and partially reduced *Re* MBH turned out to be quite different. In order to exclude changes at the active site structure during the process of reduction by β-mercaptoethanol, orientation-selective ENDOR spectra were measured for the as-isolated sample of Ni_r–B from *Re* MBH too (see Fig. 3). Due to the coupling with the additional paramagnetic center, the orientation-selection is not completely comparable and not as good as for the uncoupled Ni_r–B state in the partially reduced enzyme (Fig. 2). In addition, the spectra are broadened and not completely symmetrical, thereby hampering a reliable simulation. However, on a qualitative basis, the hf-couplings are very similar in both cases, *e.g.* in the spectrum measured at 1036 mT where the two β-protons are clearly separated from the proton matrix. Also the field dependence of the couplings appears to be identical, *e.g.* the spectrum measured close to g_y (1120.7 mT) shows one sharp line arising from the β-protons, as for the uncoupled Ni_r–B (Fig. 2B, 1120.7 mT). This indicates that no significant changes at the [NiFe] center occur during partial reduction with β-mercaptoethanol.

ESEEM

Echo envelope modulation techniques are good methods for obtaining information on nuclei with small magnetogyric ratios that are weakly coupled to the electron spin such as ^{14}N or ^{2}H. Fig. 4 shows the skyline-projection of the Fourier-transformed 3-pulse ESEEM spectrum of the Ni_r–B state of the *Dv* H_2ase (trace a) at the g_y-position ($g = 2.16$). The spectrum is dominated by three sharp lines at low frequencies. These lines show only a minor field-dependence in their positions and can therefore be attributed to the so called 'zero-field transitions' (ν_0, ν_-, ν_+). In addition, at 4 MHz

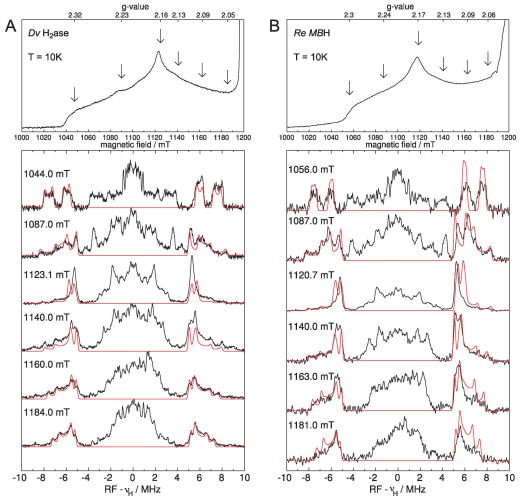

Fig. 2 Orientation-selective Q-band Davies ENDOR spectra measured at $T = 10$ K. (A) *Dv* H_2ase (black) together with simulations of the large hf-couplings from the two β-protons (red). B) *Re* MBH in D_2O buffer reduced by β-mercaptoethanol (black) together with simulations of the large hf-couplings from the two *β*-protons (red). For simulation parameters see Tables 1 and 2.

Table 1 A-Values and direction cosines for Ni_r–B, identical for *Re* MBH and *Dv* H_2ase

β-H1	a_{iso}	*x*	*y*	*z*
A_i/MHz	13.0	3.8	−1.6	−2.1
l_{ai}		0.552	0.111	0.827
l_{bi}		−0.267	−0.916	0.301
l_{ci}		0.790	−0.387	−0.475
β-H2	a_{iso}	*x*	*y*	*z*
A_i/MHz	11.5	2.7	−1.4	−1.4
l_{ai}		0.546	−0.035	−0.837
l_{bi}		−0.013	0.999	−0.050
l_{ci}		0.837	0.038	0.545

Table 2 g-Values and direction cosines used for the simulation of Ni_r–B, taken from ref. 48

Dv H_2ase	g_i	2.333	2.163	2.010
	l_{ai}	0.431	0.550	0.715
	l_{bi}	−0.741	−0.236	0.628
	l_{ci}	0.514	−0.801	0.306
Re MBH	g_i	2.300	2.173	2.010
	l_{ai}	0.431	0.550	0.715
	l_{bi}	−0.741	−0.236	0.628
	l_{ci}	0.514	−0.801	0.306

two weak signals are visible which arise from two double-quantum transitions. This pattern comprises three sharp lines and a weak transition around 4 MHz and is consistent with a nitrogen in 'exact cancellation' condition. The values from the spectrum given in Table 3 agree well with an imidazole-derived nitrogen of a histidine[37,40] close to the Ni atom, which is a common feature in many [NiFe]-hydrogenases (see Table 3).[40,52]

The spectrum of the *Re* MBH (trace b) looks similar. The three lines can be attributed to the zero-field transitions at similar frequencies as for *Dv* H_2ase. Between 3.8 and 4.0 MHz, however, only one broad band of low intensity is visible which can be attributed to a double-quantum transition (ν_{dq}) in the other non-canceled spin manifold that is caused by the anisotropy of the ^{14}N hf-coupling. The exact position of $\nu_{dq}^{\pm}$ in *Re* MBH cannot be determined due to the broadening, thus we are not able to get accurate values for the hf-coupling. Here ^{15}N-isotope labeling ($I = 1/2$) is required to remove the nuclear quadupole interaction and to simplify the spectra. It is therefore only possible to obtain an effective hf-coupling A_{eff} according to eqn (4). With the values in Table 3, A_{eff} lies in the range between 1.4 and 1.6 MHz and close to the condition of exact cancellation ($2\nu_N = 2.0$ MHz).

Discussion

The results of this study indicate that the active site structures in the oxidized Ni_r–B state in the [NiFe]-hydrogenases of *Re* and *Dv* are highly similar. However, a clear difference between the hydrogenases of *Re* and *Dv* was found regarding the $[3Fe4S]^+$-cluster in the oxidized *Re* MBH, which was coupled to additional paramagnetic species. Therefore, the discussion

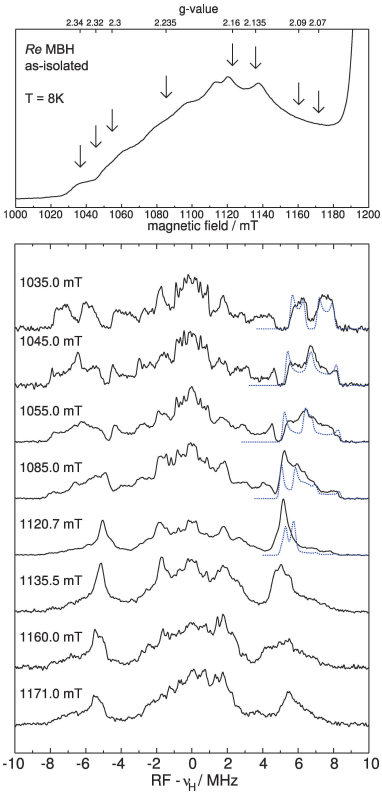

Fig. 3 Orientation-selective Q-band Davies ENDOR spectra of as-isolated *Re* MBH in D_2O buffer measured at $T = 8$ K with simulation of the β-protons (blue).

is arranged in two parts. The first part deals with the electronic structure of the [NiFe] center investigated with ENDOR and ESEEM spectroscopy and the second part describes the additional spin couplings in the EPR spectra of *Re* MBH concomitant with simulations of the EPR spectra.

Comparison of the electronic structure of the [NiFe] centers

ENDOR spectroscopy provides information on the hyperfine structure of the active site. The observed proton couplings for both the *Re* and the *Dv* hydrogenases are identical and show that the electronic structure of the Ni_r–B state must also be identical in both hydrogenases (see Table 1). The largest hf-

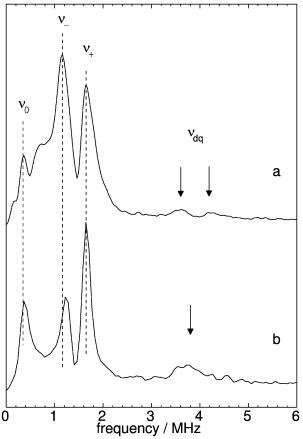

Fig. 4 Skyline-projections of 3-pulse *vs.* 2-pulse ESEEM spectra from *Dv* H_2ase (trace a) and *Re* MBH (trace b) recorded at g_y position of Ni_r–B. Experimental conditions: $T = 8$ K, microwave frequency 9.7 GHz, (a) 256 × 32 points, 64/8 increments (b) 512 × 32 points, 32/16 increments.

couplings arise from the two β-protons of a bridging cysteine. In the Ni_r–B state a spin density of up to 30% was calculated for the sulfur atom of Cys549.[18,53] This finding can be understood in terms of the crystal-field theory because the electronic ground-state for Ni_r–B is d_{z^2} and this orbital points towards this particular bridging sulfur atom leading to a significant amount of spin density. A third smaller hf-coupling was assigned previously to the proton in the OH-bridge between the Ni and Fe.[18] This coupling is mainly dipolar and could not be clearly resolved and assigned in the frozen solution spectra measured in this work.

ESEEM spectroscopy clearly indicates the presence of a histidine nitrogen close to the [NiFe] center in both hydrogenases. With the aid of DFT calculations and information derived from the X-ray structure it has been shown that the N_ε of His88 (*Dv* H_2ase) is responsible for these signals (see Scheme 2).[40,46] This histidine is hydrogen-bonded to one of the bridging cysteines of the catalytic site. With knowledge of e^2qQ/h and η it is possible to estimate the distance between the nitrogen and sulfur atoms by comparing the values with DFT calculations. The distances from the crystal structure and from DFT calculations for *Dv* H_2ase are 3.3 Å[3] and 3.4 Å,[40] respectively. The same distance is deduced for *Re* MBH.

In view of the ENDOR and ESEEM results, we conclude that the structure of Ni_r–B in *Dv* H_2ase and *Re* MBH is almost identical indicating that the [NiFe] active sites of the *Re* and *Dv* hydrogenases do not differ significantly from each other (Scheme 2).

Table 3 Nuclear quadrupole and hf parameters obtaind from the ESEEM spectra

Hydrogenase	Redox state	ν_0 [MHz]	ν_- [MHz]	ν_+ [MHz]	e^2qQ/h [MHz]	η	A_{eff} [MHz]	Ref.
Re MBH	Ni_r–B	0.39	1.25	1.65	1.94	0.38	1.4–1.6	This work
Dv H_2ase	Ni_u-A	0.32	1.26	1.58	1.90	0.34	—	49
	Ni_r–B	0.36	1.30	1.66	1.90	0.37	1.4–1.6	40, This work
D. gigas	Ni_u-A	0.4	1.2	1.6	1.9	0.4	—	52

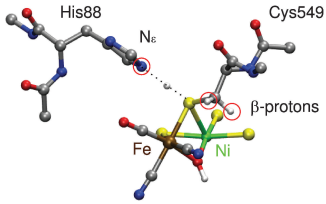

Scheme 2 Structure of Ni_r–B in the [NiFe]-hydrogenase of *D. vulgaris* Miyazaki F. His88 is hydrogen-bonded to the bridging sulfur of Cys549.

Spin couplings in the oxidized state of the Re MBH

The X- and Q-band EPR spectra of the *Re* MBH show in the as-isolated form at cryogenic temperatures ($T < 15$ K) a complex coupling pattern in the FeS region as well as for the Ni, which is different compared to standard hydrogenases.[19] Similar X-band spectra were observed for other membrane-bound [NiFe]-hydrogenases, all of which are proposed to be O_2-tolerant, *e.g.* the hydrogenase I in *A. aeolicus*[54] or the MBH of *R. metallidurans* CH34.[55]

To get a deeper insight into the origin of the resolved splittings of the Ni signals in the EPR spectra from *Re* MBH, a combined simulation of the X- and Q-band echo detected EPR spectra was performed with a focus on the Ni region (Fig. 5). The experimental Ni spectrum shows at each of the well resolved g-components (g_x and g_y) a splitting into four lines. These quartets of lines appear as doublets of doublets. This indicates that Ni_r–B is magnetically coupled to two different S = 1/2 spin systems. It has been suggested earlier for *A. vinosum* MBH that the Ni_r–B might be coupled to the $[3Fe4S]^+$-cluster and to an unknown center X^{ox}.[7,8] X^{ox} has been postulated to be either an additional iron species or a modified proximal iron–sulfur cluster, which is only paramagnetic in its oxidized form (*e.g.* a HiPIP or $[3Fe4S]^+$).[7,8]

The existence of a paramagnetic X^{ox} was used as the basis for our simulation together with the known g-values of the Ni_r–B and the uncoupled $[3Fe4S]^+$-cluster (Table 4). However, the g-values and linewidth for the additional center X^{ox} are unknown *a priori* and were used as variables in the simulations. Good agreement for the Ni signals was achieved by assuming an isotropic exchange coupling of $J_A = 780$ MHz for the large coupling and a smaller isotropic coupling of $J_B = 550$ MHz. Concerning the species X^{ox}, the best agreement for the FeS region could be achieved by assuming X^{ox} as a paramagnetic center with small g-anisotropy, *e.g.* here as a second $[3Fe4S]^+$ center with the same g-values (Table 4). Simulations assuming X^{ox} as an organic radical with g-values close to $g \approx g_e$ resulted in reasonable simulations as well (not shown). We are not able to distinguish these two cases with our simulations due to the small g-anisotropy. Sequence alignments in an earlier work have shown that *Re* H16 MBH contains two additional cysteine residues in close vicinity to the proximal [4Fe4S]-cluster, *i.e.* X^{ox} might be a cysteine based radical or a modified FeS cluster.[33]

However, since both the Ni_r–B and the $[3Fe4S]^+$-cluster are uncoupled after partial reduction with β-mercaptoethanol, a single X^{ox} species cannot explain the loss of both couplings (J_A and J_B) after partial reduction. The coupling between the [NiFe] center and the $[3Fe4S]^+$-cluster should still be present. Thus, the coupling scheme must be different and can only be explained by assuming two additional paramagnetic centers, which are both diamagnetic after partial reduction. Although their exact nature and function are unknown, they must be in a comparable distance to the [NiFe] center due to the similar exchange couplings J_A and J_B and must have a similar redox potential. The fact that the coupling pattern looks like a doublet of doublets indicates that there is no coupling between both of these centers and that they must be treated like separate S = 1/2 systems, assuming a significant coupling between the two centers would lead to an effective spin different from the two isolated S = 1/2 states and to a different coupling pattern of the Ni_r–B. However, the exchange couplings for *Re* MBH are higher than known for standard hydrogenases, where J has been deduced to be in the range of 120 MHz for the coupling between the Ni_a–C state and the reduced proximal [4Fe4S] cluster (*D. gigas*).[56] An explanation may be a closer distance of the paramagnetic centers to the [NiFe] center. However, we are not able to identify the additional center(s) in our work.

Since the EPR results indicate high similarity of the Ni_r–B state of the [NiFe] center from *Re* MBH and *Dv* H_2ase, it seems likely that the origin of the oxygen-tolerance of *Re* MBH probably does not arise from a modification at the active site but rather from a modification of the iron–sulfur clusters. Recent electrochemical studies showed that the *Re* MBH rapidly reactivates even at high potentials.[34] This finding might already indicate an important role for the proximal iron–sulfur center in providing O_2-tolerance to the active site.

Conclusion

In this work we characterized the oxidized ready state Ni_r–B of the oxygen-tolerant membrane-bound [NiFe]-hydrogenase from *Re* MBH by pulsed EPR and ENDOR spectroscopy. We compared our results to the oxygen-sensitive standard [NiFe]-hydrogenase from *D. vulgaris* Miyazaki F for which the

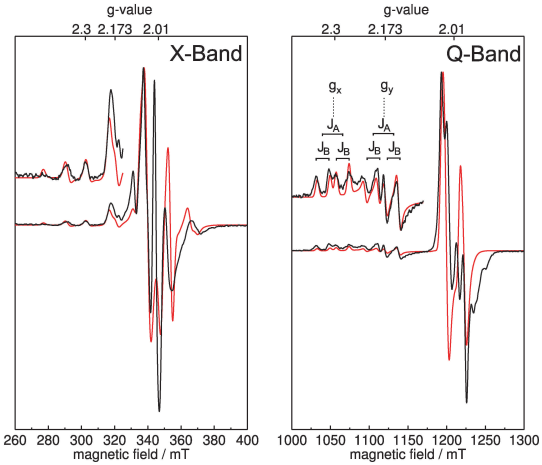

Fig. 5 Simulation of the pseudomodulated X- and Q-band echo-detected EPR-spectra from *Re* MBH obtained at $T = 8$ K. For simulation parameters see Table 4. The best agreement could be achieved in a simulation with two $[3Fe4S]^+$-clusters.

Table 4 g-Values used for the simulation of the pseudomodulated EPR spectra of *Re* MBH (see Fig. 5)

Center	g_x	g_y	g_z	J_A/MHz	J_B/MHz
Ni_r–B	2.30	2.17	2.01	780	550
[3Fe4S]	2.02	2.01	1.99		

crystal structure is known.[16] The EPR results suggest a far-reaching similarity of the Ni_r–B state in both hydrogenases. ENDOR spectroscopy provides information on the hyperfine structure of the active site. The proton couplings observed and assigned for both the *Re* MBH and the *Dv* H_2ase are identical and show that the electronic structure of the Ni_r–B state is identical in both hydrogenases (see Table 1). The largest hf-couplings arise from the two β-protons of a bridging cysteine. In the Ni_r–B state a spin density of up to 30% was calculated for the sulfur atom of Cys549 (*Dv* H_2ase) corresponding to Cys586 in *Re* MBH.[18,53]

ESEEM spectroscopy reveals the presence of a nitrogen close to the [NiFe]-center. The nuclear quadrupole parameters derived from the spectra obtained for *Re* MBH agree well with those of the *Dv* H_2ase (see Table 3), *i.e.* a histidine-nitrogen that is hydrogen-bonded to one of the bridging cysteine sulfurs is clearly present in the *Re* MBH. In the oxidized form, additional spin couplings exist between the Ni_r–B state of the [NiFe] center and two other paramagnetic centers, which are not found in standard hydrogenases.

Further studies are in preparation to identify the structure and to elucidate the function of the additional center(s) at high redox potentials. This includes *Re* MBH variants carrying amino acid exchanges close to the proximal and medial iron–sulfur clusters. In addition, pulsed EPR studies of the catalytic active Ni_a–C state of the *Re* MBH are envisaged in order to clarify whether the hyperfine structure of this redox state is also similar to that of the *Dv* H_2ase.

Acknowledgements

The authors thank Patricia Malkowski (MPI Mülheim) for the preparation of the *D. vulgaris* Miyazaki F hydrogenase. This work was supported by Deutsche Forschungsgemeinschaft Grants SFB 498 TP C1 and TP C9 and by Cluster of Excellence 'Unifying Concepts in Catalysis'.

References

1 R. Cammack, M. Frey and R. Robson, *Hydrogen as a fuel: learning from nature*, Taylor & Francis, London, 2001.
2 A. Volbeda, M. H. Charon, C. Piras, E. C. Hatchikian, M. Frey and J. C. Fontecilla Camps, *Nature*, 1995, **373**, 580–587.
3 Y. Higuchi, T. Yagi and N. Yasuoka, *Structure*, 1997, **5**, 1671–1680.
4 J. W. Peters, W. N. Lanzilotta, B. J. Lemon and L. C. Seefeldt, *Science*, 1998, **282**, 1853–1858.
5 Y. Nicolet, C. Piras, P. Legrand, C. E. Hatchikian and J. C. Fontecilla Camps, *Structure*, 1999, **7**, 13–23.
6 O. Pilak, B. Mamat, S. Vogt, C. H. Hagemeier, R. K. Thauer, S. Shima, C. Vonrhein, E. Warkentin and U. Ermler, *J. Mol. Biol.*, 2006, **358**, 798–809.
7 K. K. Surerus, M. Chen, J. W. van der Zwaan, F. M. Rusnak, M. Kolk, E. C. Duin, S. P. Albracht and E. Münck, *Biochemistry*, 1994, **33**, 4980–4993.
8 S. P. J. Albracht, *Biochim. Biophys. Acta, Bioenerg.*, 1994, **1188**, 167–204.
9 A. Volbeda, E. Garcin, C. Piras, A. L. de Lacey, V. M. Fernandez, E. C. Hatchikian, M. Frey and J. C. Fontecilla Camps, *J. Am. Chem. Soc.*, 1996, **118**, 12989–12996.

10 A. J. Pierik, W. Roseboom, R. P. Happe, K. A. Bagley and S. P. Albracht, *J. Biol. Chem.*, 1999, **274**, 3331–3337.
11 K. A. Vincent, A. Parkin, O. Lenz, S. P. J. Albracht, J. C. Fontecilla Camps, R. Cammack, B. Friedrich and F. A. Armstrong, *J. Am. Chem. Soc.*, 2005, **127**, 18179–18189.
12 M. W. Adams, *Biochim. Biophys. Acta, Bioenerg.*, 1990, **1020**, 115–145.
13 R. Cammack, V. M. Fernandez and K. Schneider, *Biochimie*, 1986, **68**, 85–91.
14 B. Bleijlevens, F. A. van Broekhuizen, A. L. De Lacey, W. Roseboom, V. M. Fernandez and S. P. J. Albracht, *JBIC, J. Biol. Inorg. Chem.*, 2004, **9**.
15 S. E. Lamle, S. P. J. Albracht and F. A. Armstrong, *J. Am. Chem. Soc.*, 2005, **127**, 6595–6604.
16 H. Ogata, S. Hirota, A. Nakahara, H. Komori, N. Shibata, T. Kato, K. Kano and Y. Higuchi, *Structure*, 2005, **13**, 1635–1642.
17 A. Volbeda, L. Martin, C. Cavazza, M. Matho, B. W. Faber, W. Roseboom, S. P. J. Albracht, E. Garcin, M. Rousset and J. C. Fontecilla Camps, *JBIC, J. Biol. Inorg. Chem.*, 2005, **10**, 239–249.
18 M. van Gastel, M. Stein, M. Brecht, O. Schröder, F. Lendzian, R. Bittl, H. Ogata, Y. Higuchi and W. Lubitz, *JBIC, J. Biol. Inorg. Chem.*, 2006, **11**, 41–51.
19 W. Lubitz, E. Reijerse and M. van Gastel, *Chem. Rev.*, 2007, **107**, 4331–4365.
20 V. M. Fernandez, E. C. Hatchikian and R. Canmmack, *Biochim. Biophys. Acta, Protein Struct. Mol. Enzymol.*, 1985, **832**, 69–79.
21 M. Brecht, M. van Gastel, T. Buhrke, B. Friedrich and W. Lubitz, *J. Am. Chem. Soc.*, 2003, **125**, 13075–13083.
22 M. Aragno and H. G. Schlegel, *The Prokaryotes: The mesophilic hydrogen-oxidizing (Knallgas) bacteria*, Springer, New York, 1992, pp. 344-384.
23 B. Friedrich and E. Schwartz, *Annu. Rev. Microbiol.*, 1993, **47**, 351–383.
24 P. M. Vignais and B. Billoud, *Chem. Rev.*, 2007, **107**, 4206–4272.
25 T. Burgdorf, O. Lenz, T. Buhrke, E. van der Linden, A. K. Jones, S. P. J. Albracht and B. Friedrich, *J. Mol. Microbiol. Biotechnol.*, 2005, **10**, 181–196.
26 K. A. Vincent, J. A. Cracknell, O. Lenz, I. Zebger, B. Friedrich and F. A. Armstrong, *Proc. Natl. Acad. Sci. U. S. A.*, 2005, **102**, 16951–16954.
27 E. van der Linden, T. Burgdorf, M. Bernhard, B. Bleijlevens, B. Friedrich and S. P. J. Albracht, *J. Biol. Inorg. Chem.*, 2004, **9**, 616–626.
28 R. P. Happe, W. Roseboom, G. Egert, C. G. Friedrich, C. Massanz, B. Friedrich and S. P. Albracht, *FEBS Lett.*, 2000, **466**, 259–263.
29 T. Buhrke, O. Lenz, N. Krauss and B. Friedrich, *J. Biol. Chem.*, 2005, **280**, 23791–23796.
30 M. Bernhard, B. Benelli, A. Hochkoeppler, D. Zannoni and B. Friedrich, *Eur. J. Biochem.*, 1997, **248**, 179–186.
31 B. Schink and H. G. Schlegel, *Biochim. Biophys. Acta, Enzymol.*, 1979, **567**, 315–324.
32 C. Kortlüke, K. Horstmann, E. Schwartz, M. Rohde, R. Binsack and B. Friedrich, *J. Bacteriol.*, 1992, **174**, 6277–6289.
33 M. Saggu, I. Zebger, M. Ludwig, O. Lenz, B. Friedrich, P. Hildebrandt and F. Lendzian, *J. Biol. Chem.*, 2009, **284**, 16264–16276.
34 M. Ludwig, J. A. Cracknell, K. A. Vincent, F. A. Armstrong and O. Lenz, *J. Biol. Chem.*, 2008, **284**, 465–477.
35 K. Schneider, D. S. Patil and R. Cammack, *Biochim. Biophys. Acta, Protein Struct. Mol. Enzymol.*, 1983, **748**, 353–361.
36 E. R. Davies, *Phys. Lett. A*, 1974, **47**, 1–2.
37 S. Dikanov and Y. Tsvetkov, *Electron spin echo envelope modulation (ESEEM) spectroscopy*, CRC press, 1992.
38 O. Lenz, A. Gleiche, A. Strack and B. Friedrich, *J. Bacteriol.*, 2005, **187**, 6590–6595.
39 T. Yagi, K. Kimura, H. Daidoji, F. Sakai and S. Tamura, *J. Biochem.-Tokyo.*, 1976, **79**, 661–671.
40 A. G. Agrawal, M. van Gastel, W. Gärtner and W. Lubitz, *J. Phys. Chem. B*, 2006, **110**, 8142–8150.
41 A. Stesmans and G. Vangorp, *Rev. Sci. Instrum.*, 1989, **60**, 2949–2952.
42 J. S. Hyde, M. Pasenkiewicz Gierula, A. Jesmanowicz and W. E. Antholine, *Appl. Magn. Reson.*, 1990, **1**, 483–496.
43 MATLAB 7.6, Mathworks 2008.
44 S. Stoll and A. Schweiger, *J. Magn. Reson.*, 2006, **178**, 42–55.
45 C. Gemperle, G. Aebli, A. Schweiger and R. R. Ernst, *J. Magn. Reson.*, 1990, **88**, 241–256.
46 T. Buhrke, M. Brecht, W. Lubitz and B. Friedrich, *JBIC, J. Biol. Inorg. Chem.*, 2002, **7**, 897–908.
47 W. B. Mims and J. Peisach, *J. Chem. Phys.*, 1978, **69**, 4921–4930.
48 O. Trofanchuk, M. Stein, C. Gessner, F. Lendzian, Y. Higuchi and W. Lubitz, *JBIC, J. Biol. Inorg. Chem.*, 2000, **5**, 36–44.
49 M. T. J. Brecht, *PhD thesis*, TU Berlin, 2001.
50 A. Müller, I. Tscherny, R. Kappl, C. E. Hatchikian, J. Huttermann and R. Cammack, *JBIC, J. Biol. Inorg. Chem.*, 2002, **7**, 177–194.
51 C. Gessner, O. Trofanchuk, K. Kawagoe, Y. Higuchi, N. Yasuoka and W. Lubitz, *Chem. Phys. Lett.*, 1996, **256**, 518–524.
52 A. Chapman, R. Cammack, C. E. Hatchikian, J. McCracken and J. Peisach, *FEBS Lett.*, 1988, **242**, 134–138.
53 M. Stein and W. Lubitz, *Phys. Chem. Chem. Phys.*, 2001, **3**, 2668–2675.
54 M. Brugna Guiral, P. Tron, W. Nitschke, K. O. Stetter, B. Burlat, B. Guigliarelli, M. Bruschi and M. T. Giudici Orticoni, *Extremophiles*, 2003, **7**, 145–157.
55 K. Knüttel, K. Schneider, A. Erkens, W. Plass, A. Müller, E. Bill and A. X. Trautwein, *B. Pol. Acad. Sci.-Chem.*, 1994, **42**, 495–511.
56 B. Guigliarelli, C. More, A. Fournel, M. Asso, E. C. Hatchikian, R. Williams, R. Cammack and P. Bertrand, *Biochemistry*, 1995, **34**, 4781–4790.
57 S. Foerster, M. Stein, M. Brecht, H. Ogata, Y. Higuchi and W. Lubitz, *J. Am. Chem. Soc.*, 2003, **125**, 83–93.

7 The proximal iron-sulfur cluster in *Ralstonia eutropha* H16

It is known from multiple sequence alignments that two additional cysteine residues are in close vicinity to the proximal [4Fe4S]-cluster in *Re* H16 MBH. Interestingly, these two cysteines can be found in all membrane-bound [NiFe]-hydrogenases that are either oxygen-tolerant or proposed to be so, e.g. the MBH from *Rm* CH34 or *A. aeolicus*. In standard [NiFe]-hydrogenases these residues are glycines.

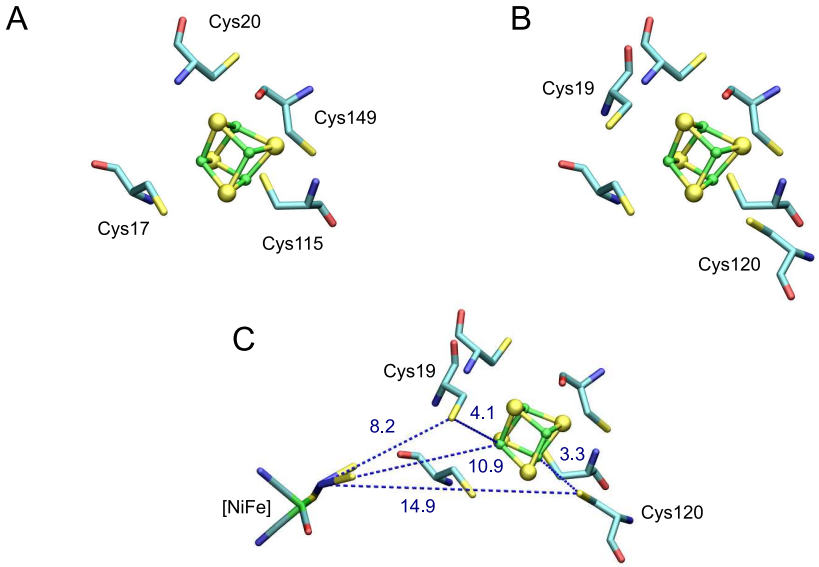

Figure 7.1: Homology model of the *Re* H16 MBH based on *D. gigas* structure. A) Proximal cluster with 4 standard cysteines B) in *Re* H16 two additional cysteines are in vicinity of the [4Fe4S]-cluster C) distances (in Å) and orientations of the additional cysteines from the Ni.

Based on the crystal-structure and sequence of the *D. gigas* [NiFe]-hydrogenase, a homology model was created[1], which is shown in Figure 7.1. The additional cysteines are located on opposite positions of the FeS cluster. The estimated distances to the nearest Fe atoms are between 3 and 4 Å; thus they could be direct ligands of the [4Fe4S]-cluster. The distances to the Ni atom are 8 and 15 Å.

The EPR spectrum of wild-type MBH shows a very complex EPR spectrum in the oxidized form (see Figure 7.2). In contrast to standard hydrogenases, additional spin-couplings between several paramagnetic centers including Ni_r-B are present (see **chapter 6**). Similar spectral features are known for the [NiFe]-hydrogenases from *Rm* CH34 and *A. vinosum*. In earlier works it has been proposed, that the proximal [4Fe4S]-cluster might be present in a HiPIP form, i.e. in a $[4Fe4S]^{3+}$ oxidation state, or that an additional Fe species might be present.[107,128] In order to identify the proximal FeS center and the origin of the spin-couplings in *Re* H16, mutations of both cysteines were carried out.

Figure 7.2 shows the EPR spectra of H16 wild-type and mutants, where the additional cysteines are exchanged vs. glycines. The top trace shows the EPR spectrum of wild-type MBH at high redox potentials, where the Ni_r-B and [3Fe4S]-cluster are coupled. In contrast to standard hydrogenases, the additional spin-couplings lead to the disappearance of the Ni signals at higher temperatures due to enhanced spin relaxation. After partial reduction with a mild reduction agent to a redox potential of +40 mV, the spectrum is simplified. The additional spin-couplings are no longer present. At g=2 a typical narrow signal of a [3Fe4S]-cluster can be seen. In addition, the Ni_r-B is uncoupled and can be observed at higher temperatures like T = 80 K (see **chapter 5**).

The EPR spectrum of the double mutant C19G/C120G, where both cysteine residues are exchanged vs. glycines, has in the as-isolated form a similar shape as the partial reduced wild-type spectrum. Both the [3Fe4S]-cluster and the Ni_r-B are uncoupled. The Ni signals are visible at higher temperatures. Addition of an excess of DCIP (+290 mV) to reach the highest oxidized states of the enzyme did not lead to any changes of the signals. This indicates that the additional paramagnetic center is not present in this mutant. The cysteines seem to play an important role in a modification of the proximal FeS center. It is possible that these residues provide binding sites for additional Fe, which might indicate a non-standard structure of the [4Fe4S]-cluster, other than cubane. Another possibility would be the presence of cysteine radicals close to the [4Fe4S]-cluster or the formation of a HiPIP type cluster.

However, only one single mutant (C19G) was stable and could be prepared. Mutants, in which all other cysteines could be exchanged vs. glycines, were instable and could not be investigated spectroscopically. Mutation of only cysteine C19 resulted in strong heterogeneity of the additional center, but not to its complete disappearance. The Ni_r-B seems to be uncoupled as well because its g_x- and g_y-signals are clearly resolved. In addition, the Ni_r-B is visible at high temperatures. At lower temperature (T = 10 K) the signal of the uncoupled [3Fe4S]-cluster clearly appears, which might indicate, that the [3Fe4S]-cluster is still influenced by the additional paramagnetic center (enhanced spin relaxation), in contrast to the [NiFe] center. However, the structure of the proximal FeS center remains unclear.

[1] by M. Stein (personal communication)

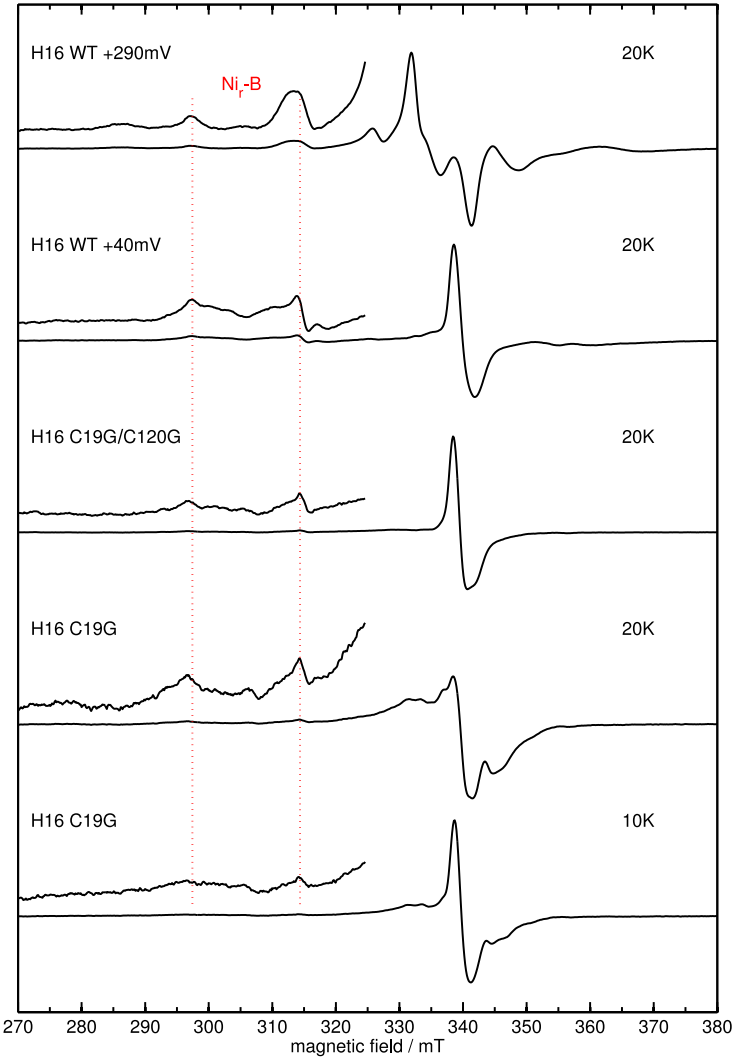

Figure 7.2: EPR spectra of heterotrimeric MBH wild-type and cysteine mutants. Experimental conditions: 1 mW microwave power, microwave frequency 9.56 GHz, 1 mT modulation amplitude, 12.5 kHz modulation frequency.

In summary, these findings indicate, that probably both cysteines are necessary for a modification of the FeS center, which can also be concluded from the sequence alignments, because oxygen-tolerant hydrogenases contain always both additional cysteines. The split FeS signal in *Re* H16 wild-type results from couplings between an unknown center X^{ox} and/or a modified proximal [4Fe4S]-cluster with the medial [3Fe4S]-cluster. The spectroscopic identification of the additional center(s) might be possible with additional mutants, e.g. conversion of the medial $[3Fe4S]^{+}$-cluster to a diamagnetic $[4Fe4S]^{2+}$-cluster will allow to detect an unperturbed proximal FeS center.

8 *In situ* investigation of the soluble hydrogenase from *R. eutropha* H16 in whole cells: a combined EPR and FTIR spectroscopic study

M. Horch, M. Saggu, L. Lauterbach, O. Lenz, P. Hildebrandt, F. Lendzian, R. Bittl and I. Zebger

to be submitted to *Angew. Chem. Int. Ed.*

Biocatalysis

DOI: 10.1002/anie.200((will be filled in by the editorial staff))

In situ investigation of the soluble hydrogenase from *Ralstonia eutropha* H16 in whole cells: a combined EPR and FTIR spectroscopic study **

*Marius Horch[†], Miguel Saggu[†], Lars Lauterbach[†], Peter Hildebrandt, Friedhelm Lendzian, Robert Bittl, Oliver Lenz, and Ingo Zebger**

[NiFe]-hydrogenases catalyze the reversible heterolytic cleavage of dihydrogen into two protons and two electrons.[1] This process plays an important role in the energy metabolism of many microorganisms. For most [NiFe]-hydrogenases, the process of H_2 cycling is extremely sensitive to molecular oxygen as O_2 holds a high binding capacity to the active site. However, some organisms are capable to catalyze hydrogen cleavage even at ambient oxygen levels.[2;3] Notably, the β-proteobacterium *Ralstonia eutropha* H16 (*Re*) harbors three different [NiFe]-hydrogenases, all of which exhibit a remarkable oxygen-tolerance.[2-4] The underlying molecular mechanisms are, however, not fully understood yet. For the regulatory hydrogenase (RH) of *Re*, a narrow gas tunnel is supposed to limit O_2 access to the active site.[4] In case of the *Re* membrane-bound hydrogenase (MBH) the reason for O_2-tolerance is so far unclear. Electrochemical experiments showed that the O_2-inhibited MBH is reactivated rapidly at high potentials.[5] This behavior might be related to an additional high-potential paramagnetic center in vicinity of the active site, as detected by EPR spectroscopy.[6] The third hydrogenase of *Re* is a cytoplasmic NAD^+-reducing hydrogenase (SH), which is composed of six subunits and closely related to the bidirectional [NiFe]-hydrogenases, found in many cyanobacteria.[2;7] For purified SH enzyme, a modified [NiFe] center has been proposed on the basis of numerous biochemical and spectroscopic studies.[2;8;9]. In contrast to standard [NiFe]-hydrogenases, in which the active site iron is kept in the low-spin Fe(II) state by one carbonyl and two cyanide ligands, the catalytic center of the SH is so far supposed to contain two more cyanides. In this context, Fourier transform infrared (FTIR) spectroscopic investigations and concomitant chemical analysis indicated one additional cyanide, coordinated to each metal atom. Especially, the unprecedented nickel-bound one was suggested to prevent the formation of the so-called Ni_u-A state, which represents the most oxidized, O_2-inactivated state in [NiFe]-hydrogenases.[9] Controversial results have been obtained for the occurrence of paramagnetic nickel states in the SH. Spectroscopic studies on SH preparations treated with an excess of NADH or dithionite revealed electron paramagnetic resonance (EPR) signals and FTIR bands attributable to the catalytic intermediate Ni_a-C and the light-induced, non-physiological, Ni_a-L state.[10;11] However, these redox-states, which are common for anaerobic standard [NiFe] Hydrogenases, were later proposed to be not involved in the SH catalytic cycle.[2;12] In fact, a reaction mechanism was suggested, in which the Ni remains in the EPR-silent Ni(II) state, and substrate as well as H_2-mediated redox changes at the active site are only reflected by shifts of the CN stretching originating from the proposed Ni-bound cyanide. Despite its O_2 tolerance, the SH can be inactivated by oxygen. This became apparent since the purified SH required a reductive activation by catalytic amounts of either NADH or NADPH.[2;12]

Information on additional SH cofactors were obtained by EPR spectroscopic experiments revealing signals for a reduced [2Fe2S]-cluster in addition to a flavine radical (FMN semiquinone) after incubation with H_2 and catalytic amounts of NAD(P)H or a solely excess of NADH. Only rigorous reduction by dithionite revealed a superposition with additional EPR signals attributable to one [4Fe4S]- and one [2Fe2S]-cluster [2].

So far, spectroscopic studies on the *Re* SH have been performed exclusively on purified tetra- and hexameric enzyme fractions.[2;9] In the present study we investigate the SH for the first time *in situ*, *i.e.* as a constituent of the cytoplasm in whole cells, by using a combined EPR and FTIR spectroscopic approach. All subsequent experiments were performed with a *Re* H16 derivative, that solely synthesizes the soluble hydrogenase at wild-type level, whereas the genes, encoding the active site-containing large subunits of the two other *Re* hydrogenases, are deleted (SH^+, MBH^-, RH^-). Thus, any interference of the SH-related spectroscopic signals with those from the RH and the MBH can be excluded.

Fig. 1 shows the EPR spectra of variously treated *Re* cells. Trace A represents the spectrum of the freshly harvested cells at T = 35K. In the low-field region, strong Ni signals are visible with resolved g_x- and g_y- components. The g-values deduced from simulation are 2.20, 2.14 and 2.01 with a linewidth of 1.8 mT and can be attributed to the Ni_a-C redox state with a formal Ni(III) as found in standard [NiFe]-hydrogenases.[13] Additionally, signals for FMN (g=2.00) and a $[2Fe2S]^+$-cluster were detected. Usually, the cytoplasm in living cells comprises dissolved NADH/NADPH reducing equivalents. Therefore, the $[2Fe2S]^+$-cluster is expected to be quantitatively reduced. Since absolute spin quantification is not possible in whole cells, relative quantifications were performed by comparing the double-integrated simulations of Ni_a-C and the

[*] [†] These authors contributed equally to the work

M. Saggu, M. Horch, Dr. F. Lendzian, Prof. P. Hildebrandt, Dr. I. Zebger
Institut f. Chemie, Sekr. PC14
Technische Universität Berlin
Straße des 17. Juni 135, D-10623 Berlin (Germany)
Fax: (+49) 30-31421122
E-mail: ingo.zebger@ tu-berlin.de

L. Lauterbach, Dr. O. Lenz
Institut f. Biologie/Mikrobiologie, Humboldt Universität zu Berlin
Chausseestr. 117, D-10115 Berlin (Germany)

Prof. R. Bittl
Institut f. Physik, Freie Universität Berlin
Arnimallee 14, D-10115 Berlin (Germany)

[**] The work was supported by the DFG SFB498 and Cluster of Excellence "Unicat".

Supporting information for this article is available on the WWW under http://www.angewandte.org or from the author

$[2Fe2S]^+$-cluster. From these values, we obtained an amount of approximately 60% Ni_a-C in freshly harvested cells, which is in agreement with the corresponding FTIR data (see below). In accordance with observations from standard hydrogenases, the Ni_a-C state in the SH was converted completely to Ni_a-L by white light illumination at T = 80K for 30 min (see trace B).[14] 10 min of dark adaptation at T > 100K led to a complete back conversion to Ni_a-C. Simulation of the difference spectra at 35K revealed the g-values 2.27, 2.10 and 2.05 with a linewidth of 1.5mT for the Ni_a-L state (trace B).

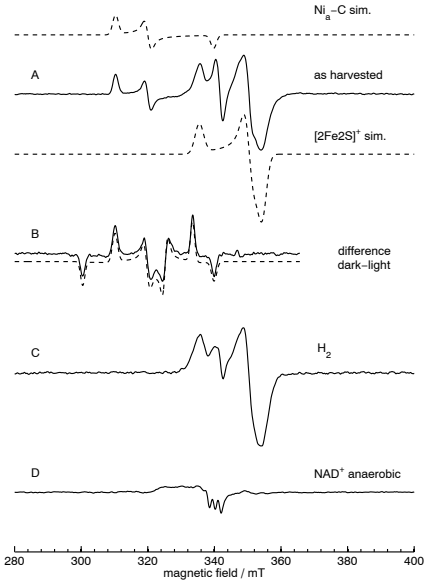

Figure 1. EPR spectra of the soluble hydrogenase recorded at T = 35K (solid) together with corresponding simulations (dashed). A) as harvested cells, B) difference of dark-adapted minus light exposed cells, C) as harvested cells exposed to H_2, D) as harvested cells oxidized anaerobically with NAD^+

Upon incubation with H_2 for 30 min, the Ni_a-C signals disappeared (trace C), whereas the $[2Fe2S]^+$-cluster and FMN signals remain. This indicates that the active site has been reduced further in a one-electron process to the fully reduced Ni_a-SR state(s). On the other hand, oxidation of SH-containing cells under anaerobic conditions using an excess of NAD^+ led to the disappearance of any Ni- and FeS-related EPR signals (trace D). Only background signals from unknown cellular paramagnetic centers were visible. Signals attributable to the oxidized Ni_r-B or Ni_u-A species, in which Ni is present in the paramagnetic Ni(III) form, could not be identified in our experiments. Similar results were obtained after re-oxidation with air.

The corresponding FTIR data of SH-containing cells are displayed in Figure 2. In the present case CO and CN band intensities in the absolute IR spectra are weak and superimposed by a strongly contoured baseline. Therefore, second derivatives of the IR absorbance spectra are shown in this study. In this representation absorption bands appear as distinct negative peaks. Trace A shows the second-derivative FTIR spectrum of freshly harvested *Re* cells. The spectrum is dominated by a CO absorption band at 1961 cm^{-1} and two corresponding CN stretching bands at 2080 and 2091 cm^{-1}. These signals can be assigned

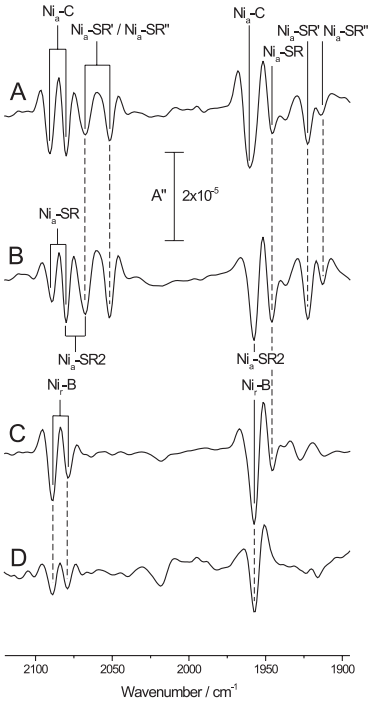

Figure 2. FTIR spectra of the soluble hydrogenase A) cells as harvested, B) after 30 min incubation under 1 bar H_2, C) oxidized with NAD^+ under anaerobic conditions and D) oxidized under aerobic conditions.

to the Ni_a-C state of the SH, whose relative amounts are consistent with the EPR data obtained from the same sample (Figure 1 A). The mentioned bands are only slightly shifted to smaller wavenumbers (2-5 cm^{-1}) with respect to previous investigations of the purified enzyme at cryogenic temperatures.[9] These deviations might be to due to temperature related changes in the hydrogen bonding network or/and a different, inherent pH in the cytoplasm compared to the purified enzyme, both influencing the absolute peak position. [15;16]

Furthermore, absorption bands in the lower frequency range of the CO and CN stretching vibrations, respectively, were observed at 1913, 1922, 2052 and 2068 cm^{-1}. The two latter bands are broadened, due to an overlap of adjacent absorptions. Since all these peaks increased in intensity by incubation with 1 bar H_2 (Trace B), they were assigned to the reduced species Ni_a-SR' and Ni_a-SR'', respectively. Additionally, signals at 1946,

Scheme 1. Postulated redox scheme for the *Re* SH in whole cells.

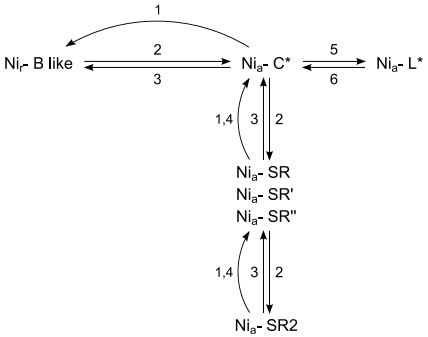

The accordingly depicted redox state transitions were shown to be reversible. Paramagnetic states are marked with an asterisk. 1) anaerobic oxidation with NAD^+ 2) reduction with H_2 and cytoplasmic NAD(P)H 3) oxidation with air 4) oxidation with N_2 5) light induction 6) dark conversion by thermal relaxation (+ΔT)

2080 and 2090 cm^{-1} were attributed to the Ni_a-SR state. More recent experiments indicated the existence of a further, oxidized intermediate state (Ni_a-S) at almost the same CO stretching frequency, which is in accordance with earlier reports. The assignment of the individual reduced species was made according to FTIR data of the bidirectional hydrogenase of *Synechocystis sp.* PCC 6803 and the *Re* MBH (Table 1). These attributions were confirmed, at least for the CO stretchings, by previously obtained spectroelectrochemical IR data of the purified *Re* SH, recorded under reductive conditions at –391 mV vs. NHE [12]. Furthermore, the signals at 1958, 2068 and 2080 were tentatively related to a further reduced, EPR-silent Ni_a-SR2 species. Incubation with an excess of NAD^+ under anaerobic conditions (Fig. 2, trace C) and O_2 (Fig. 2, trace D), respectively, yielded three exclusive signals at 1957, 2079 and 2089 cm^{-1}. These were attributed to a "Ni_r-B-like" state, which is, however, also EPR-silent. Ni_a-SR2 as a distinct reduced state and the "Ni_r-B-like" species are exclusively found in bidirectional hydrogenases with a diaphorase module. Therefore, these states were assigned on the basis of the *Synechocystis sp.* hydrogenase. [7]

Table 1. CO and CN^- stretching-mode frequencies (in cm^{-1}) of all found redox states of *Re* SH in cells and after purification[13]. The numbers in parentheses are from the soluble hydrogenase from the cyanobacterium *Synechocystis* sp. PCC 6803 (*) and the MBH from *R. eutropha* H16 (°).[7;17;18]

Redox State	ν(CO)	ν(CN)	
Ni_r-B-like	**1957** (1957*)	**2079** (2076*)	**2089** (2088*)
Ni_a-C	**1961** (1968*) 1963 @ 35K[13].	**2080** (2079*) 2084 @ 35K[13]	**2091** (2093*) 2096 @ 35K[13]
Ni_a-SR	**1946** (1948°) 1945 (-391 mV)[13]	**2080** (2068°) n.d.	**2090** (2087°) n.d.
Ni_a-SR'	**1922** (1926°) 1921 (-391 mV)[13]	**2052** (2049°) n.d.	**2068** (2075°) n.d.
Ni_a-SR''	**1913** (1919°) 1912 (-391 mV)[13]	**2052** (2046°) n.d.	**2068** (2071°) n.d.
Ni_a-SR2	**1958** (1955*)	**2068** (2063*)	**2080** (2079*)

n.d.: not determinable ; 1943/6 cm^{-1} Ni_a-S[13]

The spectroscopic data presented in this study strongly suggest, that the active site of the native SH contains a standard set of non-proteic, inorganic ligands, *i .e.* one CO and two CN^-. Freshly harvested cells exhibited significant amounts of Ni_a-C (up to 60%). Using FTIR spectroscopy, we were able to identify the catalytically active states Ni_a-C, Ni_a-SR, Ni_a-SR2, which were previously observed in other [NiFe]-hydrogenases including the bidirectional [NiFe]-hydrogenase of *Synechocystis* sp. PCC 6803. Furthermore, the Ni_a-C⇌Ni_a-L and Ni_a-C⇌Ni_a-SRx transitions turned out to be fully reversible. The latter ones are shown in the supplementary material. Anaerobic, as well as, aerobic oxidation led to the complete disappearance of the Ni_a-C signals. Instead, a FTIR spectrum was obtained, that exhibits one CO and two CN bands, which were assigned to a "Ni_r-B-like" state. However, it is not yet clear whether this redox state is a real Ni_r-B species, which is EPR-silent due to spin-couplings with other paramagnetic centers or just a "Ni_r-B-like" state with a formal Ni(II). Two further cell treatments, documented in the supplementary material, led to this "Ni-B-like" state, as well. After permeabilization of the cells by several freeze/thaw cycles it was also possible to reactivate the SH from the aerobically induced "Ni_r-B-like" state back to the catalytic active states. A fully reversible redox-behaviour, as a consequence of exchanging the gas-atmosphere from inert to oxidizing conditions and *vice versa*, was shown for *Re*, grown under litho-autotrophic conditions (see supplementary material). All redox states, identified for the SH in whole cells, are summarized in Scheme 1.

A non-standard ligation of the *Re* SH active site could not be verified by the current *in situ* study. The [NiFe] site of the native SH is rather equipped with a standard set of one CO and two CN^- ligands. This indicates, that the mechanism of oxygen-tolerance probably does not arise from additional, shielding cyanide ligands, but rather from a more complex mechanism such as postulated for the MBH from the same organism.[5;6] Further studies like a spectroelectrochemical characterization of the involved redox states are envisaged to gain a deeper insight into the reason of the remarkable oxygen-tolerance. Therefore, we are also working on the purification procedure of this enzyme, because this investigation can not be carried with whole cells.

Received: ((will be filled in by the editorial staff))
Published online on ((will be filled in by the editorial staff))

Keywords: hydrogenase · EPR spectroscopy · FTIR spectroscopy · oxygen-tolerance · biocatalysis

Reference List

[1.] R. Cammack, M. Frey, R. Robson, *Hydrogen As a Fuel: Learning From Nature*, Taylor & Francis, London and New York **2001**.

[2.] T. Burgdorf, S. Löscher, P. Liebisch, E. Van der Linden, M. Galander, F. Lendzian, W. Meyer-Klaucke, S. P. J. Albracht, B. Friedrich, H. Dau, M. Haumann, *Journal of the American Chemical Society* **2005,** *127* 576-592.

[3.] K. A. Vincent, J. A. Cracknell, O. Lenz, I. Zebger, B. Friedrich, F. A. Armstrong, *Proceedings of the National Academy of Sciences of the United States of America* **2005,** *102* 16951-16954.

[4.] T. Buhrke, O. Lenz, N. Krauss, B. Friedrich, *Journal of Biological Chemistry* **2005,** *280* 23791-23796.

[5.] M. Ludwig, J. A. Cracknell, K. A. Vincent, F. A. Armstrong, O. Lenz, *Journal of Biological Chemistry* **2009,** *284* 465-477.

[6.] M. Saggu, I. Zebger, M. Ludwig, O. Lenz, B. Friedrich, P. Hildebrandt, F. Lendzian, *Journal of Biological Chemistry* **2009,** *284* 16264-16276.

[7.] F. Germer, I. Zebger, M. Saggu, F. Lendzian, R. Schulz, J. Appel, *Journal of Biological Chemistry* **2009,** *in press, doi:* 10.1074/jbc.M109.028795.

[8.] R. P. Happe, W. Roseboom, G. Egert, C. G. Friedrich, C. Massanz, B. Friedrich, S. P. J. Albracht, *Febs Letters* **2000,** *466* 259-263.

[9.] E. Van der Linden, T. Burgdorf, M. Bernhard, B. Bleijlevens, B. Friedrich, S. P. J. Albracht, *Journal of Biological Inorganic Chemistry* **2004,** *9* 616-626.

[10.] A. Erkens, K. Schneider, A. Müller, *Journal of Biological Inorganic Chemistry* **1996,** *1* 99-110.

[11.] Gessner, C., PhD thesis, TU Berlin, **1996**.

[12.] E. Van der Linden, T. Burgdorf, A. L. De Lacey, T. Buhrke, M. Scholte, V. M. Fernandez, B. Friedrich, S. P. J. Albracht, *Journal of Biological Inorganic Chemistry* **2006,** *11* 247-260.

[13.] S. Foerster, M. van Gastel, M. Brecht, W. Lubitz, *Journal of Biological Inorganic Chemistry* **2005,** *10* 51-62.

[14.] M. Brecht, M. van Gastel, T. Buhrke, B. Friedrich, W. Lubitz, *Journal of the American Chemical Society* **2003,** *125* 13075-13083.

[15.] A. L. De Lacey, V. M. Fernandez, M. Rousset, R. Cammack, *Chemical Reviews* **2007,** *107* 4304-4330.

[16.] C. Fichtner, C. Laurich, E. Bothe, W. Lubitz, *Biochemistry* **2006,** *45* 9706-9716.

[17.] S. Kurkin, S. J. George, R. N. F. Thorneley, S. P. J. Albracht, *Biochemistry* **2004,** *43* 6820-6831.

[18.] B. Bleijlevens, F. A. van Broekhuizen, A. L. De Lacey, W. Roseboom, V. M. Fernandez, S. P. J. Albracht, *Journal of Biological Inorganic Chemistry* **2004,** *9* 743-752.

[19.] S. Stoll, A. Schweiger, *Journal of Magnetic Resonance* **2006,** *178* 42-55.

Supporting Material

Experimental Section

For the construction of *Re* HF798 (SH^+ MBH^- RH^-) the SH expression in HF500 [1] with the characteristics (*hoxGΔ hoxHΔ hoxCΔ*; MBH^- SH^- RH^-, $HoxJ^{G422S}$) was restored by introducing *hoxH* on pCH1500 into HF500 *via* an allelic-exchange procedure.[2] pCH1500 was constructed as follows: The 1897 bp. *Ecl136II* fragment of plasmid pCH472 [3], containing *hoxH, was* cloned into the 7.3 kb *PmeI* digested pLO1 fragment.[2] The exchange was verified by PCR of the corresponding inserts.

If not otherwise noted, *Re* cells were grown heterotrophically in FGN medium [4], supplemented with 1µM $NiCl_2$,$ZnCl_2$ and SL6 [5], under continuous shaking at 120 rpm. For one distinct preparation (Fig. S2) cells were cultivated lithoautotropically in the same mineral salts, but without fructose and glycerol under an atmosphere of 80% H_2, 10% O_2 and 10% CO_2. Cells were harvested by centrifugation at an A_{436} of 12 and washed twice with 50 mM potassium phosphate buffer, pH 7.0. After resuspension in the same buffer (A_{436} ~ 2000), the cells were stored on ice. For SH oxidation in whole cells, the cell membranes were permeabilized by treatment with 33 mg/ml cetyl-trimethyl-ammonium bromide.[6] Oxidation was performed either anaerobically by adding excessive amounts of NAD^+ (5 mM) or aerobically in the presence of O_2. Reduced SH was prepared by 30 min incubation of whole cells with 1 bar H_2 in a glove box at ambient temperature.

H_2-oxidizing activity in soluble extracts was determined by a spectrophotometric NAD^+ reduction assay. [9] The in-gel activity staining assay was described in [7]. Protein concentration was determined according to the BCA method.[8]

EPR spectroscopy was performed using a Bruker ESP300E spectrometer equipped with an Oxford ESR900 helium flow cryostat. The samples were placed in a rectangular microwave cavity working in the TE_{102} mode. Simulations of the spectra have been performed with the MATLAB toolbox *EasySpin* (version 3.1.0.).[19] Experimental conditions: 2 mW microwave power, microwave frequency 9.56 GHz, 1 mT modulation amplitude, 12.5 kHz modulation frequency.

FTIR spectra were recorded on a Bruker Tensor 27 spectrometer equipped with a liquid nitrogen-cooled MCT detector with a spectral resolution of 2 cm^{-1}. The sample compartment was purged with dried air or N_2. The sample was held in a temperature-controlled (10°C) gas-tight IR-cell for liquid samples (volume ~ 7 µL, path length = 50 µm), equipped with CaF_2 windows.

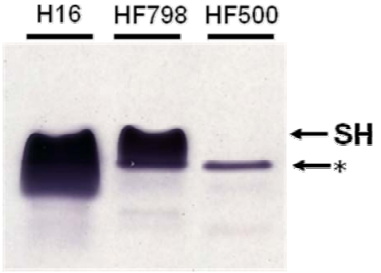

Figure S1 In-gel SH activity staining. Soluble extracts (100 µg of protein per lane) were separated on a native polyacrylamide gradient gel (4–15 %).. The gel was incubated with 50 mM Tris/HCl, pH 8, flushed with 1 bar H_2 for 30 min. SH activity staining was induced by the addition of 500 µM NAD and 60 µM NBT followed by a subsequent incubation for 2 h at 37°C. The blue-colored band marked by an asterisk is not related to hydrogenase activity.

The soluble extract of HF798 displayed approximately one third SH activity in comparison to the wildtyp H16 (Figure S1 and Table S1.).

Table S1. SH activity measured in soluble extracts of different Re derivatives. The given values represent the arithmetic mean of two independent experiments.

Strain	SH activity H2(NAD+ [Units x mg-1]
H16	1.29 ± 0.26
HF798	0.46 ± 0.22
HF500	<0.001

Additional IR-spectroscopic results

Various experiments were performed to demonstrate the reversibility of redox transitions between the catalytically active and inactive states of the *Re* SH *in situ*. All studies were performed on vital cells, which were at least partially grown under exceedingly physiological, litho-autotrophic conditions. Resulting FTIR spectroscopic data of these examinations are displayed in the following second derivative spectra.

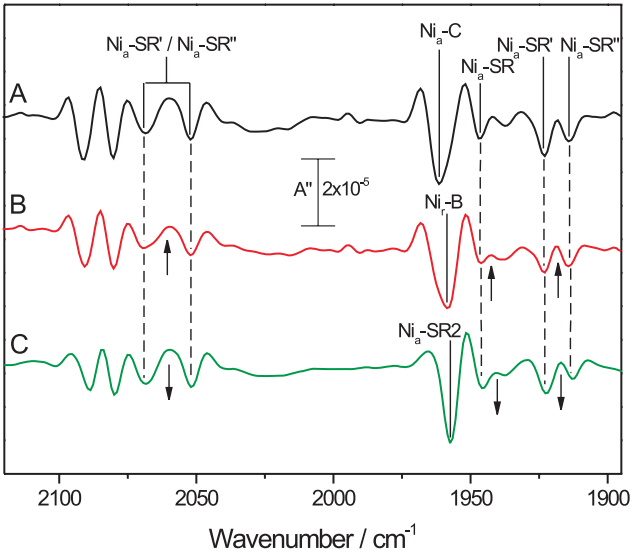

Figure S2 FTIR spectra of the soluble hydrogenase A) cells as harvested B) oxidized under aerobic conditions C) after 30 min incubation with 1 bar H_2

Fig. ***S2*** represents the reversibility of a partial oxidation of the soluble hydrogenase in whole cells. A permeabilization of the cells was realized by three successive freeze-thaw cycles. Trace A displays a FTIR spectrum of the freshly harvested cells. The result of a partial oxidation by air is shown in trace B. Here, the CO peak, corresponding to Ni_a-C, decreases while the respective Ni_r-B-like related signal has emerged. Furthermore, all signals, which are related to the reduced states of the enzyme, are lowered in intensity. The re-reduction originating from this state is represented by the spectrum, given in trace C. At this, all signals corresponding to the reduced states re-increased.

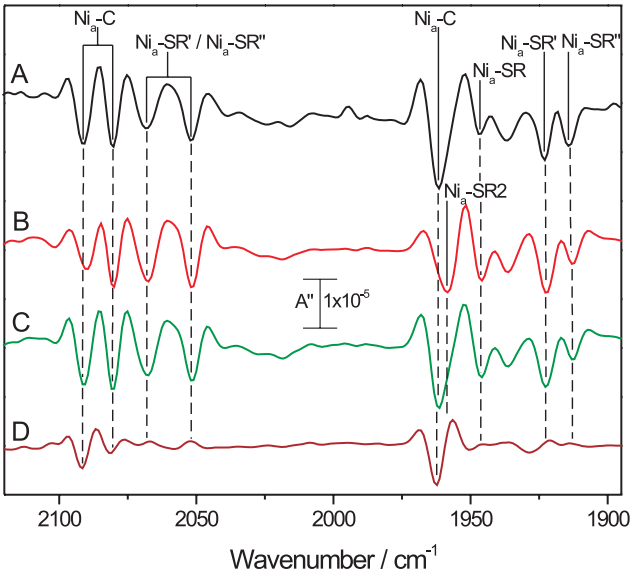

Figure S3 Second derivative FTIR spectra of the soluble hydrogenase A) freshly harvested cells B) after 30 min of incubation with 1 bar H_2 C) following subsequent long time incubation with N_2 D) difference spectrum C – B

Reduction and re-oxidation of the *Re* SH in whole cells is shown in Fig. S3. In this context, the spectral features, exhibited by the SH in freshly harvested cells, were shown to be fully reversible. Trace A shows the freshly harvested cells. Incubation with H_2 resulted in trace B. Here, the intensity of the peaks corresponding to the reduced states is increased. In particular, the Ni_a-SR2 related absorption in the CO region has emerged, while the respective Ni_a-C related signal vanished in return. The reappearance of the latter peak by long time incubation with N_2 is shown in trace C. Furthermore, the corresponding signals in the CN region have re-emerged, while the peaks, related to the enzyme's reduced states, decreased in intensity. The mentioned incidents are highlighted by the difference spectrum C – B, which is given in trace D.

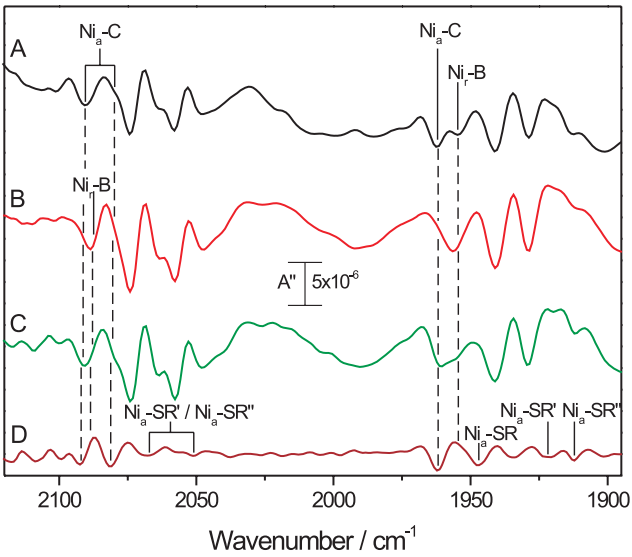

Figure S4 Second derivative FTIR spectral data of the soluble hydrogenase, cultivated under litho-autotrophic conditions A) cells as harvested B) after exposure to O_2 in air-saturated buffer C) after subsequent gas exchange by N_2 purging D) difference spectrum C - B

The FTIR spectral data, given in Fig. S4, display the reversibility of a total oxidation of the soluble hydrogenase in whole cells, cultivated under exceedingly physiological, lithoautotrophic conditions. Non-assigned strong IR absorption bands are related to increased amounts of non-functional and partially degraded protein, as it is usually observed under turn-over conditions. A spectrum of the freshly harvested cells is given in trace A. Ni_r-B-like related peaks emerged through exposure of the cells to air saturated buffer under aerobic conditions (trace B). Concurrently, Ni_a-C associated signals decreased. The latter peaks re-emerge subsequently to gas exchange by N_2 purging, as shown in trace C. Additionally, signals corresponding to the reduced states re-appeared. These processes are notably amplified by the difference spectrum C – B, which is given in trace D.

Literature Supplementary Material

[1.] Kleihues L., Lenz O., Bernhard M., Buhrke T., and B. Friedrich *American Society for Microbiology* **2000**, *182* 2716-2724
[2.] Lenz, O., Schwartz, E., Dernedde, J., Eitinger, M. and B. Friedrich *J. Bacteriol.* **1994** *176* 4385–4393.
[3.] Massanz, C., and B. Friedrich. *Biochemistry* **1999** *38* 14330–14337.
[4.] Friedrich, B., Heine, E., Fink, A., and C. G. Friedrich *J. Bacteriol*. **1981** *145* 1144-1149.
[5.] Eberz G. and B. Friedrich *J Bacteriol*. **1991** *173* 1845–1854.
[6.] Andersson M., Holmberg H. and P. Adlercreutz *Biotech. and Bioengineering* **1998** *57* 79-86
[7.] Schneider K. and H. Schlegel *Biochemica et Biophysica Acta* **1976** *452* 66-80
[8.] C.M. Stoscheck *Methods in Enzymology* **1990** *182* 50-69
[9.] Burgdorf T., Löscher S., Liebisch P., Van der Linden E., Galander M., Lendzian F., Meyer-Klaucke W., Albracht S.P., Friedrich B., Dau H. and Haumann M. *J. Am. Chem. Soc*. **2005** *127*, 576-592

9 Overexpression, isolation and spectroscopic characterization of the bidirectional [NiFe]-hydrogenase from *Synechocystis* sp. PCC 6803

F. Germer, I. Zebger, M. Saggu, F. Lendzian, R. Schulz and J. Appel

published in *J. Biol. Chem.* (**2009**), *284*, 36462-36472

THE JOURNAL OF BIOLOGICAL CHEMISTRY VOL. 284, NO. 52, pp. 36462–36472, December 25, 2009

Overexpression, Isolation, and Spectroscopic Characterization of the Bidirectional [NiFe] Hydrogenase from *Synechocystis* sp. PCC 6803*[S]

Received for publication, June 2, 2009, and in revised form, September 26, 2009 Published, JBC Papers in Press, September 28, 2009, DOI 10.1074/jbc.M109.028795

Frauke Germer[‡], Ingo Zebger[§], Miguel Saggu[§], Friedhelm Lendzian[§], Rüdiger Schulz[‡], and Jens Appel[¶1]

From the [‡]Botanisches Institut, Universität Kiel, Am Botanischen Garten 1-9, D-24118 Kiel, Germany, the [§]Max-Volmer-Laboratorium, Technische Universität Berlin, Strasse des 17, Juni 135, D-10623 Berlin, Germany, and the [¶]School of Life Sciences, Arizona State University, Tempe, Arizona 85287

The bidirectional [NiFe] hydrogenase of the cyanobacterium *Synechocystis* sp. PCC 6803 was purified to apparent homogeneity by a single affinity chromatography step using a *Synechocystis* mutant with a Strep-tag II fused to the C terminus of HoxF. To increase the yield of purified enzyme and to test its overexpression capacity in *Synechocystis* the *psbAII* promoter was inserted upstream of the *hoxE* gene. In addition, the accessory genes (*hypF, C, D, E, A,* and *B*) from *Nostoc* sp. PCC 7120 were expressed under control of the *psbAII* promoter. The respective strains show higher hydrogenase activities compared with the wild type. For the first time a Fourier transform infrared (FTIR) spectroscopic characterization of a [NiFe] hydrogenase from an oxygenic phototroph is presented, revealing that two cyanides and one carbon monoxide coordinate the iron of the active site. At least four different redox states of the active site were detected during the reversible activation/inactivation. Although these states appear similar to those observed in standard [NiFe] hydrogenases, no paramagnetic nickel state could be detected in the fully oxidized and reduced forms. Electron paramagnetic resonance spectroscopy confirms the presence of several iron-sulfur clusters after reductive activation. One [4Fe4S]$^+$ and at least one [2Fe2S]$^+$ cluster could be identified. Catalytic amounts of NADH or NADPH are sufficient to activate the reaction of this enzyme with hydrogen.

Hydrogenases are metalloenzymes that catalyze the reversible cleavage of H_2 into two protons and two electrons. Three types of hydrogenases are recognized, two contain a binuclear metal center (FeFe or NiFe) and the third type harbors a mononuclear iron center. Despite being unrelated in an evolutionary context (1, 2) all three classes share a $Fe(CO)_x(RS^-)$ motif in their active sites (3, 4).

In the cyanobacterial phylum two functionally different [NiFe] hydrogenases are present, an uptake and a bidirectional enzyme (5, 6). *Synechocystis* PCC 6803, as a non-nitrogen fixing cyanobacterium, possesses only a bidirectional [NiFe] hydrogenase, which is investigated in this study. It is a pentameric enzyme utilizing NAD(P)$^+$ as a substrate (Fig. 1). HoxY and HoxH form the hydrogenase moiety and HoxE, HoxF, and HoxU comprise the diaphorase unit (5, 7–9). Physiologically it was shown that the hydrogenase functions as a valve for an excess of electrons (10–13). It is suggested that cyclic electron transport, respiration via the NDH-1 complex, and the bidirectional hydrogenase are competing for reducing equivalents (13). Furthermore, it has been proposed that the enzyme could be part of respiratory complex I (8). For a schematic representation of the suggested metabolic pathways see Fig. 1. The bidirectional hydrogenase shows its highest activity in cells with high photosynthetic activity and low respiration rates (10), although it should be stressed that it is only active under anaerobic conditions. The *hox* genes are constitutively expressed in the presence of O_2 (10, 14), but the enzyme is inactive under aerobic conditions. In the absence of O_2 the hydrogenase regains its activity in less than a minute (10, 11). Crude extracts or the partially purified enzyme can be activated under anaerobic conditions within minutes by excess NADH or NADPH in the absence of H_2 (12). Most other known [NiFe] hydrogenases, except *e.g.* the three oxygen-tolerant hydrogenases in *Ralstonia eutropha* H16 (*Re* H16), (namely) the soluble NAD$^+$-reducing (15, 16), the regulatory (17), and the membrane bound hydrogenase (18), are inactivated by oxygen under electron poor conditions, presumably by the formation of a hydroperoxo-bridge. Their reactivation in the presence of hydrogen takes hours (19–21).

[NiFe] hydrogenases consist minimally of a large subunit in which the active site is deeply buried and a small subunit with at least one FeS cluster. All enzymes with a bimetallic active site harbor a [4Fe4S] cluster near the active site, the so-called proximal cluster. A medial [3Fe4S] cluster and a distal [4Fe4S] cluster are common features in some [NiFe] hydrogenases, as exemplified by the enzymes of *Desulfovibrio gigas* (22, 23), *Allochromatium vinosum* (20, 24–26), or the *Desulfovibrio vulgaris* Miyazaki F (21, 27–29).

The active site in [NiFe] hydrogenases has been characterized as a $NiFe(CN)_2(CO)$ center by x-ray crystallography (22, 23, 28, 30) and by Fourier transform infrared spectroscopic

* This work was supported by grants from Linde AG, the foundation of the Universität Kiel and state of Schleswig-Holstein (to F. G.). We also acknowledge the DFG for financial support within the CoE "UniCat" (F. L.) and SFB 498 (I. Z., M. S., F. L.).

[S] The on-line version of this article (available at http://www.jbc.org) contains supplemental Figs. S1–S3 and Tables S1–S3.

[1] To whom correspondence should be addressed. Tel.: 480-965-1865; Fax: 480-965-6899; E-mail: jens.appel@asu.edu.

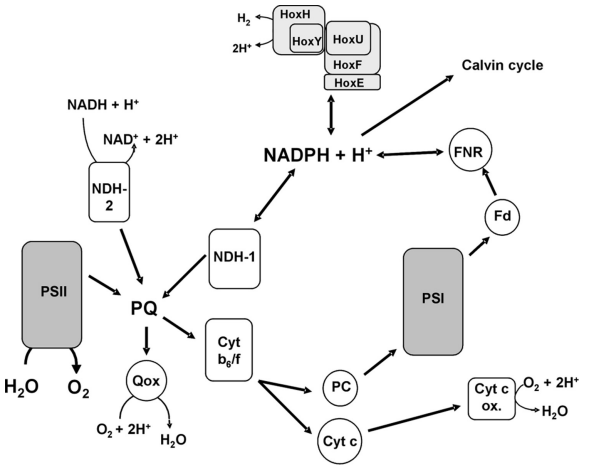

FIGURE 1. **Schematic model of the metabolic position of the bidirectional [NiFe] hydrogenase (HoxEFUYH) in *Synechocystis* sp. PCC 6803.** *Arrows* represent electron transport. The abbreviations are: *NDH-1*, NADPH-dehydrogenase (complex I); *NDH-2*, type 2 NADH-dehydrogenase, *PSI*, photosystem I; *PSII*, photosystem II; *Cyt b_6/f*, cytochrome b_6/*f* complex; *PQ*, plastoquinone; *Fd*, ferredoxin; *FNR*, ferredoxin:NADP reductase; *PC*, plastocyanin; *Cyt c ox.*, cytochrome *c* oxidase; *Qox*, quinol oxidase.

(FTIR)[2] studies (4, 21, 31–33), showing that the iron atom carries three inorganic diatomic ligands, two cyanides and one carbon monoxide. Nickel is coordinated by the sulfur atoms of four cysteines. Two of them are linked to the iron. In aerobically isolated enzymes, crystallographic studies indicate a third bridging ligand, which is a mono-oxo (hydroxo) ligand in the Ni_r-B (ready state), whereas a bridging di-oxo (hydroperoxide) species has been suggested in the Ni_u-A (unready state) (34, 35). The exact nature of the ligand in the Ni_u-A state is still under discussion (29). In these oxidized states, the enzyme is inactive but can be activated by reduction with hydrogen. Upon activation the oxygen ligand is removed (36, 37). The two states Ni_r-B and Ni_u-A differ in their activation kinetics. Ni_r-B activation takes place within a time frame spanning from seconds to minutes, whereas the Ni_u-A state requires hours (4, 19–21). Both states can be monitored with electron paramagnetic resonance (EPR) spectroscopy, via the low spin Ni^{3+} ion. In one-electron reactions these states are converted to their respective reduced states, Ni_u-S and Ni_r-S, which are also catalytically inactive, but EPR-silent. All redox states can be distinguished by FTIR spectroscopy via their characteristic band positions of the CO and CN stretching vibrations (4, 21, 26, 32). For an overview about the different states of standard [NiFe] hydrogenases, see Refs. 4 and 29. It is proposed that at least three of the various redox states identified in [NiFe] hydrogenases are directly involved in the catalytic cleavage and formation of H_2. Ni_a-S (EPR-silent) is the most oxidized that is converted by reduction to the intermediate Ni_a-C (EPR-active), which is then fully reduced to Ni_a-SR (EPR-silent). Each of the one-electron reduction steps is accompanied by a proton transfer step. Although nickel cycles between diamagnetic +II and paramagnetic +III states, the iron in the active site remains in its valence state during catalysis (25, 38). The splitting of H_2 is known to be a heterolytic process ($H_2 \rightleftharpoons H^- + H^+$) (3) and the electrons are believed to be transferred via FeS clusters between the active site and the redox partners of the enzyme.

The bidirectional, soluble NAD^+-reducing hydrogenase from *Re* H16 (SH) is a close relative of the cyanobacterial bidirectional hydrogenase and the best characterized of its class. For this enzyme a non-standard coordination of the active [NiFe] site was proposed with one additional cyanide ligand bound to each iron and nickel (15, 16, 39). Such a ligation would possibly protect the catalytic center from binding of oxygen and the related inactivation. The protein was activated by hydrogen in the presence of catalytic amounts of NADH or NADPH (16). Under such conditions, no evidence of paramagnetic nickel species could be detected by EPR spectroscopy (16). However, in some enzyme preparations significant amounts of Ni_a-C could also be induced electrochemically or by an excess of NADH or dithionite (39).

Oxygenic photosynthetic microorganisms are a matter of intense interest for the production of hydrogen by solar power. The bidirectional hydrogenase is the enzyme naturally involved in this process in cyanobacteria (10–12). In this work we present a newly developed rapid and gentle purification protocol for *Synechocystis* sp. PCC 6803 and the first characterization of the enzymes active site and its iron-sulfur centers by a combination of FTIR and EPR spectroscopy.

MATERIALS AND METHODS

Cell Growth—The wild type strains *Synechocystis* sp. PCC 6803, *Nostoc* sp. PCC 7120, and the *Synechocystis* mutants were grown in BG-11 (40) supplemented with 5 mM TES, pH 8, at 28 °C and 50 μE m^{-2} s^{-1} bubbled with air. For purification, *Synechocystis* mutant strain E3 was cultured in 5-liter glass bot-

[2] The abbreviations used are: FTIR, Fourier transform infrared; EPR, electron paramagnetic resonance; SH, soluble hydrogenase; *Re*, *Ralstonia eutropha*; TES, 2-{[2-hydroxy-1,1-bis(hydroxymethyl)ethyl]amino}ethanesulfonic acid; Tricine, *N*-[2-hydroxy-1,1-bis(hydroxymethyl)ethyl]glycine; MALDI-TOF, matrix-assisted laser desorption ionization time-of-flight; T, tesla.

TABLE 1
Primer sequences used during cloning procedures

Primer	Sequence 5′–3′
Anahyp1	CATATGGCGACTGAGGAAATTCG
Anahyp2	TAGCTAGTCGACGATTAAGGAAAAACTGGTAC
E-in1	GGTTCGTGCCTTCATCCGTCGACTGATTGGGAGAGCCT AAACC
E-out1	TCTGAGCGATGAACTGAGAAAC
E-in2	TACCGCCACCTAACAATTCGGTACCAGGATTTTCATATG ACCGTTGCCAC
E-out2	AACTGTTACTTAACCAAGGTTG
Gm1	GTCGACGGATGAAGGCACGAACC
Gm2	GTCGACGAATTGTTAGGTGGCG
HoxF-in1	GAACTGCGGGTGGCTCCAGCTAGCGACTTTGAGTAATTC TTCATA
HoxF-out1	CTTTTTAGAAGGGGAAGCTA
HoxF-in2	GAGCCACCCGCAGTTCGAGAAATAGTTCGGATCCTTATC CACTCAGTTA
HoxF-out2	CAGTGGCTTGGATAAATTCT

tles. The cells were harvested at 20 min by centrifugation at 6,000 × *g*.

Cloning Procedures—DNA cloning and PCR amplification were performed using standard procedures (41). All primer sequences used during the cloning procedure are listed in Table 1. To insert a *psbAII* promoter upstream of the *hoxE* gene from *Synechocystis*, a PCR product was amplified using the primer pairs E-out1/E-in1 and E-in2/E-out2. The gentamycin cassette that had been amplified with primers Gm1 and Gm2 was then fused to these two PCR products as described (42). The resulting product was ligated into pCRII-TOPO (Invitrogen). In the final step this vector was cut by KpnI and NdeI, and the *psbAII* promoter of pDH1 (42) was excised with the same enzymes and inserted into these sites.

For construction of the Strep-tag II mutant (E3), the Strep-tag II sequence with an Alanin-Serin-linker (Fig. 2) was fused to the C terminus of the HoxF protein. Then, two PCR products from the genomic DNA of *Synechocystis* PCC 6803 were amplified using primer pairs HoxF-out1/HoxF-in1 and HoxF-in2/HoxF-out2. The overlapping parts of the Strep-tag II sequence in these products could be fused together with a second PCR. Primer HoxF-in2 contained the restriction site for the enzyme BamHI, at this site the kanamycin resistance cassette from pUC4K was inserted as a selection marker in the same orientation as *hox* genes. To get a *hyp* gene expression construct, the respective operon of *Nostoc* sp. PCC 7120 was amplified by PCR using primers Anahyp1 and Anahyp2. The resulting 6.7-kb PCR product was cloned downstream of the *psbAII* promoter into *Synechocystis* expression vector pDH2. The latter vector was constructed by cutting the kanamycin cassette out of pDH1 with restriction enzymes XhoI and SacI, and ligating the chloramphenicol resistance cassette from pKS-CAT (HindIII and SacI digested) into the pDH1 vector in a half-blunt end ligation reaction. This construct was transformed into the Strep-tag II mutant E3. All constructs were sequenced before transformation in *Synechocystis*.

Enzyme Purification—All purification steps were carried out at 4 °C under aerobic conditions. After washing and resuspending the pellet in buffer W (100 mM Tris-HCl, 150 mM NaCl, pH 8.0) the cells were disrupted by three passages through a chilled French pressure cell (Sim Amicon) at 20,000 p.s.i. To obtain the soluble fraction the extract was centrifuged at 24,000 × *g* for 1 h. Subsequently, a concentrated ammonium sulfate solution was slowly added to a final concentration of 20%. After centrifuging for 30 min at 11,000 × *g*, the supernatant was applied to a 5-ml gravity flow Strep-Tactin-Sepharose column (IBA, Göttingen, Germany). Unbound proteins were removed by washing 5 times with 1 column volume of buffer W. Recombinant protein was eluted by adding buffer E (buffer W with 2.5 mM desthiobiotin (IBA, Göttingen, Germany)) and the elution fraction was concentrated by centrifugation at 7,500 × *g* in centrifugal filters (Amicon Ultra 4, 10 K, Millipore, Eschborn, Germany).

Enzyme Assays—H_2 production was measured with a Clark-type electrode (43) in the presence of 5 mM methyl viologen and 10 mM sodium dithionite (10). Protein concentrations were determined by the Bradford assay (Bio-Rad, Laboratories) using bovine serum albumin as a standard (44).

Immunoblot Analysis—Proteins were separated by electrophoresis in 16.5% Tricine-SDS gels (45), and either stained with Coomassie Brilliant Blue or transferred to nitrocellulose membranes (Porablot, Macherey-Nagel, Düren, Germany). Proteins were detected with antibodies raised against *Synechocystis* HoxF (1:1000) and HoxH (1:100) (10) or against the HypD (1:500) (46) of *R. eutropha* and the ECL system (Amersham Biosciences). Strep-tag II antibodies, obtained from IBA (Göttingen, Germany) were used as described by the manufacturer. As a protein marker, the prestained protein ladder PageRuler (Fermentas, St. Leon-Rot, Germany) was used.

MALDI-MS Analysis and Edman Degradation—The excised gel slices were bleached, reduced with dithiothreitol, and acylated with jodacetamide. After digestion with trypsin, all mass spectra were acquired with a MALDI-TOF mass spectrometer (ABI Voyager-STR). The measurements were carried out with an α-cyano-4-hydroxycinnamic acid matrix. They were calibrated externally and internally using a standard Sequazyme Peptide Mass Standard kit and by the peptides generated by the autoproteolysis of trypsin. Protein identification by mass spectrometry data was achieved using the Protein Prospectors MS-Fit program (University of California, San Francisco, CA) and the Mascot search engine (version 2.0, Matrix Science Ltd.).

Determination of the subunit stoichiometry was performed using a Procise 492 protein sequencer (Applied Biosystems, Foster City, CA). The integrated peak areas of the separated 3-phenyl-2-thiohydantoin-derivatives during 13 Edman degradation cycles were used for quantification of the relative protein amounts.

Sample Treatment—Protein samples were filled in X-Band EPR tubes (Rototec Spintec 707-SQ-250). For reductive activation catalytic amounts (5 mol % of protein) of NADH or NADPH were added and the samples were flushed with 100% H_2 gas for 30 min in a glove box with an anaerobic atmosphere (5% H_2, 95% N_2). Sodium dithionite solution was prepared in an anoxic buffer, and the reduction was carried out under an argon atmosphere by adding a 20-fold excess to the sample. Furthermore, excess NADH was added to another sample that had been incubated with hydrogen and frozen after 30 min. In order to produce the highest oxidized state(s) in the enzyme, experiments with an excess of 2,6-dichloroindophenol were also carried out. Aliquots of the protein samples after various chemical

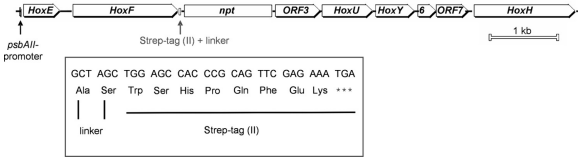

FIGURE 2. **Scheme of the *hox* operon with the Strep-tag II fused to *hoxF* in *Synechocystis* sp. PCC 6803.** The *psbAII* promoter was inserted upstream of the [NiFe] hydrogenase operon. The Strep-tag II sequence was fused with an Alanin-Serin-linker to the C terminus of *hoxF*. The construct contains a kanamycin resistance cassette. *HoxE*, *F*, *U*, *Y*, and *H* encode the structural hydrogenase genes. The function of open reading frames (*ORF*) 3, 6, and 7 is not yet known.

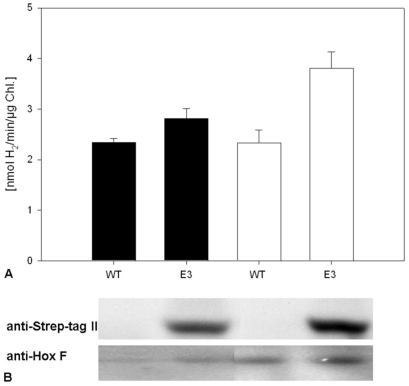

FIGURE 3. **Hydrogenase activity as measured in the presence of methyl viologen and dithionite (*A*) and Western blot analysis with anti-HoxF and anti-Strep-tag II (*B*) of wild type and mutant cultures grown in BG-11.** *WT*, *Synechocystis* sp. PCC 6803 wild type; *E3*, mutant with *psbAII* promoter upstream of the *hox* operon and Strep-tag II fused to the C terminus of HoxF. Cells were cultivated at 50 μE m^{-2} s^{-1} (*black bars*) and 200 μE m^{-2} s^{-1} (*white bars*). Triplicate measurements are shown; *error bars* represent the standard deviation.

treatments were taken for the FTIR spectroscopic investigations, whereas the main fraction was studied by EPR spectroscopy.

Infrared Spectroscopy—Infrared spectra were recorded on a Bruker Tensor 27 FTIR spectrometer equipped with a liquid nitrogen-cooled MCT detector at a spectral resolution of 2 cm^{-1}. The sample (0.1–0.6 mM protein) was held in a temperature-controlled (10 °C), gas-tight liquid cell (volume ~7 μl, path length ≈50 μm) with CaF_2 windows, whereas the sample chamber was purged with dried air. To follow the inactivation process after various chemical reactions, spectra were collected subsequently as a function of time while allowing air to penetrate slowly into the liquid cell.

Subsequently, the FTIR spectra were baseline corrected by means of a spline function implemented within OPUS 4.2 software supplied by Bruker. The spectra shown in this work were normalized with respect to the integral intensity of the CO stretching bands.

EPR Spectroscopy—X-Band EPR measurements at 9.5 GHz were carried out on a Bruker ESP300E spectrometer equipped with a rectangular microwave cavity working in the TE_{102} mode. The samples were placed in an Oxford ESR 900 helium-flow cryostat controlled with an Oxford ITC502 to allow measurements at temperatures between room temperature and 4 K. The microwave frequency was detected with an EIP frequency counter (Microwave Inc.). To obtain accurate g values the magnetic field was calibrated with an external standard (lithium particles embedded in LiF matrix) with a known g value of 2.002293 (47). Simulations of the spectra were performed with the MATLAB toolbox *EasySpin* (48). Background corrections were done by subtracting a spectrum containing only buffer solution from the spectrum of hydrogenase that was measured under the same conditions. For absolute quantification, the double-integrated spectra were compared with the spectra of a $CuSO_4$ standard of known concentration.

RESULTS

Overexpression—The genes of the bidirectional [NiFe] hydrogenase from *Synechocystis* PCC 6803 (*hoxE*, *hoxF*, *hoxU*, *hoxY*, and *hoxH*) are located in one operon (28, 30). In the gene cluster three open reading frames of unknown function (open reading frames 3, 6, and 7) are situated (Fig. 2). Six accessory proteins HypA-F (hydrogenase pleiotropic proteins) and one protease (HoxW) are necessary for post-translational processing of the hydrogenase (42, 49). To yield a sufficient amount of the [NiFe] hydrogenase for its characterization and to test the overexpression capacity in *Synechocystis* PCC 6803, the *psbAII*-promoter was inserted upstream of the *hoxE* gene in *Synechocystis*. The resulting mutants were used for another mutation process (Fig. 2), where a Strep-tag II sequence was fused to the C terminus of *hoxF*. The Strep-tag II contains eight amino acids with highly selective binding affinity for streptavidin variant Strep-Tactin, which is used for affinity chromatography.

Synechocystis wild-type cells and the produced mutants were cultivated at light intensities of 50 and 200 μE m^{-2} s^{-1}. Hydrogenase activity was measured in these cultures. Fig. 3*A* shows the resulting H_2 production rates. The hydrogenase activity of the *Synechocystis* mutant with a *psbAII* promoter upstream of the *hox* operon and with a Strep-tag II fused to the C terminus of HoxF (E3) is higher compared with the wild type. This result is reflected by comparison of the expression levels of HoxF in the mutant and the wild-type. In Fig. 3*B* a Western blot using the antibodies against HoxF and Strep-tag II demonstrate that the amount of HoxF in the mutant cells is higher compared with wild-type. The mutants cultivated at 200 μE m^{-2} s^{-1} (*white bars*) generally show higher H_2 production rates than those cultivated at 50 μE m^{-2} s^{-1} (*black bars*). This result agrees with the fact that the *psbAII* promoter is light induced. It

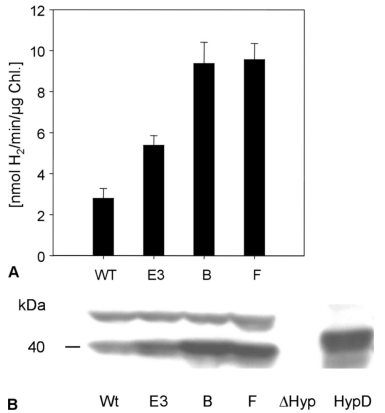

FIGURE 4. **Hydrogenase activity as measured in the presence of methyl viologen and dithionite (*A*) and Western blot analysis with antibody against HypD (*B*).** *WT*, *Synechocystis* sp. PCC 6803; *E3*, mutant with *psbAII* promoter upstream of the *hox* operon and Strep-tag II fused to the C terminus of HoxF; *B* and *F*, two E3 mutants with the *hyp* operon from *Nostoc* sp. PCC 7120 under the control of the *psbAII* promoter; *HypD*, *R. eutropha* strain HF632, which harbors the maturation proteins of the membrane-bound hydrogenase operon, as the positive control.[3] *ΔHyp*, strain HF632 with deletion of the complete *hyp* region, as the negative control. The protein of higher molecular weight detected in the cyanobacterial strains is due to an unspecific reaction of the antibody because it is not visible in the *R. eutropha* strains. Triplicate measurements are shown; *error bars* represent the standard deviation.

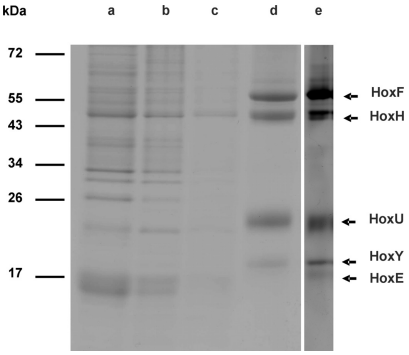

FIGURE 5. **Electrophoresis in 16.5% Tricine-SDS gels of the purified [NiFe] hydrogenase from *Synechocystis* sp. PCC 6803.** Coomassie Blue staining of crude extract (*a*), the first flow-through fraction (*b*), the first wash fraction (*c*), and the elution fraction with the highest protein concentration (*d*) from affinity chromatography. In *e*, a silver stain of the same elution fraction is shown.

encodes for the D1 protein of photosystem II, which is damaged at a higher pace at high light intensities because of stronger photooxidation. Consequently, the cells increase the expression of this gene (50).

We supposed that expression of the normal wild-type level of *hyp* genes might limit the formation of an active hydrogenase and that their overexpression could increase its yield. The *hyp* genes in *Synechocystis* are spread over the chromosome as single genes and are localized in different gene clusters (42). Because of this constraint, we overexpressed *hyp* genes (*hypF*, *C*, *D*, *E*, *A*, and *B*) from *Nostoc* sp. PCC 7120, which are in a single gene cluster, under the control of the *psbAII* promoter in the *Synechocystis* mutant containing the Strep-tag II and the *psbAII* promoter upstream of the *hox* operon. The result is presented in Fig. 4. Insertion of the *hyp* operon from *Nostoc* (see mutants B and F) led to a higher hydrogenase activity compared with the *Synechocystis* wild-type and compared with the mutant without this *hyp* operon. The expression of Hyp proteins from *Nostoc* sp. PCC 7120 in *Synechocystis* was confirmed by Western blot using an antibody against HypD. The crude extracts of mutants B and F contained more HypD than wild-type or the E3 mutant.

Purification—The soluble [NiFe] hydrogenase of the cyanobacterium *Synechocystis* sp. PCC 6803 could be purified to apparent homogeneity by affinity chromatography using a *Synechocystis* mutant with a Strep-tag II fused to the C terminus of HoxF. In the elution fraction of the purified enzyme all five subunits (HoxEFUYH) could be detected by Tricine-SDS-PAGE (Fig. 5). The identity of these bands was confirmed by MALDI-mass spectrometry (data not presented). Edman degradation in combination with sequencing of the purified enzyme established a subunit stoichiometry of HoxEFUYH. All subunits had unblocked N termini and could be sequenced, and aside from HoxF all subunits were detected without the N-terminal methionine. The unique amino acids occurring in five cycles (5–8, 10) of the degradation could be used to establish a ratio of 0.2:2:2:1:1 for E:F:U:Y:H (supplemental Table S1).

A complete small-scale purification procedure is summarized in Table 2. Beginning with 7.5 g of cells (wet weight) 13 μg of enzyme could be gained. The specific activity of the isolated fraction was 87.78 units/mg of protein with methyl viologen as the electron donor. The enzyme was purified 1155-fold. This high purity of the preparation could be confirmed by silver staining of the elution fraction (Fig. 5). For spectroscopic investigation the purification process was scaled up.

EPR Spectroscopy—In the isolated form of *Synechocystis* hydrogenase small signals attributable to an oxidized $[3Fe4S]^+$-cluster and an organic radical (probably chlorophyll impurities) were seen (supplemental Fig. S1). However, signal intensity did not correspond to stoichiometric amounts. The overall signal intensity corresponded to 0.05 spins/protein, indicating that the [3Fe4S] signal might arise from an oxidative damaged [4Fe4S] cluster in a small fraction of the sample during purification. Addition of an excess of 2,6-dichloroindophenol, to obtain the highest oxidized state of the enzyme, did not change the overall shape of the spectrum (supplemental Fig. S1) indicating that this hydrogenase does not harbor a $[3Fe4S]^+$ cluster as found in standard [NiFe] hydrogenases such as those from *D. vulgaris* Miyazaki F (28) or *D. gigas* (22). Furthermore, no traces

TABLE 2
Small-scale purification of the [NiFe] hydrogenase from *Synechocystis* sp. PCC 6803 (1 unit = production of 1 μmol of H_2/min^{-1})

Sample	Volume	Protein	Total protein	Activity	Total activity	Specific activity	Purification factor	Activity yield
	ml	*mg/ml*	*mg*	*units/ml*	*units*	*units/mg*	*-fold*	*%*
Crude extract	5.00	13.60	68.00	1.034	5.170	0.076	1	100
Affinity chromatography	0.50	0.025	0.013	2.195	1.097	87.782	1155	21

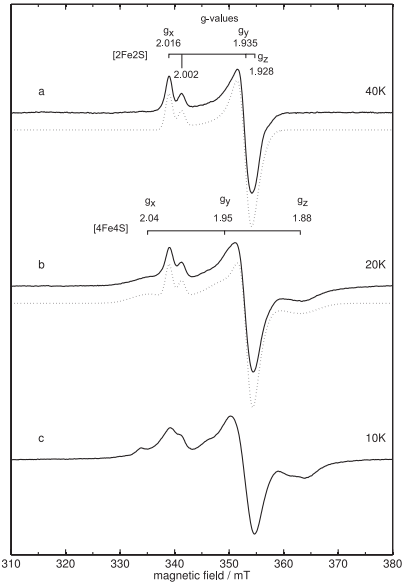

FIGURE 6. **EPR spectra of reduced *Synechocystis* hydrogenase (*solid*) together with corresponding simulations (*dotted*).** Catalytic amounts of NADPH (5 mol %) were added to the protein solution and the sample was incubated with hydrogen for 30 min. For simulation parameters, see Table 3. *a*, T = 40 K, signal of a reduced $[2Fe2S]^+$ is detected. The cluster appears in two different forms with slightly different g_x values. *b*, T = 20 K, additional $[4Fe4S]^+$ appears. *c*, T = 10 K, clusters are magnetically coupled and give rise to a splitting of the spectral components. Experimental conditions: 9.5 GHz microwave frequency, 1 mT modulation amplitude, 12.5 kHz modulation frequency, and 1 milliwatt microwave power.

of the Ni_r-B or Ni_u-A states were found in the EPR spectra. Their g values would be in the range of 2.33 to 2.01 (*e.g.* in *A. vinosum* Ni_r-B, $g_x = 2.33$, $g_y = 2.16$, $g_z = 2.01$, and Ni_u-A, $g_x = 2.32$, $g_y = 2.24$, $g_z = 2.01$ (4, 29)).

After addition of catalytic amounts of NADPH (5 mol %) and incubation with hydrogen for 30 min at room temperature, the signal of a reduced iron-sulfur cluster could be detected at 40 K (Fig. 6*a*). The g values of this cluster are $g_x = 2.016$, $g_y = 1.935$, and $g_z = 1.928$ with a line width of 1.5 mT. The temperature dependence and microwave power saturation behavior indicate that this cluster is most likely a reduced $[2Fe2S]^+$ cluster rather than a [4Fe4S] cluster as already discussed for the FeS clusters in complex I (51). Spin quantification yields about one spin/protein, *i.e.* this cluster is present in virtually 100% of the protein. However, there seem to be two forms of this [2Fe2S] cluster with different g_x values (see Table 3). This behavior is known from other iron-sulfur proteins where two forms were also observed in varying amounts depending on solvent and freezing conditions (52). Two populations with slightly different g_x values might arise from partial protonation of an amino acid in close vicinity to the cluster. Moreover, it is also possible that two different $[2Fe2S]^+$ clusters are present, which have by coincidence the same g_y and g_z values. We are unable to distinguish these two cases, because the signal intensity corresponds only to one spin/protein.

When the temperature was decreased to 20 K signals from a second type of iron-sulfur cluster appeared with g values, $g_x = 2.04$, $g_y = 1.95$, and $g_z = 1.88$ (Fig. 6*b*). The line width is 5 mT and the signal could not be saturated. The saturation behavior, temperature dependence, as well as the g-anisotropy are typical for reduced $[4Fe4S]^+$ clusters rather than for $[2Fe2S]^+$ clusters, as found in other organisms (18, 53–55). Absolute quantification indicates about 1.9 spins/protein for the overall EPR signal, originating from both types of FeS cluster. The double-integrated simulations of both clusters have similar intensities as well as indicating the presence of both clusters in virtually 100% of the protein.

At a temperature of 10 K the spectrum becomes more complex and the lines are broadened, which is probably due to magnetic coupling of both clusters. The spin intensity still corresponds to two spins/protein and it was not possible to disentangle the spectrum with power saturation studies (supplemental Figs. S2 and S3). From this we conclude that the $[4Fe4S]^+$ cluster and the $[2Fe2S]^+$ cluster(s) are in spatial proximity to each other.

Because up to eight iron-sulfur clusters are expected in this protein (supplemental Table S2) (8), different reduction methods have been performed. Surprisingly, all of them produced the same signals (see Fig. 7). Besides reductive activation with catalytic amounts of NADPH and hydrogen incubation, reduction was also performed with catalytic amounts of NADH and H_2 (Fig. 7*b*). Also incubation of excess NADH and hydrogen did not change the shape of the signal, only an increased amount of a flavin radical was observed centered around g = 2.003 (see *inset* Fig. 7). This radical is visible at higher temperatures, *e.g.* 230 K, and has a line width of 1.9 mT. To reduce all cofactors the sample was treated with excess sodium dithionite. However, no significant change of signal shape or intensity was observed. Therefore, it is obvious that the enzyme was already in the catalytically active state.

TABLE 3
g tensor principal values observed for the iron-sulfur cluster in *Synechocystis* hydrogenase (obtained by simulation)

Cluster	*Synechocystis* PCC 6803		*A. variabilis*[a]		*P. furiosus*,[b] [2Fe2S]
	[2Fe2S][c]	[4Fe4S][d]	[2Fe2S]	[4Fe4S]	
g_x	2.016/2.002	2.04	2.021	2.05	2.03
g_y	1.935	1.95	1.94		1.93
g_z	1.928	1.88	1.935	1.88	1.92
Line width (mT)	1.5	5.0			

[a] From Ref. 56.
[b] From Ref. 57.
[c] g-strain was included with 0, 0.01, and 0.02 for g_x, g_y, and g_z.
[d] g-strain was included with 0.03, 0, and 0.025 for g_x, g_y, and g_z.

By EPR spectroscopy no signals attributable to paramagnetic Ni(III) or Ni(I) species were found in the reduced enzyme (Figs. 6 and 7). Ni_a-C or Ni_a-L type signals are known from reduced standard hydrogenases (*e.g.* in *A. vinosum* at g values of Ni_a-C, 2.21, 2.15, and 2.01; and Ni_a-L1, 2.26, 2.12, and 2.05, see Ref. 29).

The absence of a Ni_u-A, Ni_r-B, Ni_a-C, or Ni_a-L signal indicates that either the [NiFe] site remains under oxidative and reductive conditions in a diamagnetic Ni(II)-state, or that the nickel center couples to another nearby unpaired electron to an overall EPR-silent state. This is in agreement with earlier studies performed on the soluble hydrogenases from *Anabaena variabilis* (56), *Pyrococcus furiosus* (57), *Nocardia opaca* 1b (58), and *A. vinosum* (59).

FTIR Spectroscopy—With this technique it is in general possible to characterize all redox states of the active site of [NiFe] hydrogenases, whether paramagnetic or EPR-silent diamagnetic. These states can be assigned by means of the specific absorption frequencies of the diatomic ligands and their respective band shifts due to changes of the electron density and/or coordination environment (4, 21, 26, 32).

Fig. 8 shows the first FTIR spectra of the [NiFe] hydrogenase from *Synechocystis* sp. PCC 6803. In the oxidized, as isolated form of this enzyme, only three bands can be resolved in the spectral region characteristic for the CN (2076 and 2088 cm^{-1}) and CO (1957 cm^{-1}) stretching vibrations (Fig. 8*e*). This suggests a coordination arrangement as it is observed in standard [NiFe] hydrogenases, with two cyanides and one CO bound to the iron of the active site (20–22, 32).

The detectable redox states after various chemical treatments were assigned by a comparison with those observed in standard [NiFe] hydrogenases and the Ni_a-C state found in certain preparations of the soluble bidirectional hydrogenase of *R. eutropha*. Furthermore, the redox states of the hydrogenase dimer of the soluble hydrogenase from *A. vinosum* were incorporated, which, however, could so far only be tentatively assigned via their CO stretching frequencies. An overview about characteristic band positions of the diatomic ligands is given in Fig. 10. Differences in the exact band location, which are also listed in supplemental Table S3, can be explained by variations in the embedding protein matrix in vicinity of the active site, see below (4, 21).

The spectrum after a treatment with 10 times excess 2,6-dichloroindophenol (not shown here) was identical with that from the as isolated sample. Therefore, we assume that this spectrum characterizes the highest oxidized state of the investigated enzyme, although EPR-silent (supplemental Fig. S1).

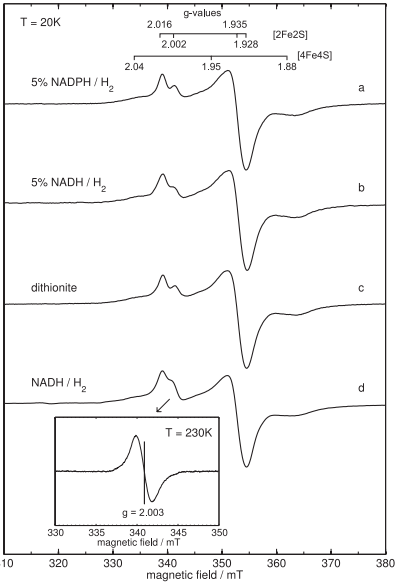

FIGURE 7. **Comparison of reduced *Synechocystis* hydrogenase at T = 20 K using different reduction methods.** The *inset* shows the resolved signal of the flavin radical at 230 K. *a*, with catalytical amounts of NADPH (5 mol %) and a 30-min H_2 incubation; *b*, with catalytical amounts of NADH (5 mol %) and 30-min H_2 incubation; *c*, with 10-fold excess NADH and 30-min H_2 incubation; *d*, with 20-fold excess sodium dithionite added under argon atmosphere. Experimental conditions: 9.5 GHz microwave frequency, 1 mT modulation amplitude, 12.5 kHz modulation frequency, and 1 milliwatt microwave power.

Because the CO and CN vibration band positions match best with the respective band positions of the diatomic ligands, as found in the Ni_r-B state of standard NiFe hydrogenases, we assigned this state as the "Ni_r-B-like" ready state. This implies that in the case of the cyanobacterial bidirectional enzyme the active site or its vicinity must be modified to suppress the appearance of an EPR-signal.

This most oxidized state of the enzyme can be easily activated by hydrogen, when catalytic amounts of NADH or NADPH are present. The corresponding spectrum after such a reductive treatment is displayed in Fig. 8*a*. It displays a dominating species with absorption bands at 2079/2063 cm^{-1} for the cyanides and 1955 cm^{-1} for the CO, respectively. The observed band positions, and the fact that no Ni(I/III) signals were detected in the corresponding EPR spectra, are in good agreement with the assignment to an activated, fully reduced, EPR-silent Ni_a-SR species. Incubation of the enzyme with a 20-fold excess of dithionite or NADH/NADPH in combination with hydrogen leads to the same IR and EPR spectra. This result

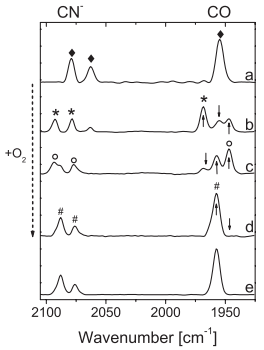

FIGURE 8. **FTIR spectra of the fully reduced sample of SH *Synechocystis* PCC 6803 at pH 8 (5 mol % NADPH + H_2) (*a*) and its slow reoxidation (*b*–*d*).** ♦, Ni_a-SR (*a*) and the corresponding spectra of various enriched redox states during the slow reoxidation with air, which are comparable with those observed in [NiFe] standard hydrogenases: *, Ni_a-C (*b*); ○, Ni_a-S (*c*); and reoxidized #, Ni_r-B-like (*c* and *d*). The latter is identical to isolated state before reduction (*e*). The spectra are normalized with respect to the entire area of the CO-stretching region. *Arrows* indicate the change of the relative amount of the involved redox state as a function of the oxygen content.

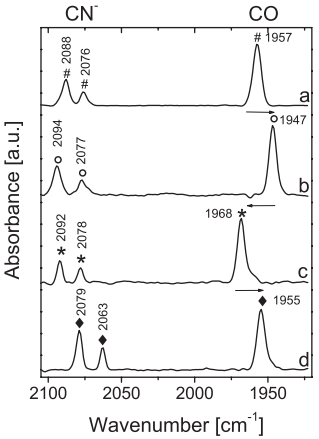

FIGURE 9. **FTIR spectra of the oxidized (as isolated) SH *Synechocystis* PCC 6803.** #, Ni_r-B-like (*a*) and the corresponding spectra of various states, which are comparable with those identified in [NiFe] standard hydrogenases and have been obtained after appropriate subtraction of the enriched components from Fig. 6 at pH 8.0: ○, Ni_a-S (*b*); *, Ni_a-C-like (*c*); and ♦, Ni_a-SR (*d*). The spectra are normalized with respect to the overall area of the CO-stretching region. *Arrows* indicate the relative shift of the CO stretching vibration compared with the previous redox state.

confirms that the spectral data presented here describe indeed the most reduced redox state of this enzyme.

During the controlled, slow penetration of air into the IR transmission cell, another Ni_a-C-like, reduced species with a CO stretching vibration at 1968 cm^{-1} and the related CN stretching at 2093 and 2079 cm^{-1} appeared readily during its transformation from the fully reduced Ni_a-SR state in the IR spectra (Fig. 8*b*). The latter band overlaps with cyanide absorption bands of other redox states, see Fig. 9. However, so far there was no EPR spectroscopic proof for a Ni_a-C state, because this transitional/intermediate state, with a redox potential close to that of the Ni_a-SR, could not be stabilized in sufficient amounts under the applied conditions for EPR spectroscopic investigations.

Within the ongoing slow reoxidation process, the relative concentration of the Ni_a-C-like state decreased again and another transitional redox state was observed before the enzyme was fully and reversibly reoxidized to its initial (as isolated) state. The corresponding stretching vibrations of such a Ni_a-S like, EPR-silent state were located at 1947 cm^{-1} (CO) and 2078/2093 cm^{-1} (CN^-). Adequate subtraction of the pure and enriched states of the spectra displayed in Fig. 8 reveals the individual spectra of the corresponding involved redox states as shown in Fig. 9.

DISCUSSION

Hydrogen production by photosynthetic organisms is a matter of interest to ensure future energy supply by alternative environmentally friendly sources. Oxygenic photosynthesis produces reducing equivalents and oxygen directly from water. Despite cyanobacteria being the only prokaryotes able to perform oxygenic photosynthesis a detailed biochemical characterization of the cyanobacterial [NiFe] hydrogenases is missing. Our results show, that the bidirectional [NiFe] hydrogenase from *Synechocystis* PCC 6803 can be purified under aerobic conditions to apparent homogeneity as a functional heteropentameric protein, HoxEFUYH. The stoichiometry of the subunits indicates that the amount of HoxF and -U is 2-fold higher as compared with the small and large subunits of hydrogenase (HoxYH). This is a surprising finding and very interesting in light of the quantification of transcript levels of their respective genes that found a 3× higher amount of *hoxU* compared with *hoxH* for *Synechococcus* sp. PCC 7942, although both are encoded in the same operon (60). The low abundance of HoxE indicates that it is either partly removed during the purification procedure or that it is only present in some of the complexes *in vivo*. A similar variability concerning an additional subunit, HoxI, unrelated to the cyanobacterial hydrogenases, which depends on the ionic strength of the buffers used, was also found for the hexameric SH of *R. eutropha* (61).

Anaerobic reduction of the [NiFe] hydrogenase from *Synechocystis* leads to high activity within a few seconds. To compensate for low preparation yields of the wild type hydrogenase we tried to overexpress the enzyme in *Synechocystis*. The task was challenging due to the genetic complexity of hydrogenase assembly (49). The overexpression of *hox* genes leads to an increase in activity (Fig. 3), but it was still below the level expected from the *psbAII* promoter, which is one of the strongest in cyanobacteria. We therefore assumed that expression of the *hyp* genes might be limiting. Due to a scattered distribution

of *hyp* genes in *Synechocystis*, the clustering of *hyp* genes in *Nostoc* sp. PCC 7120, and the high sequence homology of both hydrogenases (62) an expression of the *hyp* operon from *Nostoc* in *Synechocystis* seemed to be reasonable. *Nostoc* possesses one set of *hyp* genes that seems to be involved in the maturation of both of its [NiFe] hydrogenases. Our results confirm the possibility of overexpressing these *hyp* genes in *Synechocystis* and their heterologous use in the maturation of its bidirectional hydrogenase (Fig. 4).

EPR spectroscopy reveals the presence of functional iron-sulfur centers after reductive activation. In our studies we found signals corresponding to one $[4Fe4S]^+$ and at least one $[2Fe2S]^+$ cluster. Both clusters are in close proximity at temperatures below 10 K because they are magnetically coupled. Additionally, a signal appears at higher temperatures that can be attributed to a flavin (line width 1.9 mT). All observed paramagnetic centers could be reversibly activated/inactivated.

The spectral shape at low temperatures is similar to the spectra from the cyanobacterium *A. variabilis* (56), the hyperthermophilic archaeon *P. furiosus* (57), and the NAD-linked hydrogenase from *N. opaca* 1b (58). In the first case signals from reduced $[2Fe2S]^+$ and $[4Fe4S]^+$ clusters could be identified. In the *P. furiosus* hydrogenase one [2Fe2S] cluster was found, which is magnetically coupled to another iron-sulfur center at low temperatures. For the *N. opaca* hydrogenase it could be shown that the [2Fe2S] and [4Fe4S] clusters are located in the diaphorase subunit. Because of sequence similarities between this hydrogenase and the cyanobacterial bidirectional enzyme, it seems plausible that the [2Fe2S] center is bound by HoxU, whereas the [4Fe4S] center could be bound by either HoxF or HoxU, but any final conclusion needs to await further direct experimental evidence. Interestingly in all of these hydrogenases no signals of a paramagnetic nickel species were observed, which seems to be a common feature in hydrogenases of this type.

The FTIR spectroscopic investigations suggest a standard hydrogenase-like coordination of the iron in the [NiFe] site, with one CO and two CN^-. At least four different redox states of the active site have been identified. In particular two transitional states were detected only during the controlled reoxidation of the fully reduced species with air. In this way, a reversible inactivation of the enzyme to its initial, fully oxidized state was accomplished.

The direction and the degree of the observed blue and red shifts, especially of the CO stretching vibration within the various redox transitions, is comparable with those detected in the anaerobic [NiFe] standard hydrogenase from *D. vulgaris* Miyazaki F between the Ni_r-B, Ni_a-S, Ni_a-C, and Ni_a-SR states (see Figs. 9 and 10 and supplemental Table S3) (21).[3] Taking the π-electron back-bonding character of the $^-C{\equiv}O$ bond into account, the shift to lower wavenumbers from a Ni_r-B(III)-like state to a Ni_a-S(II) state should be caused by an increase of electron density at the active site. The corresponding CN stretches exhibit a weaker π-electron acceptability and shift to slightly higher wavenumbers. This effect is not unusual for

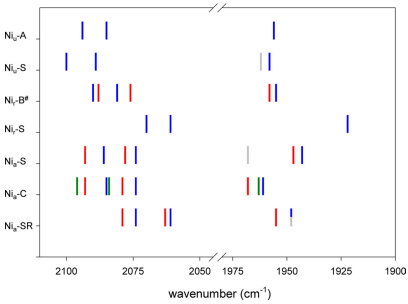

FIGURE 10. **Comparison of the positions of the CN^- and CO stretching modes of the [NiFe] hydrogenases from *D. vulgaris* Miyazaki F (*blue*) (21, 62), *A. vinosum* SH (*gray*) (59), *R. eutropha* SH (*dark green*) (39), and *Synechocystis* sp. PCC 6803 (*red*).** #, no EPR signal of the "Ni_r-B"-like state was observed.

redox transitions in standard [NiFe] hydrogenases (see below), as well as for CN^-/CO containing model compounds, and could be explained by a decrease of hydrogen bonding strength between neighboring amino acids and the cyanide ligands (*e.g.* due to a deprotonation) (21, 63).

A comparable but inverse effect, with constant, respectively, slightly lower values for CN stretching (explainable by increase of the hydrogen bonding, *e.g.* due to a protonation of cyanide adjacent amino acids) is observed from the Ni_a-S(II) to Ni_a-C(III)-like transition for all standard hydrogenases (see Fig. 10 and supplemental Table S3) (21). The corresponding CO band position shifts to higher wavenumbers, reflecting a decrease of the electron density at the active site. In turn, another shift to lower wavenumbers was found for transition from Ni_a-C(III)-like to Ni_a-SR(II), which is common for various standard [NiFe] hydrogenases and found for both types of the diatomic ligands, the CO and less pronounced also for the CN stretches (4, 21, 26, 32). Slight deviations (up to $\pm$ 7 cm^{-1}) in the absolute band positions could be explained by a variation of amino acids in the proximity of the bimetallic active site.

We could not find hints of any Ni(III) or Ni(I) species by means of EPR spectroscopy for the fully oxidized and reduced species. Because it seems unlikely that in the different [NiFe] hydrogenases different redox states of the nickel ion are used during catalysis these findings indicate an efficient coupling of any Ni(III) or Ni(I) ion with another nearby paramagnetic species to an overall, EPR-silent system. Any such coupling could also explain the low amount of EPR-detectable [FeS] clusters compared with the expected ones. Our experiments do not exclude the presence of a Ni_a-C state, because the corresponding transient species was observed in the IR spectra only during slow reoxidation by air and could not be stabilized in sufficient amounts for an EPR spectroscopic investigation.

Another, unlikely explanation is, that the [NiFe] site remains in a diamagnetic Ni(II) state, whereas electron density at the active site is changed by one of the coordinating ligands to the nickel during catalysis by donation or acceptance of electron

[3] M. Pandelia and W. Lubitz, personal communication.

density. This ligand could be modified by NADH/NADPH in such a way that catalytic hydrogen cleavage can take place, involving at least two transitional states, before the enzyme is fully reduced. In this respect recent studies of an [Fe] hydrogenase complex are interesting (64). It was proposed, that the methenyl-H_4MP^+ substrate can bind to the active site and accept the hydride during catalysis to form a methylene-H_4MP. In this process the H_2 molecule might bind side-on to the low spin Fe(II), which preserves its valence state during the catalytic cycle. In general it seems that the absence of a paramagnetic nickel species is a general principle in cyanobacterial bidirectional hydrogenases because the enzyme from *A. variabilis* neither showed nickel-specific signals in the oxidized nor reduced state (56).

A comparison with the presently available initial IR spectroscopic data of the isolated hydrogenase HoxYH modul of the (bidirectional) HoxEFUYH-type [NiFe] hydrogenase from *A. vinosum* reveals similarities with respect to some of the observable redox states. Thus, inter alia in an oxidized state, an active intermediate state, and a fully reduced state, all EPR-silent, were detected. These were tentatively assigned via the CO-stretching frequencies. The corresponding cyanide absorptions, however, are not well resolved and could not be unambiguously assigned (59), see Fig. 10. Depending on the particular preparation of the *A. vinosum* enzyme, minor amounts of Ni_u-A and Ni_r-B were identified by EPR spectroscopy. However, Ni_a-C could not be observed in any of the preparations.

The presence of a Ni(II) center in the oxidized state has been suggested for other hydrogenases, *e.g.* in the also bidirectional, but oxygen tolerant, soluble hydrogenase from *R. eutropha* H16 (15, 16, 39). In this hydrogenase, however, four instead of two CN stretching vibrational bands were detected besides one CO absorbance band. These additional IR bands were attributed to two more cyanides at the bimetallic center, one coordinated to the iron, and the other to the nickel atom. The latter was supposed to protect the active site and keep it in a Ni(II) low-spin state.

Another example where the [NiFe] active site was EPR-silent in the highest oxidized state is the cyanobacterial-like uptake hydrogenase from *A. ferrooxidans* in its native cell environment (66). Also in this case the presence of a different ligand at the nickel of the active site was suggested, which preserves the Ni(II) state. The FTIR spectra without additional light treatment reveals a mixture of two EPR-silent forms in air: Ni_s-S and Ni_f-S with CO and CN absorption bands at 1951, 1949 cm^{-1} and 2082/2093, 2077/2096 cm^{-1}, respectively. The main difference between these states is their slow and fast sensitivity with respect to light exposure. In a hydrogen atmosphere, Ni_s-S is fully converted to the Ni_f-S form. The purification process of the enzyme, however, leads to a modification of the active site, which shows EPR-detectable as well as silent states, similar to those observed in anaerobic standard hydrogenases (65).

None of the mentioned hydrogenases really exhibits a close similarity to both, the observed redox behavior and the characteristic IR spectroscopic band pattern of the diatomic ligands in the hydrogenase of *Synechocystis* sp. PCC 6803. It reveals a standard-like coordination of the active site with respect to the number of diatomic ligands (two cyanides and one carbon monoxide) and at least four standard-like redox states. However, no nickel-specific EPR signal was detected, and catalytic amounts of NADH/NADPH as in case of the soluble, oxygen-tolerant enzyme of *R. eutropha* (SH) were sufficient for its activation. Thus, the cyanobacterial enzyme, with its active site structure and fast activation kinetics, is situated between anaerobic [NiFe] standard hydrogenases and the SH from *R. eutropha*. With respect to these properties, it is very well suited to rapidly changing conditions faced by an oxygenic phototroph. It is rapidly activated under anoxic conditions, able to produce hydrogen, and on the other hand, quickly inactivated in the presence of oxygen, so as to not waste reductive power needed for carbon fixation. Further studies, including spectroelectrochemical FTIR redox titrations of the involved states are envisaged to gain a deeper insight into the redox behavior of this enzyme.

Acknowledgments—We thank Bärbel Friedrich, Humboldt University Berlin, for the gift of the antibody against HypD of R. eutropha. Help from WITA GmbH, Teltow-Berlin for Edman degradation/sequencing, and PLANTON GmbH for MALDI-MS analysis is gratefully acknowledged.

REFERENCES

1. Vignais, P. M., Billoud, B., and Meyer, J. (2001) *FEMS Microbiol. Rev.* **25,** 455–501
2. Vignais, P. M., and Billoud, B. (2007) *Chem. Rev.* **107,** 4206–4272
3. Armstrong, F. A., and Fontecilla-Camps, J. C. (2008) *Science* **321,** 498–499
4. De Lacey, A. L., Fernandez, V. M., Rousset, M., and Cammack, R. (2007) *Chem. Rev.* **107,** 4304–4330
5. Appel, J., and Schulz, R. (1998) *J. Photochem. Photobiol.* **47,** 1–11
6. Tamagnini, P., Leitão, E., Oliveira, P., Ferreira, D., Pinto, F., Harris, D. J., Heidorn, T., and Lindblad, P. (2007) *FEMS Microbiol. Rev.* **31,** 692–720
7. Schmitz, O., Boison, G., Hilscher, R., Hundeshagen, B., Zimmer, W., Lottspeich, F., and Bothe, H. (1995) *Eur. J. Biochem.* **233,** 266–276
8. Appel, J., and Schulz, R. (1996) *Biochim. Biophys. Acta* **1298,** 141–147
9. Schmitz, O., Boison, G., Salzmann, H., Bothe, H., Schütz, K., Wang, S. H., and Happe, T. (2002) *Biochim. Biophys. Acta* **1554,** 66–74
10. Appel, J., Phunpruch, S., Steinmüller, K., and Schulz, R. (2000) *Arch. Microbiol.* **173,** 333–338
11. Cournac, L., Mus, F., Bernard, L., Guedeney, G., Vignais, P. M., and Peltier, G. (2002) *Int. J. Hydrogen Energy* **27,** 1229–1237
12. Cournac, L., Guedeney, G., Peltier, G., and Vignais, P. M. (2004) *J. Bacteriol.* **186,** 1737–1746
13. Gutthann, F., Egert, M., Marques, A., and Appel, J. (2007) *Biochim. Biophys. Acta* **1767,** 161–169
14. Gutekunst, K., Phunpruch, S., Schwarz, C., Schuchardt, S., Schulz-Friedrich, R., and Appel, J. (2005) *Mol. Microbiol.* **58,** 810–823
15. Happe, R. P., Roseboom, W., Egert, G., Friedrich, C. G., Massanz, C., Friedrich, B., and Albracht, S. P. (2000) *FEBS Lett.* **466,** 259–263
16. Van der Linden, E., Burgdorf, T., Bernhard, M., Bleijlevens, B., Friedrich, B., and Albracht, S. P. (2004) *J. Biol. Inorg. Chem.* **9,** 616–626
17. Buhrke, T., Lenz, O., Krauss, N., and Friedrich, B. (2005) *J. Biol. Chem.* **280,** 23791–23796
18. Saggu, M., Zebger, I., Ludwig, M., Lenz, O., Friedrich, B., Hildebrandt, P., and Lendzian, F. (2009) *J. Biol. Chem.* **284,** 16264–16276
19. Fernandez, V. M., Hatchikian, E. C., and Cammack, R. (1985) *Biochim. Biophys. Acta* **832,** 69–79
20. Kurkin, S., George, S. J., Thorneley, R. N., and Albracht, S. P. (2004) *Biochemistry* **43,** 6820–6831
21. Fichtner, C., Laurich, C., Bothe, E., and Lubitz, W. (2006) *Biochemistry* **45,**

9706–9716
22. Volbeda, A., Charon, M. H., Piras, C., Hatchikian, E. C., Frey, M., and Fontecilla-Camps, J. C. (1995) *Nature* **373,** 580–587
23. Volbeda, A., Garcin, E., Piras, C., De Lacey, A. L., Fernandez, V. M., Hatchikian, E. C., Frey, M., and Fontecilla-Camps, J. C. (1996) *J. Am. Chem. Soc.* **118,** 12989–12996
24. Coremans, J. M., van der Zwaan, J. W., and Albracht, S. P. (1992) *Biochim. Biophys. Acta* **1119,** 157–168
25. Surerus, K. K., Chen, M., van der Zwaan, J. W., Rusnak, F. M., Kolk, M., Duin, E. C., Albracht, S. P., and Münck, E. (1994) *Biochemistry* **33,** 4980–4993
26. Bleijlevens, B., van Broekhuizen, F. A., De Lacey, A. L., Roseboom, W., Fernandez, V. M., and Albracht, S. P. (2004) *J. Biol. Inorg. Chem.* **9,** 743–752
27. Asso, M., Guigliarelli, B., Yagi, T., and Bertrand, P. (1992) *Biochim. Biophys. Acta* **1122,** 50–56
28. Higuchi, Y., Yagi, T., and Yasuoka, N. (1997) *Structure* **5,** 1671–1680
29. Lubitz, W., Reijerse, E., and van Gastel, M. (2007) *Chem. Rev.* **107,** 4331–4365
30. Ogata, H., Mizoguchi, Y., Mizuno, N., Miki, K., Adachi, S., Yasuoka, N., Yagi, T., Yamauchi, O., Hirota, S., and Higuchi, Y. (2002) *J. Am. Chem. Soc.* **124,** 11628–11635
31. Happe, R. P., Roseboom, W., Pierik, A. J., Albracht, S. P., and Bagley, K. A. (1997) *Nature* **385,** 126
32. De Lacey, A. L., Hatchikian, E. C., Volbeda, A., Frey, M., Fontecilla-Camps, J. C., and Fernandez, V. M. (1997) *J. Am. Chem. Soc.* **119,** 7181–7189
33. De Lacey, A. L., Stadler, C., Fernandez, V. M., Hatchikian, E. C., Fan, H. J., Li, S., and Hall, M. B. (2002) *J. Biol. Inorg. Chem.* **7,** 318–326
34. Ogata, H., Hirota, S., Nakahara, A., Komori, H., Shibata, N., Kato, T., Kano, K., and Higuchi, Y. (2005) *Structure* **13,** 1635–1642
35. Volbeda, A., Martin, L., Cavazza, C., Matho, M., Faber, B. W., Roseboom, W., Albracht, S. P., Garcin, E., Rousset, M., and Fontecilla-Camps, J. C. (2005) *J. Biol. Inorg. Chem.* **10,** 239–249
36. Garcin, E., Vernede, X., Hatchikian, E. C., Volbeda, A., Frey, M., and Fontecilla-Camps, J. C. (1999) *Structure* **7,** 557–566
37. Higuchi, Y., Ogata, H., Miki, K., Yasuoka, N., and Yagi, T. (1999) *Structure* **7,** 549–556
38. Huyett, J. E., Carepo, M., Pamplona, A., Franco, R., Moura, I., Moura, J. J., and Hoffman, B. M. (1997) *J. Am. Chem. Soc.* **119,** 9291–9292
39. van der Linden, E., Burgdorf, T., de Lacey, A. L., Buhrke, T., Scholte, M., Fernandez, V. M., Friedrich, B., and Albracht, S. P. (2006) *J. Biol. Inorg. Chem.* **11,** 247–260
40. Rippka, R., Deruelles, J., Waterbury, J. B., Herdman, M., and Stanier, R. (1979) *J. Gen. Microbiol.* **111,** 1–61
41. Sambrook, J., and Russel, D. W. (2001) *Molecular Cloning: A Laboratory Manual,* Cold Spring Habor Laboratory Press, Cold Spring Harbor, NY
42. Hoffmann, D., Gutekunst, K., Klissenbauer, M., Schulz-Friedrich, R., and Appel, J. (2006) *FEBS J.* **273,** 4516–4527
43. Wang, R., Healey, F. P., and Myers, J. (1971) *Plant Physiol.* **48,** 108–110
44. Bradford, M. M. (1976) *Anal. Biochem.* **72,** 248–254
45. Schägger, H. (2006) *Nat. Protoc.* **1,** 16–22
46. Jones, A. K., Lenz, O., Strack, A., Buhrke, T., and Friedrich, B. (2004) *Biochemistry* **43,** 13467–13477
47. Stesmans, A., and Van Gorp, G. (1989) *Rev. Sci. Instrum.* **60,** 2949–2952
48. Stoll, S., and Schweiger, A. (2006) *J. Magn. Reson.* **178,** 42–55
49. Böck, A., King, P. W., Blokesch, M., and Posewitz, M. C. (2006) *Adv. Microb. Physiol.* **51,** 1–71
50. Máté, Z., Sass, L., Szekeres, M., Vass, I., and Nagy, F. (1998) *J. Biol. Chem.* **273,** 17439–17444
51. Ohnishi, T. (1998) *Biochim. Biophys. Acta* **1364,** 186–206
52. Mukai, K., Kimura, T., Helbert, J., and Kevan, L. (1973) *Biochim. Biophys. Acta* **295,** 49–56
53. Guigliarelli, B., More, C., Fournel, A., Asso, M., Hatchikian, E. C., Williams, R., Cammack, R., and Bertrand, P. (1995) *Biochemistry* **34,** 4781–4790
54. Guigliarelli, B., and Bertrand, P. (1999) *Adv. Inorg. Chem.* **47,** 421–497
55. Schumann, S., Saggu, M., Möller, N., Anker, S. D., Lendzian, F., Hildebrandt, P., and Leimkühler, S. (2008) *J. Biol. Chem.* **283,** 16602–16611
56. Serebryakova, L. T., Medina, M., Zorin, N. A., Gogotov, I. N., and Cammack, R. (1996) *FEBS Lett.* **383,** 79–82
57. Bryant, F. O., and Adams, M. W. W. (1989) *J. Biol. Chem.* **264,** 5070–5079
58. Schneider, K., Cammack, R., and Schlegel, H. G. (1984) *Eur. J. Biochem.* **142,** 75–84
59. Long, M., Liu, J., Chen, Z., Bleijlevens, B., Roseboom, W., and Albracht, S. P. (2007) *J. Biol. Inorg. Chem.* **12,** 62–78
60. Schmitz, O., Boison, G., and Bothe, H. (2001) *Mol. Microbiol.* **41,** 1409–1417
61. Burgdorf, T., van der Linden, E., Bernhard, M., Yin, Q. Y., Back, J. W., Hartog, A. F., Muijsers, A. O., de Koster, C. G., Albracht, S. P., and Friedrich, B. (2005) *J. Bacteriol.* **187,** 3122–3132
62. Ludwig, M., Schulz-Friedrich, R., and Appel, J. (2006) *J. Mol. Evol.* **63,** 758–768
63. Lai, C. H., Lee, W. Z., Miller, M. L., Reibenspies, J. H., Darensbourg, D. J., and Darensbourg, M.Y. (1998) *J. Am. Chem. Soc.* **120,** 10103–10114
64. Hiromoto, T., Warkentin, E., Mo, J., Ermler, U., and Shima, S. (2009) *Angew. Chem. Int. Ed.* **48,** 6457–6460
65. Schröder, O., Bleijlevens, B., de Jongh, T. E., Chen, Z., Li, T., Fischer, J., Förster, J., Friedrich, C. G., Bagley, K. A., Albracht, S. P., and Lubitz, W. (2007) *J. Biol. Inorg. Chem.* **12,** 212–233

10 Conclusion and outlook

The focus of this thesis was laid on the spectroscopic characterization of oxygen-tolerant [NiFe]-hydrogenases. An important aspect was to study these biological systems in a preferably native environment, i.e. in whole cells or cytoplasmic membrane fragments. EPR spectroscopy was applied to probe all paramagnetic Ni and FeS species. In addition, FTIR spectroscopy was used to identify all redox states of the [NiFe] center, formed during the activation and catalytic cycle. The central aim of the studies was to investigate structure/function-relationships and to get deeper insight into the mechanisms of oxygen-tolerance of the *Re* H16 hydrogenases. The spectroscopic results for the *Re* H16 hydrogenases were compared with those obtained for the *D. vulgaris* Miyazaki F standard hydrogenase, for which crystal structures are available.

Membrane-bound hydrogenase from *Re* H16

The membrane-bound hydrogenase was the most extensively studied hydrogenase in this work. Both the heterotrimeric complex and the solubilized heterodimeric hydrogenase were spectroscopically investigated (**chapter 5**). Earlier EPR work dealt only with the purified heterodimeric protein. In these preparations a content of only 15% Ni_r-B was detectable. The combined EPR and FTIR study performed in this work on the heterodimeric form revealed that a large fraction remains in an EPR-silent state of an inactive form (up to 80% depending on the pH and the preparation). Remarkably, the catalytic activity of MBH is highest at pH 7.0 for the heterotrimeric form. Upon solubilization, the point of highest activity is shifted to pH 5.5 indicating that this process is connected with some kind of conformational change. Therefore, the studies were extended to the heterotrimeric complex, where the hydrogenase heterodimer is still attached to a cytochrome *b*, acting as the natural redox partner. Inside the cytoplasmic membrane, its physiological environment, the MBH was fully active and reacted in a fully reversible manner with its substrate H_2.

All catalytically active redox states, as known from standard [NiFe]-hydrogenases, except the unready state Ni_u-A, were identified. However, the EPR spectrum of the MBH in the oxidized form is obviously different from standard hydrogenases. Usually, standard hydrogenases show signals from a $[3Fe4S]^+$-cluster and resolved Ni_r-B/Ni_u-A signals. In contrast, the MBH displays a complex EPR spectrum with a superposition of several magnetically coupled paramagnetic species. The Ni site remains mainly in the Ni_r-B state ($\geq$80%), which could be activated with hydrogen within minutes. Both the $[3Fe4S]^+$-cluster and the Ni_r-B were coupled to an additional high-potential paramagnetic center. This additional center could be selectively reduced under mild conditions, leading to an EPR spectrum of the [3Fe4S]-cluster and Ni_r-B very similar to standard hydrogenases.

Since all relevant redox states known from standard [NiFe]-hydrogenases were found with FTIR spectroscopy, pulsed EPR studies were performed on the Ni_r-B state on cytoplasmic membrane

fragments containing MBH wild-type to obtain detailed information about the electronic and spatial structure of the [NiFe] center (**chapter 6**).

ENDOR spectroscopy showed that the electronic structure of the Ni_r-B state in *Re* H16 is similar to *D. vulgaris* Miyazaki F in frozen solution samples. The hf-couplings arising from two β-protons of one of the bridging cysteines were resolved and could be simulated for both the *Re* H16 and *D. vulgaris* with the same parameters.

With ESEEM spectroscopy, the presence of a histidine in the second coordination sphere of the [NiFe] center could be found. The nitrogen of this histidine is connected via a hydrogen-bond to one of the bridging sulfur atoms.

Pulsed EPR spectra were recorded at two different microwave frequencies (X- and Q-Band). With multifrequency experiments it was possible to disentangle field-dependent and field-independent interactions. A combined simulation of both the X- and Q-Band EPR spectra was performed, which revealed in more detail the origin of the additional spin-couplings in *Re* H16. From the analysis of the spin-couplings the presence of two different coupling partners for the Ni_r-B could be confirmed. However, the nature of these partners remains unclear, but the most plausible explanation up to now is a modified proximal FeS center, which is paramagnetic in the oxidized form (**chapter 7**).

From multiple sequence alignments it was found that all oxygen-tolerant membrane-bound [NiFe]-hydrogenases, including the *Re* H16 MBH, contain two additional cysteine residues in close vicinity to the proximal FeS-cluster. Mutations of these cysteines to glycines, which are found in standard [NiFe]-hydrogenases, resulted in EPR spectra similar to the partial reduced wild-type. Mutation of only one cysteine resulted in a strong heterogeneity of the additional center, indicating that both cysteines are responsible for an alteration of the proximal FeS center (**chapter 7**). However, it was not possible to reveal the nature of the additional center, e.g. whether it is a HiPIP, a modified [3Fe4S]-cluster or a cystein radical.

In summary, the reason for the remarkable oxygen-tolerance of the MBH is probably not due to an alteration of the [NiFe] center. The pulsed EPR data show a high similarity to a standard [NiFe] center. It is rather a more complex mechanism including the additional high-potential center, which is related to the proximal FeS cluster. This center might act as an electron donor in the catalytic cycle to avoid formation of the Ni_u-A state, which usually inhibits the enzyme.

Soluble hydrogenase from *Re* H16

The soluble hydrogenase was investigated for the first time in whole cells, i.e. in its natural environment (**chapter 8**). FTIR data showed, that the [NiFe] center behaves like a standard-type [NiFe] center with one CO and two CN ligands attached to the Fe. Five redox states known from standard hydrogenases could be identified. In whole cells the catalytically active form Ni_a-C/Ni_a-L and the fully reduced Ni_a-SR states were found. Oxidation with NAD^+ under anaerobic conditions or with O_2 revealed a diamagnetic Ni_r-B-like state with similar vibrational frequencies to those observed in standard [NiFe]-hydrogenases. With respect to the missing EPR signal, this state has either a formal Ni^{2+} oxidation state or the Ni_r-B is coupled to a nearby unpaired electron to an overall EPR-silent state, e.g. with a FeS-cluster.

These results are in sharp contrast to earlier studies on purified SH, where a modified [NiFe] center has been postulated. Based on the unusual FTIR spectra of purified heterotetrameric SH and chemical cyanide determination, two additional CN-ligands have been proposed. One cyanide was proposed to be bound directly to the Ni atom to protect the active site from oxygen.

In this work no indications for additional CN^--ligands were found, which suggests that the unusual FTIR properties suggested previously probably originated from heterogeneities of the sample. Therefore, the O_2-tolerance of the SH probably does not arise from a modified [NiFe]-center. Since several standard-like redox states were found by FTIR spectroscopy, the reason for O_2-tolerance might be more complex, such as observed in the MBH.

Bidirectional [NiFe]-hydrogenase from *Synechocystis* sp. PCC 6803

A combined EPR and FTIR study of a [NiFe]-hydrogenase from (**chapter 9**), an oxygenic phototrophic bacterium, was performed. The bidirectional hydrogenase from *Synechocystis* is closely related to the SH from *Re* H16. Therefore the spectrocopic properties of the SH could be used as a reference system. FTIR spectroscopy revealed at least four different redox states with similar vibrational spectra as found for standard [NiFe]-hydrogenases, suggesting a coordination of the Fe with two CN^- and one CO. In the oxidized as-isolated form the Ni site remains in a Ni_r-B-like EPR silent state, as found for the SH from *Re* H16. The hydrogenase could be activated with catalytic amounts of NADH or NADPH and incubation under H_2. After activation, three more redox states could be identified with FTIR, one of them similar to Ni_a-C. This intermediate state could not be enriched in sufficient amounts for EPR studies. Thus, it is not clear whether this state is Ni_a-C or a diamagnetic Ni_a-C-like state. Ni_a-SR and Ni_a-S were verified as the other two states, which could be shown by slow reoxidation of the fully reduced enzyme.

No paramagnetic Ni species could be detected with EPR spectroscopy under the applied experimental conditions. In the oxidized form the enzyme was EPR-silent. After activation signals from one [4Fe4S]- and at least one [2Fe2S]-cluster were visible. Similar EPR spectra have been found for other soluble hydrogenases, e.g. from *N. opaca*. This is a surprising result since up to eight FeS-cluster are expected from the biochemical binding motifs. It is possible that some of them are in close proximity and couple to EPR-silent states. At higher temperatures a resolved signal of a flavin-type radical could be observed, which may represent the site for NADH or NADPH conversion.

From its redox and activation behaviour, the bidirectional hydrogenase is placed between standard [NiFe]-hydrogenases and oxygen-tolerant hydrogenases, like the SH from *Re* H16. However, the latter enzyme is oxygen-tolerant, while the cyanobacterial hydrogenase needs to be activated under anaerobic conditions.

Outlook

Important aspects of the oxygen-tolerant MBH from *R. eutropha* regarding the structure of the [NiFe] and the FeS centers have been revealed in this thesis. However, the physiological function of the additional paramagnetic center, which couples to Ni_r-B remains unclear. To solve the structure of the proximal FeS center, a mutant in which the medial [3Fe4S]-cluster is converted to a

[4Fe4S]-cluster may provide further information. A [4Fe4S]-cluster is diamagnetic in its oxidized form and the complex coupling pattern in the EPR spectrum should change in the ideal case and simplify the spectrum, which would help to identify the unknown center(s). Further Q-Band EPR experiments with single point mutants of the cysteines near the proximal FeS center may provide more information about the origin of the additional couplings of the Ni signals and the locations of the additional center(s).

Pulsed EPR/ENDOR experiments have shown, that the electronic structure of the Ni_r-B redox state from *Re* H16 is similar to the Ni_r-B found in standard [NiFe]-hydrogenases. However, it is not clear whether the electronic structure of the Ni_a-C state is similar as well. The purified heterodimeric protein cannot be used for these experiments due to the 1:1 mixture of Ni_a-C and Ni_a-L. The conditions to enrich the Ni_a-C redox state in cytoplasmic membranes are quite difficult because strong background signals appear in the spectral region where Ni_a-C is expected after incubation with hydrogen. However, improved purification procedures are in progress, e.g. purifcation of the heterotrimeric MBH, using different detergents. It is expected that this system will also work completely reversible, when the natural electron acceptor is still attached.

Another aspect, which needs further investigations, is the spectroscopic behavior and the structure of the soluble hydrogenase from *Re* H16. The mechanism of oxygen-tolerance for the SH needs to be reconsidered due to the fact that in whole cells the [NiFe] center has a standard-like structure. For future experiments, the procedure of purification needs to be improved to study the enzyme under well-controlled conditions, which are difficult to establish in cells, e.g. controlled pH or redox potentials.

Nevertheless, it has been shown in this thesis that partial redox control in complex biological systems such as whole cells is possible. Thus, spectroscopy of whole cells can be be used to investigate the catalysis of enzymes when they are still attached to their natural redox partners. This allows studies under completely physiological conditions. In addition, such *in situ* experiments are good criterions to quantify the quality of purified proteins because the reversibility of catalytic processes in purified hydrogenases is not always given.

For the soluble hydrogenase from *Synechocystis* only four different redox states were identified with FTIR spectroscopy. Spectroelectrochemical experiments could help to identify more intermediate states including their corresponding redox potentials. This may allow the enrichment of certain redox states for EPR spectroscopic investigations. From such studies a more detailed picture of the reaction mechanism is expected.

The goal is to understand in detail the molecular mechanisms of oxygen-tolerance of hydrogenases and use this knowledge for technological applications like bio-hydrogen production or fuel cells.

Danksagung

Ich möchte mich bei allen Personen bedanken, die mich während meiner Promotion unterstützt haben, insbesondere bei

- Prof. Dr. Peter Hildebrandt für die Möglichkeit, in seinem Arbeitskreis zu promovieren und vielen hilfreichen Diskussionen,
- Dr. Friedhelm Lendzian für die hervorragende Betreuung während der Promotion,
- Dr. Ingo Zebger für eine gute Zusammenarbeit, insbesondere während der vielen gemeinsamen EPR/FTIR Nächte im Labor,
- Prof. Dr. Robert Bittl vor allem für die Übernahme der Betreuung gegen Ende meiner Arbeit und wertvollen Diskussion bezüglich Puls EPR,
- Prof. Dr. Thomas Friedrich für die Übernahme des Prüfungsvorsitzes,
- Dr. Marcus Ludwig, der die meisten Proben der MBH präpariert hat, insbesondere die heilige innere Membran,
- Dr. Christian Teutloff für die Einführung in die Puls EPR und vielen langen Abenden an der FU sowie dem Korrekturlesen,
- Dr. Marc Brecht für viele wertvolle Diskussionen und Ideen bezüglich Hydrogenasen,
- Dr. Oliver Lenz für viele konstruktive Diskussionen, die Bereitstellung einiger Abbildungen sowie dem Korrekturlesen,
- Tobias Goris für die Präparation der FeS-Mutanten
- Lars Lauterbach für die SH Präparationen
- Frauke Germer und Prof. Dr. Jens Appel für die Bereitstellung der *Synechocystis* Hydrogenase,
- Prof. Dr. Wolfgang Lubitz und Dr. Maria-Eirini Pandelia für die Bereitstellung der *Dv* Miyazaki F Hydrogenase und einer guten Kooperation,
- allen Kollegen im Büro PC316 (Steve Kaminski, Tillmann Utesch, Marius Horch, David von Stetten, Matthias Schenderlein) für eine motivierende Atmosphäre,
- Marina Böttcher, Nina Heidary, Jacek Kozuch, Dr. Anja Kranich, Jürgen Krauss, Dr. Uwe Kuhlmann, Khoa Ly, Wiebke Meister, Dr. Diego Millo, Dr. Maria Andrea Mroginski, Dr. Hendrik Naumann, Lars Paasche, Jacqueline Priebe, Yvonne Rippers, Johannes Salewski, Claudia Schulz, Murat Sezer, Francisco Velazquez Escobar, Dr. Inez Weidinger und allen weiteren Mitgliedern des Max-Volmer Laboratoriums für eine angenehme Arbeitsatmosphäre,
- allen weiteren Mitgliedern der AG Bittl für eine angenehme Arbeitsatmosphäre während der Messungen an der FU.